COO-2763-1
Distribution Category UC-66a

EXPLORATION CRITERIA FOR LOW PERMEABILITY GEOTHERMAL RESOURCES

Progress Report
for Period June, 1975--March 1, 1977

D. Norton

Under Contract No. EY-76-S-02-2763

March 1977

Prepared For
Energy Research and Development Administration

University of Arizona
Tuscon, Arizona 85721

DISCLAIMER

EXPLORATION CRITERIA FOR LOW PERMEABILITY GEOTHERMAL RESOURCES

Abstract

The decision to drill deep holes in a prospective geothermal system implies that geothermal energy resources exist at depth. The drill hole location and budget result from hypotheses regarding the location and depth of the resource within the overall system. Although operational decisions normally dictate the practicality of drilling, the characteristics of a system should assume a more significant role in the decision process. In order to increase the emphasis on collecting and interpreting data that are diagnostic of system characteristics, we must first understand how unique various surface or shallow subsurface data are in assessing the nature of the resource.

The following progress report summarizes the results of numerical simulations of heat and mass transport around igneous plutons and the synthesis of geologic data. To date, the results of the study describe the transient nature of thermal resources and the ambiguities which must be accounted for in using current technology to assess the nation's geothermal resources.

Statement of Problem

Recognition that energy resources occur in finite quantities, that they are nonrenewable, and that consumption of energy is required in order to utilize these resources, has resulted in programs whose objectives are assessment of the magnitude and recoverability of various geothermal energy resources. Since the geothermal energy resources occur in subsurface environments which are not well understood, the tasks which can potentially fulfill the program objectives are poorly defined. Therefore, the resource assessment problem for geothermal energy requires description of the unique features of the resource and development of methods useful in direct or indirect measurement of the resource characteristics.

Geothermal resources occur as a natural consequence of processes which disperse anomalous concentrations of thermal energy in the earth's upper crust. These heat and mass transport processes are active around thermal anomalies, such as igneous or metamorphic intrusions, for long periods of time, circa 10^6 years, and affect large volumes of rocks, circa 10^5 km^3. As a consequence, the characteristics of these resources as we know them today have been deduced from data collected over an extremely short time interval, with respect to the total age of the resource, or from data which represent the total integrated history of the resource at a few positions in this larger system. The observations made on active

geothermal systems are not representative of the entire system.

Simulation of heat and mass transport processes which occur in and around thermal anomalies in the upper crust provides a key to understanding the geologic past and extent of hydrothermal systems, Norton and Knight, 1977. Basic mathematical equations which represent the processes and numerical approximations of these equations permit computer simulation of large and long-lived natural systems. An analysis of the transport equations which simulate the processes reveals those parameters and variables which are characteristic of the system, and an analysis of the numerical approximations to idealized systems provides a first order approximation of the magnitude of the variables.

Objective of the Research

The objective of this research was to analyze low permeability geothermal systems related to high temperature plutons in the upper crust in order to ascertain those characteristics of these systems which could be detected by surface and shallow subsurface exploration methods. The analyses were designed to utilize computer simulation of idealized systems and to integrate data and concepts, available in the literature, which relate to the transport processes.

Methods of Analysis

Notions of temperatures and pressures in geothermal systems are primarily derived from production or exploration wells,

which are usually restricted to small portions of the total system. Knowledge of these parameters over the entire hydrothermal system is necessary in order to analyze the time dependence of transport variables in the region of a cooling pluton. Simulation of cooling plutons by numerical methods is one method by which these variables can be defined for an idealized geothermal system.

Fluid flow caused by thermal anomalies related to igneous plutons is effectively scaled and represented in two-dimensions by partial differential equations which describe the conservation of mass, momentum, and energy for the fluid-rock system, Norton and Knight, 1977:

$$(1)\quad \gamma\frac{\partial T}{\partial t} + q\nabla H = \nabla\cdot\kappa\nabla T \qquad \text{(conservation of energy)}$$

and

$$(2)\quad \frac{\nu\nabla\cdot\nu}{k}\frac{}{k}\nabla\Psi = R\,\frac{\partial\rho}{\partial y} \qquad \text{(conservation of momentum)}$$

where T is the temperature, Ψ the streamfunction, q the fluid flux, t the time, H, ρ, and ν are the enthalpy, density, and viscosity of the fluid, k is the permeability of the rock, κ the thermal conductivity and γ the volumetric heat capacity of the fluid saturated media, R the Rayleigh number, ∇ the gradient operator, and y the horizontal distance in the two-dimensional section to which these equations apply.

Equations (1) and (2) are approximated by finite difference numerical equations which permit computation of the values of the dependent variables at discrete points in the domain

from initial and boundary values specified for the system. The numerical analysis provides the option to include variable transport properties of the fluid (H_2O-system) and rock, general boundary and initial conditions, and radioactive and volumetric heat sources in a two-dimensional domain. The transport process related to the transient thermal anomaly is approximated by a time sequence of steady state numerical solutions to (1) and (2), computed at explicitly stable time intervals. An alternating-direction-implicit finite difference method, which accounts for the transportive characteristics of the system, is used to approximate the spatial derivatives at discrete intervals on the order of 0.1 to 0.5 of the system height. Fluid pressure in the system is computed at each steady state step by integration of Darcy's Law in which the fluid properties, viscosity and density, are expressed as a function of temperature and pressure.

The methods used by Norton and Knight, 1977, were used to define the temperature variations in the environment of cooling plutons, such as might be present in geothermal systems, as a function of time. The fluid flux, heat fluxes (conductive and convective), porosity, intrinsic electrical resistivity, and energy content were also computed. Our intent was not to analyze specific geothermal systems but to systematically vary input parameters in order to understand their effect on the variables which might be measured in an exploration-assessment program.

The numerical methods used generally approximated the governing partial differential equations within 10% in space and time. However, the overall geologic reality of the analyses depended on the degree to which the parameters used approximated natural conditions and was, therefore, more difficult to evaluate.

Attempts to apply details of specific results to a natural system will undoubtedly be unsuccessful. We feel the results will be most effectively used as a tool for understanding the uniqueness of certain exploration data and for understanding some of the gross characteristics of the system, as guidance in the collection and interpretation of data, and as a basis for more refined and sophisticated numerical studies. This study represents a first order approximation to transport processes which generate geothermal resources.

Discussion of Results

Theoretical studies of shallow igneous heat sources have resulted in several new concepts regarding the nature of geothermal resources and the uniqueness of methods utilized to search for these resources. These results pertain to the overall geothermal system, which consists of a high temperature intrusion, host rocks, and fluids. Details regarding reservoir characteristics of various rock units are not considered because the resource assessment problem which appears to be of first order importance is that of detecting shallow thermal systems. The detection of produceable reservoirs normally

follows after the overall system has been detected and delimited.

Geothermal resources in regions of igneous activity are, for purposes of this study, conveniently classified into three types, as defined by the processes which tend to disperse the anomalous thermal energy: (1) Thermal energy in rocks whose bulk permeability is sufficiently large that fluids (liquid or vapor) can be recovered from conventional production wells. Examples of this resource are the rocks from which energy is being recovered today, e.g., Wairakei, Larderello, Geyser, etc. The bulk rock permeabilities are on the order of $\geq 10^{-11}$ cm^2 in the systems, figure 1, region C. (2) Thermal energy in rocks which have permeabilities too small, $< 10^{-11}$ cm^2, for direct production of energy by conventional wells but whose permeabilities are greater than the minimum value ($\sim 10^{-14}$ cm^2) at which heat transport by fluid convection predominates over heat transport by conduction, figure 1, region B. (3) Thermal energy in rocks whose permeabilities are less than the value at which heat transport by convection predominates over heat transport by conduction, figure 1, region A.

This classification of subsurface thermal energy resources is derived directly from consideration of the transport processes which form the resources, and it provides a viable basis for designing exploration programs since these resource characteristics are predictable.

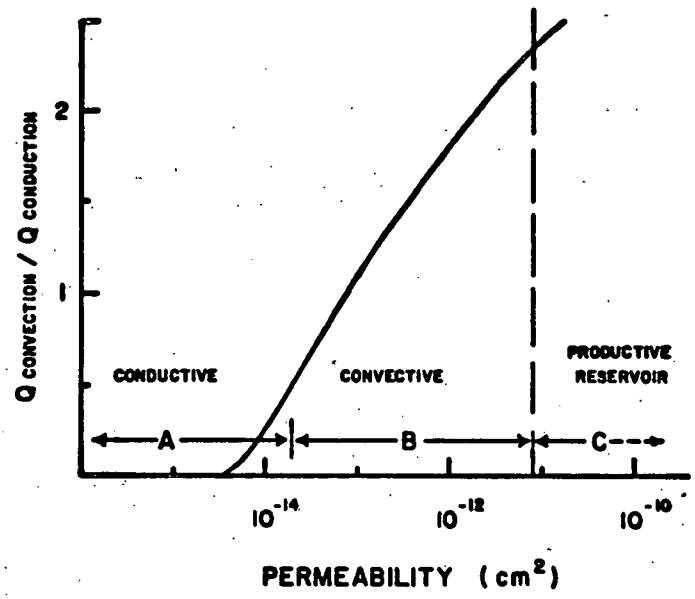

Figure 1

The original concept of "hot-dry-rock" resources seems to relate more to a reservoir type than to an overall system such as we are considering. We would expect to find relatively impermeable but high energy content blocks of rock within the relatively fractured regions of either A or B type resources, as well as in C. This is certainly evident in the producing geothermal systems where drill holes have missed the zones of abundant fracturing; they are hot and dry. In general, rocks contain pore fluids in their flow porosity from the groundwater table to several kilometer depths in the crust, albeit insufficient for direct production of energy. Indeed, significant fluid circulation is probably characteristic of most shallow pluton environments. And, as a consequence of extensive fluid circulation, resources associated with plutons have characteristics that are not uniquely interpreted by conventional methods, since these methods often require the presence of a steady heat source which cools by conduction of thermal energy.

The age of geothermal resources on the geologic time scale has a direct affect on the type of exploration methods which can be used to effectively detect these resources. Consequently, another degree of non-uniqueness is introduced into the interpretation of data normally used in exploring for geothermal systems. The age of the geothermal resource with respect to the causative thermal anomaly is important in all types of systems, but it is particularly relevant for those systems in which fluid circulation contributes to heat transport. Therefore, the characteristics of systems are discussed with respect to three rather arbitrary age intervals, crudely defined on the basis of major differences in their characteristics. The elapsed age obviously depends on geologic conditions in the subsurface; so, for purposes of discussion, the near-surface (1 - 2 km) thermal characteristics of a 4.5 km tall, $\sim$ 2 km wide, semi-infinite dike emplaced at 4.5 km will be considered. Plutons emplaced at $\sim$ 4.5 km depths will not cause perturbation in temperatures at 1 - 2 km depths for tens of thousands of years after emplacement of the pluton; from the time of initial emplacement to the time at which perturbations in temperature are evident at shallow depths is referred to as Stage I. Near-surface thermal perturbations then tend to a maximum, at which point the energy resource is nearest to the surface, Stage II; and, finally, the system decays to background temperatures, Stage III.

With these subdivisions of time in mind, let us now

examine the predicted distribution of several variables in the following schematic diagrams. Temperature as a function of depth, directly above the causative pluton, in three systems, A, B, and C, corresponding to the regions A, B, and C in figure 1, at an elapsed time equivalent to Stage II is summarized below:

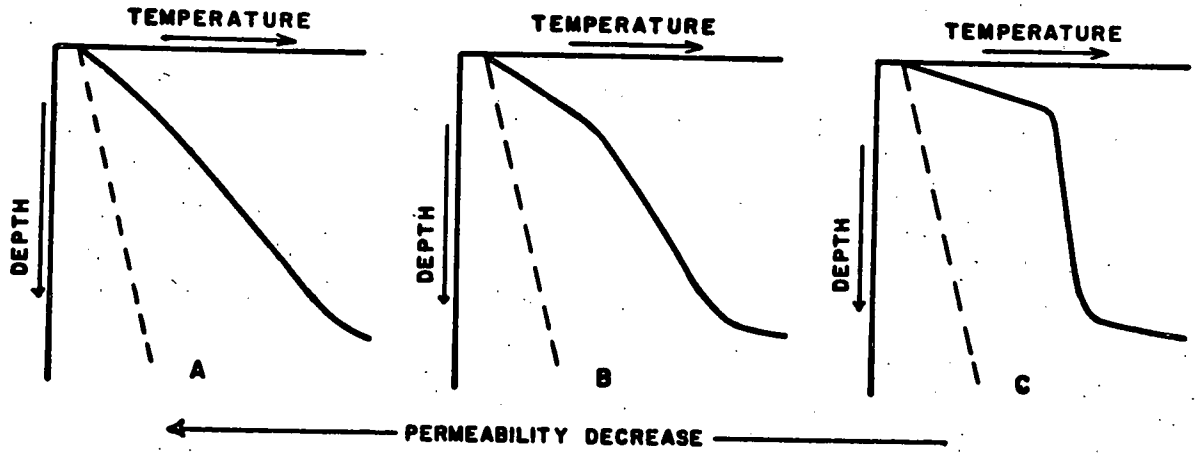

Figure 2

Thermal profile variations are simply a function of permeability of the host rocks surrounding the thermal anonaly since all other system parameters were held constant. Increases in permeability result in thermal profiles which are very steep near the top boundary, below which temperature changes very little with depth but then increases to the temperature of the causative pluton.

The interval of nearly constant temperature is the result of convective heat transport by circulating fluids and may

extend for several kilometers and persist for tens of thousands of years in the system. This type of thermal gradient has long been recognized in active geothermal systems. As a consequence of its nonlinear character, temperatures cannot be predicted at depth on the basis of shallow temperature gradient data. More significantly, the temperatures are grossly over-estimated by conventional methods.

The variation in temperature as a function of depth with time in a system with permeabilities in the B-region of figure 1 can be seen in figure 3. Note that the largest near-surface

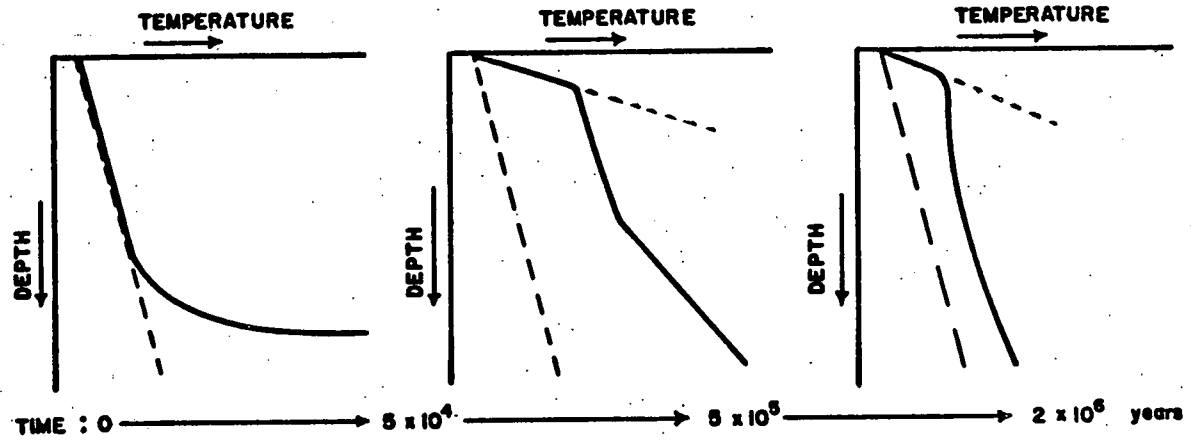

Figure 3

temperature gradients occur at Stage III of the decay of the thermal anomaly. Independent evidence regarding subsurface and energy distribution is required for "older" systems, and in Stage I systems the gradients will predict temperatures at depth which are much lower than actual temperatures.

Upward migration of thermal energy away from the intrusive body gives rise, in turn, to several other characteristics that all basically relate back to the rate and style of heat transport in the system. Upward migration of thermal energy in all systems, regardless of permeability values, causes pore fluid expansion and concomitant decrease in effective pressures, P_e, to a value which causes the rock to fracture. Although the manner in which these fractures will propagate and their dimensions are not known, an increase in interconnected porosity and an energy release in the form of microearthquakes undoubtedly occurs. The propagation of a $P_e = 0$ isobar away from a pluton which cools by conductive heat transport only illustrates the extent of this effect.

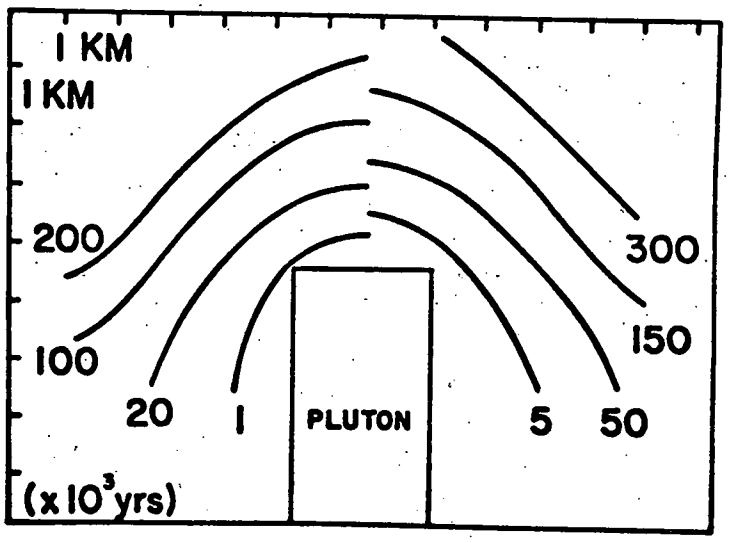

Figure 4

Assuming a distribution of fluid-filled isolated pores in the host rocks, the frequency of microearthquakes associated with

rock failure at P_e = 0 can be computed. Although the frequency

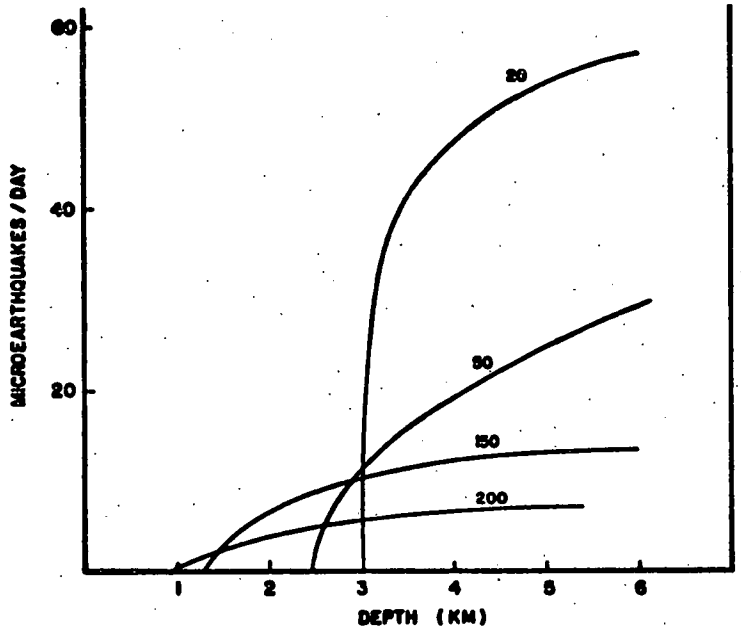

Figure 5

of events is greatest during the initial cooling period, the majority of these events occur <u>after</u> the causative pluton has cooled to below its solidus temperature. For this particular system, on the order of 20 - 60 events/day were predicted. The distribution of the events as a function of depth and time is illustrated in figure 6.

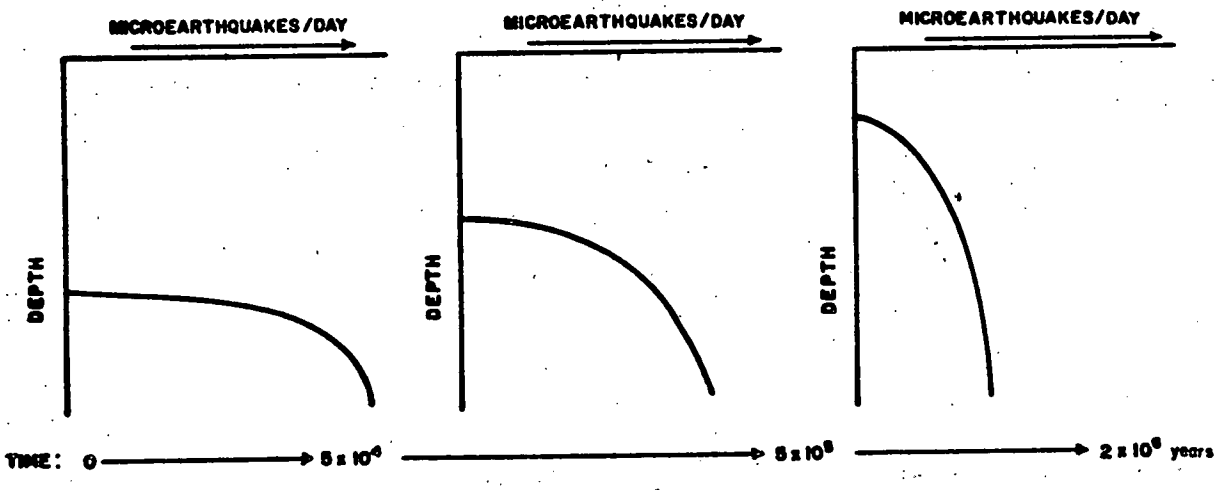

Figure 6

As a consequence of the thermal expansion of pore fluids in residual pores, the generation of zero effective pressure, and rock failure by fracture, the interconnected porosity of the rock mass will undoubtedly be increased. Depending on the geometry of these newly interconnected pores, bulk rock permeability and electrical porosity will be increased. The porosity variations with depth as a function of time, which results from this process, are depicted in figure 7.

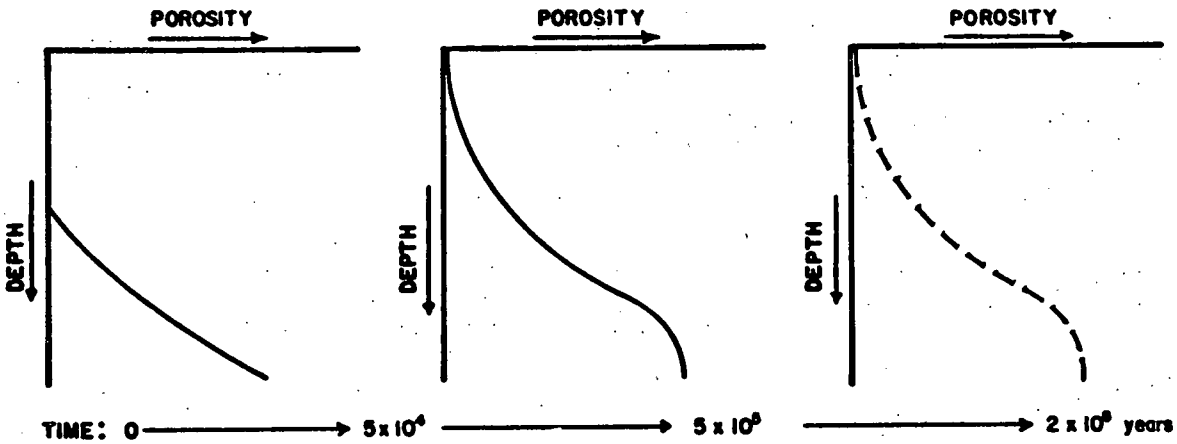

Figure 7

Increase in interconnected porosity and associated decrease in fluid resistivity with increasing temperature, figure 8, results in the formation of regions in which the intrinsic electrical resistivity is anomalously low. Intrinsic electrical resistivity, ρ_{rock}, can be related to porosity and fluid resistivity, ρ_f, by Archie's function: $\rho_{rock} = \hat{k}\rho_f\phi^{-n}$, where n is $\sim$ 2 for fractured media, and ϕ is effective electrical porosity. The low-magnitude anomaly is primarily

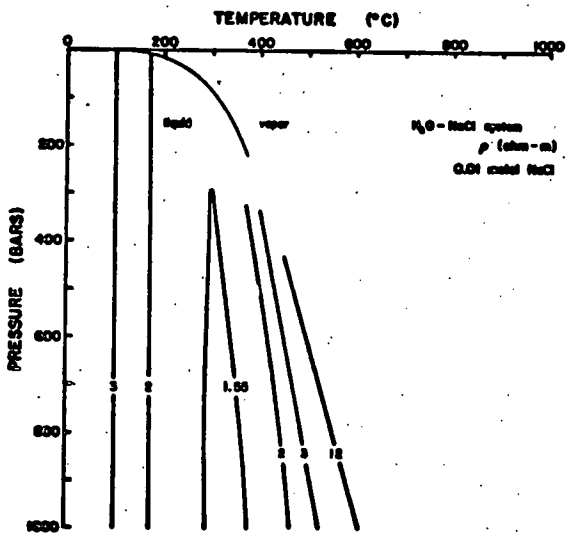

Figure 8

the result of porosity changes since intrinsic resistivity is probably related to $^{1}/\phi^{2}$, figure 9, as suggested by Archie's function, and is probably not detectable by present electrical resistivity measurement methods.

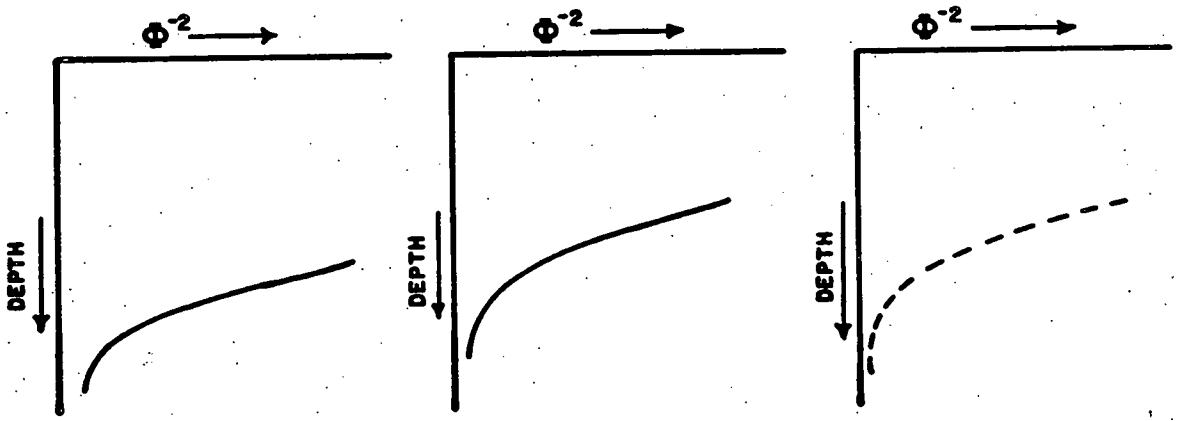

Figure 9

The ϕ^{-2} versus depth plots with respect to time depict the variation in bulk rock resistivity as a result of porosity changes. Porosity values are not well defined once the system has developed to maximum thermal effects near the surface, because mineral fluid reactions will tend to fill pores, and decreasing pore fluid pressure will allow the pores to collapse.

Note that we are assuming only fluid resistivity and porosity effects on intrinsic resistivity and that the time and space variation in mass abundance of conductive minerals deposited by the circulating fluids are not considered. The effect of fluid composition on the bulk rock resistivity is much larger than temperature or pressure variations, but is less than the effect of porosity variations.

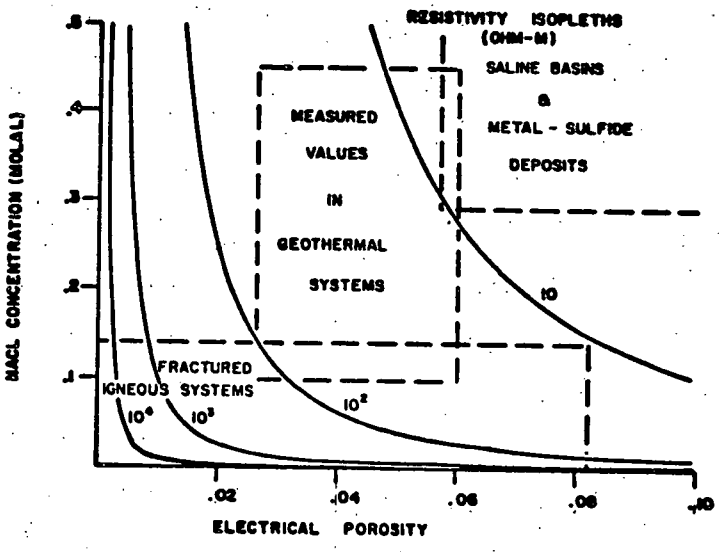

Figure 10

Salinity-porosity effects which result in low intrinsic resistivities are not unique for hydrothermal systems however. As can be seen in figure 10, metal-sulfide deposits and high porosity sedimentary basins containing saline fluids are also characterized by low intrinsic resistivity values.

Circulation of fluids around plutons results in a redistribution of thermal energy which closely mimics the rock temperature for systems containing relatively pure H_2O at temperatures < 350°C. In systems containing relatively high permeability host rocks, $k > 10^{-14}$ cm^2, the transport of thermal energy upward toward the top boundary (surface) is more rapid and results in higher energy concentrations than those systems whose host rock permeabilities are < 10^{-14} cm^2, cf. below.

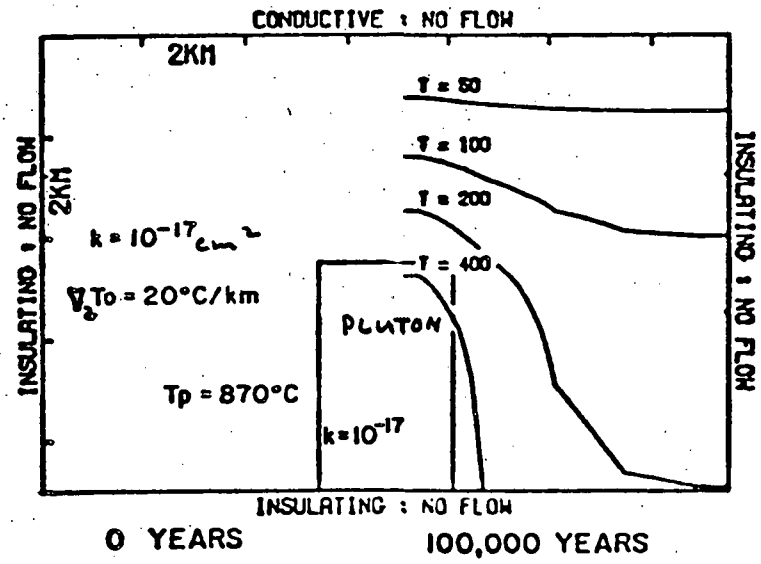

Figure 11

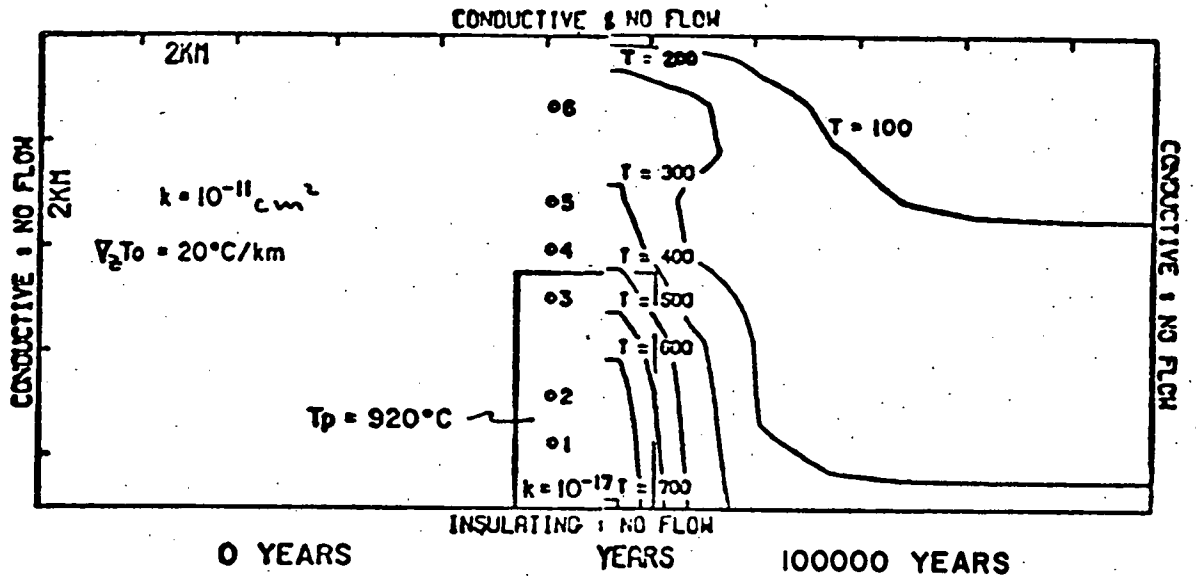

Figure 12

Thermal energy begins to increase at 1 km depth at an elapsed time of $\sim 1.5 \times 10^5$ years in the low permeability case and at an elapsed time of $\sim 5 \times 10^4$ years in the high permeability case. However, in the system which cools primarily by conduction, the 200°C isotherm never gets closer to the surface than 1.75 km, whereas in the system in which fluid convection of thermal energy predominates, the 200°C isotherm is within 0.5 km of the surface for several tens of thousands of years.

Thermal anomalies in relatively permeable host rocks might develop broad regions of abnormally low conductive heat flux around the margins of the system, coincident with the zones of downward fluid circulation. As can be seen in the figure, circulating fluid convects near-surface low energy fluids downward and depresses the isotherms below the regional values. These regions of abnormally low heat flux could be useful in outlining the regions of upward fluid circulation,

obviously the regions of greatest thermal energy potential, e.g., high energy concentration, large mass, and shallow depths.

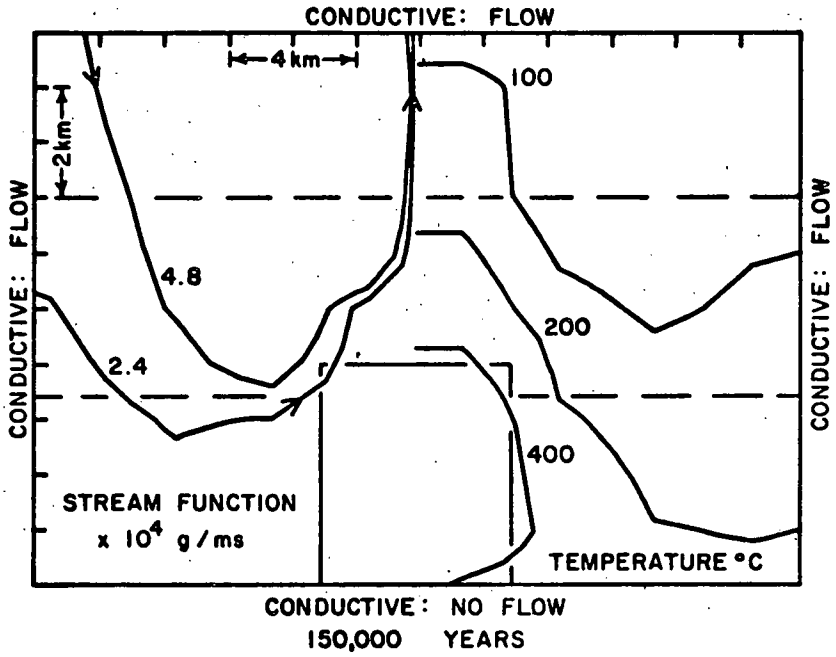

Figure 13

The above relationships, as well as consideration of the seismic velocity variations which result from coupled temperature and porosity changes, are now being refined and related to actual systems. Chemical effects are only being considered in a cursory manner because the numerical tools required to adequately simulate these processes are not yet available. These effects are clearly the most significant contribution to the intrinsic electrical resistivity of rocks in geothermal systems. However, proper analysis of the chemistry will not be possible for about another year. An example of the state-of-the-art in using fluid chemistry to predict the chemical composition of subsurface environments is reproduced in Appendix II.

Geologic Reality

An important conclusion of this study is to reemphasize the non-uniqueness of predictions regarding the presence of geothermal resources. In order to effectively detect subsurface resources, existing exploration methods must be significantly improved. Furthermore, because of the intrinsic properties of rocks in the region around cooling plutons, deep drill holes may not adequately define these resources. These conclusions are based on a few very simple geological facts; the consequence of these facts is realized in the numerical models discussed above.

The most important parameter in defining the nature of heat transport in the subsurface, as indicated by the numerical studies, is bulk rock permeability. Geologic observations confirm the significance of this parameter, since host rocks and igneous rocks are, in general, relatively permeable in the upper crust. This observation is qualitatively supported by the fact that eroded equivalents to the system modeled above show evidence that large amounts of fluid have circulated through systematically developed fractures in these rocks. This evidence is in the form of hydrothermal alteration minerals, gains and losses of components from the rocks, shifts in hydrogen and oxygen isotope values, and composition of fluid inclusions. Many pluton and adjacent host rocks appear to have had permeabilities $> 10^{-14}$ cm^2 during some stage of their formation. The systematic distribution of continuous fractures

in some pluton environments suggests much larger permeabilities, Villas and Norton, 1977. Numerous igneous plutons appear to have had relatively low permeabilities, but the surrounding host rocks usually show evidence that fluid circulation was significant.

Magma intrusion into the upper crust, thermal energy transport away from the crystallizing body, concomitant volume increases in the magma+solid pluton, and temperature increases in the host rocks all result in significant changes in the stress conditions which often result in thorough fracturing of the rocks. Although the physics of this entire process is not well understood, it is clear that shallow igneous systems will contain permeable rocks.

The regions of volcanic activity contain plutons emplaced over a time span of a few million years, and each pluton may have a thermal life on the order of a few hundred thousand years. As we noted in the numerical studies, this transient feature of the thermal sources must be considered in evaluating resources.

The pragmatic question is: How can we increase the confidence level of predictions based on surface or shallow drill hole information? The following is a synthesis of data utilizations and limitations concerned with this question.

1. Temperature

Thermal gradient data are useful if the drill hole conditions where they are collected are thoroughly

documented. In particular, those data collected above the groundwater table can be very misleading. Projection of thermal gradient data requires independent information on subsurface conditions, e.g., permeability and thermal conductivity.

The nonlinearity of thermal gradients is a function of bulk rock permeability; coupled with paleo-temperatures, this information could potentially be used to define the bulk permeability of the system.

2. Conductive Heat Flux

Conductive heat flux relates directly to the thermal gradient comments. Those fluxes estimated from temperatures measured above the groundwater table should correlate with numerical models which have conductive and impermeable top boundary conditions, whereas those measured in the vicinity of springs should correlate with conductive and permeable boundary conditions.

Regions of downward fluid circulation around the pluton should be detectable as regions of abnormally low conductive heat flux. These regions define the outer limits of the high thermal energy portion of the system.

The magnitude and width of the conductive thermal anomaly can be used to define the depth and width of the thermal source only in a steady state system in which there is no convective heat transport. However, other information in detailed thermal surveys, e.g., low

amplitude noise, may be useful in defining these parameters in a convection dominated system.

3. Convective Heat Flux

This variable is a direct measure of system permeability and is probably not measurable because of the low mass fluxes, but it does deserve consideration.

4. Electrical Resistivity

Electrical resistivities on the order of 500 Ω-m or less cannot be attributed to simple temperature increases at depth. These values clearly require abnormally large electrical porosities, fluid salinities, and/or conductive minerals. The coupled temperature and porosity increases in the subsurface can account for a 2x decrease in intrinsic resistivities, and salinity can account for a 10^2 decrease at an electrical porosity of 0.1.

Fluid circulation in pluton environments always results in the formation of hydrothermal minerals, some of which are conductive. Furthermore, the metal-sulfides tend to deposit in regions above the top of the pluton.

5. Microearthquakes and Tilts

Magma emplacement and magma crystallization generate seismic noise for the first few 10^4 years, or, in general, < 10% of the pluton's total duration. Thereafter, temperature increases in the surrounding host rocks appear to be the principal process by which seismic noise is generated. Detailed mapping of the seismic noise would

provide depth information on the location of the zero effective pressure front and could possible provide an indirect measure of the elapsed time of the system.

Tilts associated with thermal expansion of the rocks could be as large as a fraction of a cm/yrs.

6. Chemistry

Bulk chemical and stable light isotope concentrations, as well as temperature and electrical resistivity of springs and borehole fluids, provide a data base which permits estimation of subsurface rock compositions and temperature, cf. Norton and Panichi, 1977, and mass abundance of mineral phases in surface and subsurface rocks, Villas and Norton, 1977.

A First Approximation of Real Systems

The exploration for geothermal resources has resulted in successes, surprises, and many unanswered questions. This section attempts to apply some of the insight into geothermal systems, obtained through the numerical studies, to natural systems. We have reviewed data from several systems; the results are presented below.

Those geothermal systems which represent the "A" (conduction dominated) type have been identified only as subsystems within the "B" or "C" type. We do not know of a thermal resource related to an igneous pluton in which heat transport throughout the system is by pure conduction. The "C" type are exemplified by systems from which energy is currently being

produced. "B" type systems include those that may contain reservoirs of the "C" type, but the latter have not been detected.

The most interesting consideration is the time stage to which various systems can be assigned. Stage I is mostly speculation since the only evidence would be found through remote measurements of magmatic activity at several kilometer depths. Seismic zones might provide examples of this stage, such as the Intermountain Seismic Belt defined by Smith et al., 1974, along which "swarms" of seismic activity have been noted and an incipient spreading of the continental crust has been suggested. A few occurrences of very young basalt cinder cones and flows, and some thermal activity, are present along this zone. A second example is found along the extension of the volcanic time trend on the San Francisco Peak region.

Stage II systems include Yellowstone, Geysers, Wairakei, Larderello, and possibly Coso and Long Valley.

Stage III systems are typified in the extreme by mineral deposits, such as porphyry copper. These systems have moderate thermal anomalies resulting from oxidation of sulfide and radiogenic sources (U, Th, K), electrical resistivity lows caused by metal sulfides, and thoroughly altered rocks. The Marysville project is clearly another example of Stage III systems.

Another style of "thermal" system which is very common in the Basin and Range Province is depicted by the intermontane

basins, an example being Safford Valley, Arizona, Norton and Gerlach, 1975. Very porous sediments fill a basin which is ∿ 1.5 km deep, saline pore fluids and evaporite bearing formations are present, and the fluid circulation path of groundwater is from the surrounding mountains which rise to 2 km above the valley, as well as from the Gila River which flows through the valley. There are thermal springs which flow from the basin margin faults and scattered occurrences of "young" looking basalts which intrude the sediments. The valley is characterized by low electrical resistivity and anomalous heat flow. However, the entire "thermal" system could be the result of forced fluid convection through the anhydrite bearing rocks, hydration of anhydrite to gypsum, and associated heat of reaction, or a significant volume of basalt may underlie the valley.

A PRELIMINARY ANALYSIS OF THE COSO GEOTHERMAL SYSTEM

by D. Norton and J. Knight

Introduction

The objective of this communication is to present a preliminary and partially completed analysis of the Coso system. The studies to develop exploration criteria useful in the detection of hot dry rock systems are in a preliminary stage at the University of Arizona; however, we have utilized the numerical modeling capability of the laboratory to analyze the Coso system.

The decision to drill deep holes in a geothermal system implicitly hypothesizes that a thermal energy resource exists at depth. Significant concentrations of thermal energy at shallow depths in the earth's crust are transient features in geologic time. The processes which tend to disperse the energy anomaly give rise to features that are diagnostic of the extent and character of the energy resource. We have synthesized the geological, geophysical, and geochemical data from Combs, Duffield, Austin, Jenkins, and Schultz. A hypothetical geologic cross-section has been prepared on the basis of this data. The section includes a thermal energy source of igneous origin. Initial and boundary conditions were assigned, thereby defining an initial value problem. The initial value problem was then solved using computer programs described in Appendix I. The results from the computed model were then compared with measured data.

The analysis suggests the Coso system is a permissive energy prospect which may contain in the subsurface: 1) regions of sufficient permeability and energy content to permit direct production of high temperature fluid,

and 2) regions of low permeability but high heat content rock which will require in-situ fracturing prior to production.

Also of note are certain characteristics of the model system which may also appear in the Coso System: 1) The surface heat flux due to convective fluid flow is significantly larger than the conductive heat flux. 2) The subsurface energy distribution is significantly different from a system in which the igneous body cools by simple conductive heat transfer, even though the permeabilities are below those necessary for direct production of high temperature fluid.

Other possible models need to be examined. A very plausible model of this system would be a distribution of much smaller, very impermeable, shallow plutons that were emplaced during the initial volcanic event and are nearly cooled to ambient conditions.

Analysis of the Energy Content and Distributions in Model Systems

Initial Conditions

The heat flow, p-wave velocities, seismic noise hypocenters, resistivity, closely spaced high angle normal faults, ring faults, thermal springs, and outcropping igneous rocks (< 10,000 to 20,000 years old) define a geological cross-section, figure 1. Our interpretation of the above data suggests a shallow, < 1 km, zone of relatively low resistivity material in the vicinity of Sugarloaf Mountain that may be caused by high porosity rocks saturated with saline fluids or 2-3 wt% sulfide minerals in the rock; we assume this to be a zone of relatively high permeability since the anomaly coincides with the zone containing abundant fractures. A somewhat broader zone of microearthquake hypocenters (< 3 km) is correlated with the near surface zone of abundant fractures and low resistivity and could represent the base of the high permeability zone (10^{-9} - 10^{-10} cm^2). A second zone of microearthquake activity is recognized, 4-6 km deep and 8 km wide, which may be due to thermal expansion of pore fluids and subsequent hydrofracturing of the rocks. The third zone of microearthquake activity, > 6 km, may be due to tectonic movement and thermal fracturing associated with an igneous intrusive body. The p-wave discontinuity at 5 km depth is taken to be an indication of change in the regional abundance of continuous fractures and could represent a decrease in rock permeability. These assumptions, then, define a possible permeability and heat source configuration at depth. Age-dating suggests the Coso system is around 15,000-20,000 years old, and our transient models were tested against the heat flux observed at Coso today with time $\simeq$ 20,000 years in the models.

The size and energy content of the igneous heat sources were more or less arbitrarily defined. The total energy content of the pluton at the time of its emplacement as a magma represents the energy available above the normal background. The total energy for three model plutons per unit length of the pluton ranges from 7×10^{15} kcal to 1×10^{16} kcal. This is on the order of the U.S. annual electrical energy consumption.

ENERGY SOURCE CHARACTERISTICS

	Width	Height	Depth to top	T	ΔT^*	H_{TOTAL}	H_{ANOM}
COSO1	4 km	3 km	6 km	960°C	750°C	8×10^{15}kcal	6×10^{15}kcal
COSO2	4	4	5	960	750	1×10^{16}	9×10^{15}
PLO6	2.6	4	5	920	750	7×10^{15}	6×10^{15}

C_p (rock) = 0.26 cal/gr°C, ρ (rock) = 2.75 gr/cm^3, and heat content is per km length of pluton. H_{ANOM} is the heat content above the normal background, $\Delta T^* \cdot C_p$.

COSO1 - The initial and boundary conditions for this model, figure 1a, were derived from the geologic section, figure 1. The heat flux and cooling characteristics of the system were found to be significantly different from present day features of the Coso system. The depth of burial, 6 km, of the heat source and its confinement within relatively low permeability host rocks slowed the energy transfer rate. After a time interval of 22,000 years, the surface conductive heat flux was still 1.6 HFU, and at 50,000 years the thermal perturbation is barely discernible at 2 km depth, figure 2. We felt the age of the igneous events at Coso required a model system age that was younger than 20,000 years; therefore, a shallower, 5 km deep, heat source was modeled.

Figure 1

Initial conditions for model COSO1 (left side) and geophysical and geological observations used to estimate the initial conditions (right side). The section is centered near Sugarloaf Mountain and is bounded by caldera-like ring faults (Duffield, 1975). The central portion of the section contains abundant faulting and high electrical conductivity, implying greater permeability (k). The major p-wave velocity discontinuity at 5 km depth coincides with a permeability discontinuity. Microseismic hypocenters are grouped into three divisions (Combs, 1975): 1. Deep, > 6 km, hypocenters are centrally grouped and interpreted as representing a tectonic activity associated with a buried pluton (small circles), 2. Intermediate, > 3 km < 6 km, hypocenters circumscribe the deeper hypocenters and are interpreted as representing tectonic fracturing and hydrofracturing above the pluton (medium sized circles), 3. Shallow, < 3 km, hypocenters which circumscribe both classes of deeper hypocenters are interpreted as tectonic movement on near surface faults (large circles). The geothermal gradient ($30^{\circ}C\ km^{-1}$) and thermal conductivity (5×10^{-3} cal-$(cm^2\text{-sec-}^{\circ}C)^{-1}$) are consistent with the background heat flux of 1.5 HFU (Combs, 1975).

The temperature distribution in COSO1 after 50,000 years. The $T = 100^{\circ}C$ isotherm is barely affected by the thermal anomaly at depth.

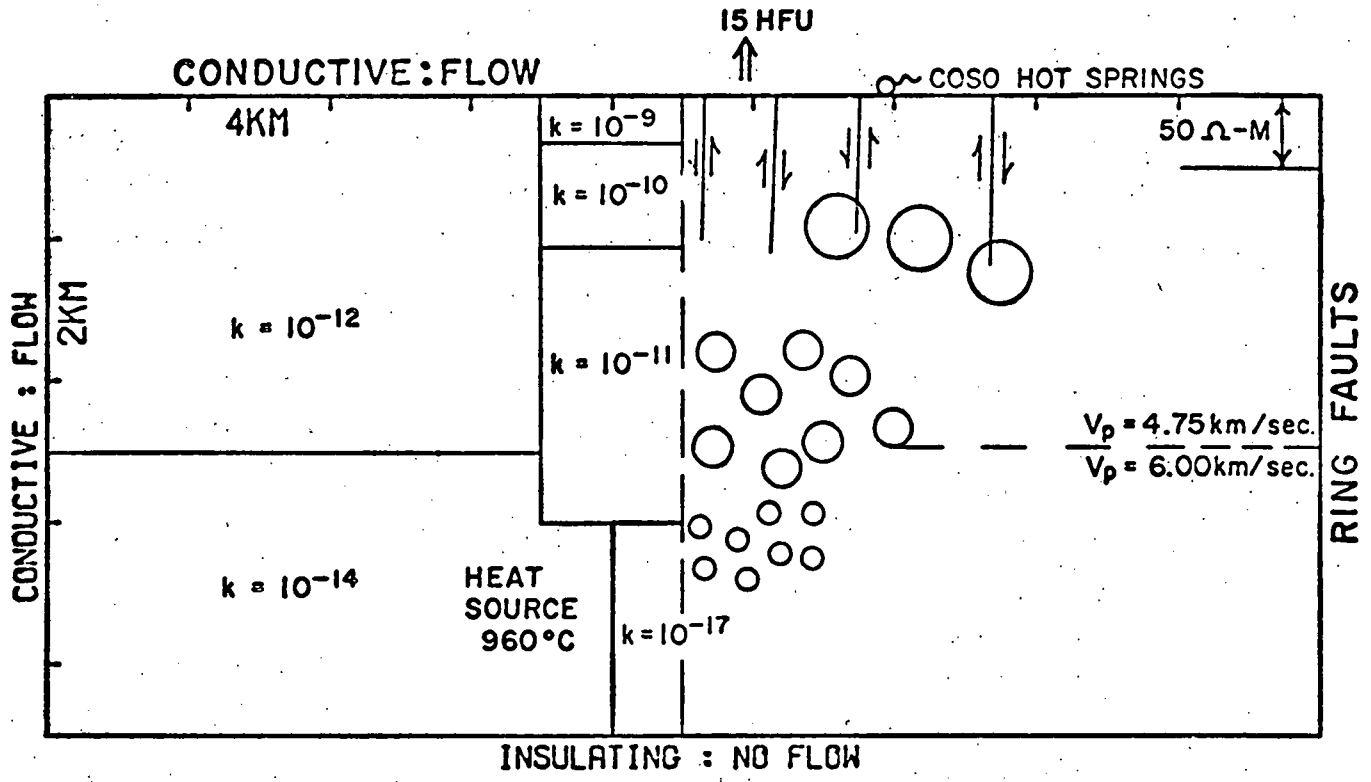

INITIAL & BOUNDARY CONDITIONS

GEOLOGICAL CONDITIONS

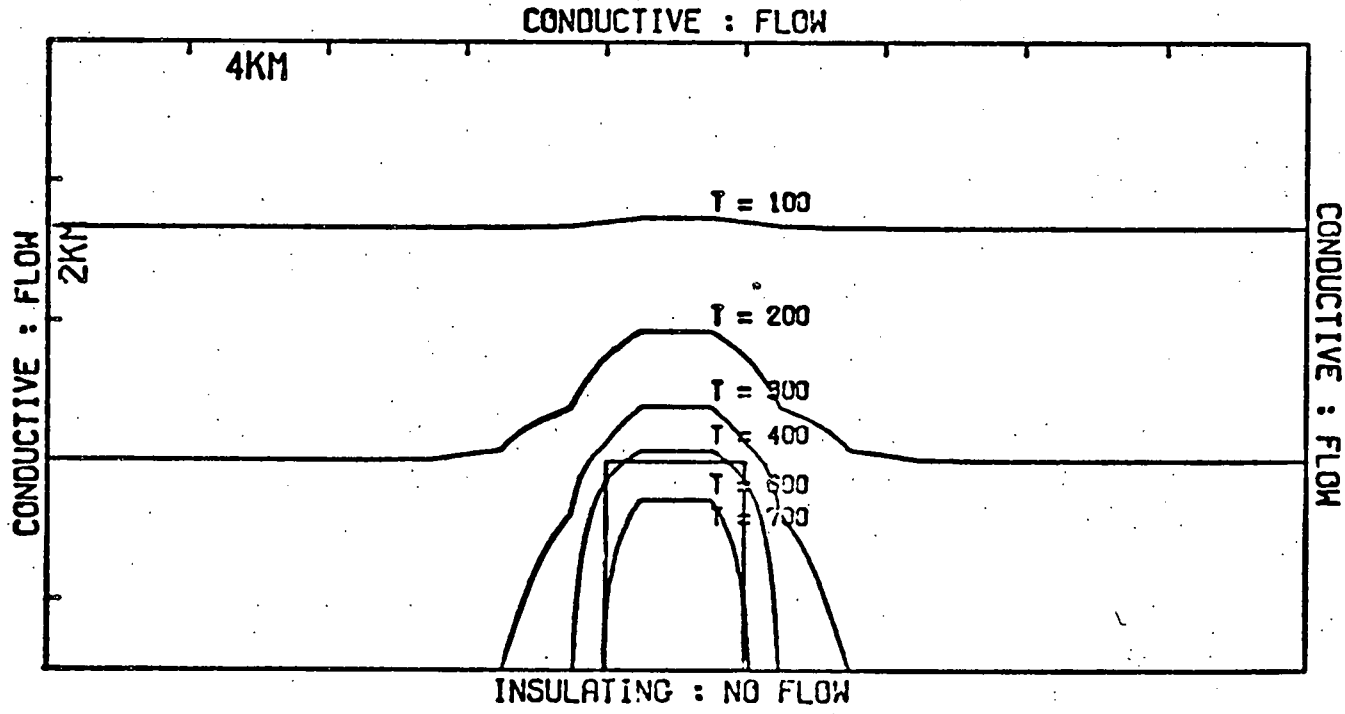

TEMPERATURE TIME = 50000 YEARS

COSO2 - Initial and boundary conditions for this model were modified from COSO1 to afford for more rapid heat transfer to shallow regions of the system, figure 2. The conditions are still compatible with the geologic cross-section in figure 1. The pluton top now coincides with the transition between the basement p-wave discontinuity and the intermediate hypocenters. The deep hypocenters now coincide with the heat source. This is consistent with a pluton which is either moving or cooling and fracturing. Therefore, a time dependent permeability was introduced into the heat source, cf. figures 2-3.

The conductive and convective heat fluxes produced by this system demonstrate some of the ambiguities in evaluating simple conductive heat flow anomalies and also indicate the magnitude of convective heat transfer in systems whose permeabilities are marginal for direct production of high temperature fluid. The convective heat flux near the surface, 100 m deep, is significantly greater than the corresponding conductive heat flux, e.g., at 20,000 and 25,000 years the vertical component of convective heat flux at 100 m depth is 4.5 times greater than the vertical component of conductive flux.

The discharge of convecting fluids at either the surface or groundwater table for this system appears to be small, although mass flux data on the thermal springs could not be found for comparison.

Surface Discharge of Convecting Fluid

time	mass flux (g/cm^2 sec) X 10^7	mass flow Kg/sec	total fluid Kg X 10^{-12}
5,000 yr	1.9	7.6	1.2
10,000 yr	2.0	8.0	2.5
15,000 yr	2.6	10.3	4.1
20,000 yr	3.7	14.7	6.4
25,000 yr	4.6	18.4	9.3
30,000 yr	5.3	21.0	12.6

The total thermal energy content of the subsurface rocks in the COSO2 model averages about 25 cal/gr between 0-1 km depth. In 4 km^3 of rock this amounts to 3 X 10^{14} kcal of energy, or about 3% of the energy in the initial anomaly associated with the pluton.

Figure 2

LEFT SIDE

Initial conditions for model COSO2. This model is similar to COSO1, but regional permeabilities and pluton height have been increased to produce larger heat fluxes near the surface.

RIGHT SIDE

Temperature contours 5,000 years after initial conditions.

LEFT SIDE

Permeability (k) in model COSO2 at 17,500 years after initial conditions. The permeability in the upper portion of the pluton has been increased to simulate fracturing of the pluton as the pluton cools below its solidus temperature.

RIGHT SIDE

Temperature contours 19,000 years after initial conditions and 1,500 years after fracturing of pluton. Note the perturbation in the 150, 100, and 50°C isotherms is increasing.

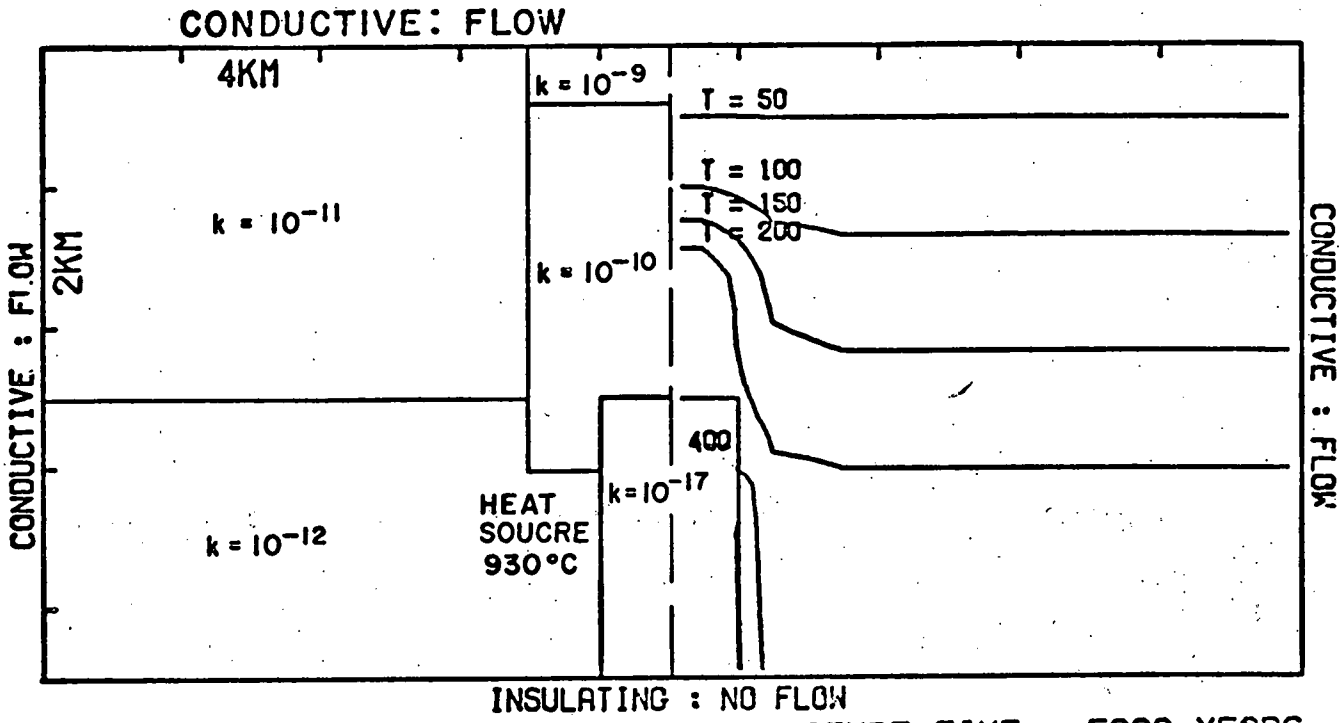

INITIAL & BOUNDARY CONDITIONS

TEMPERATURE TIME = 5000 YEARS

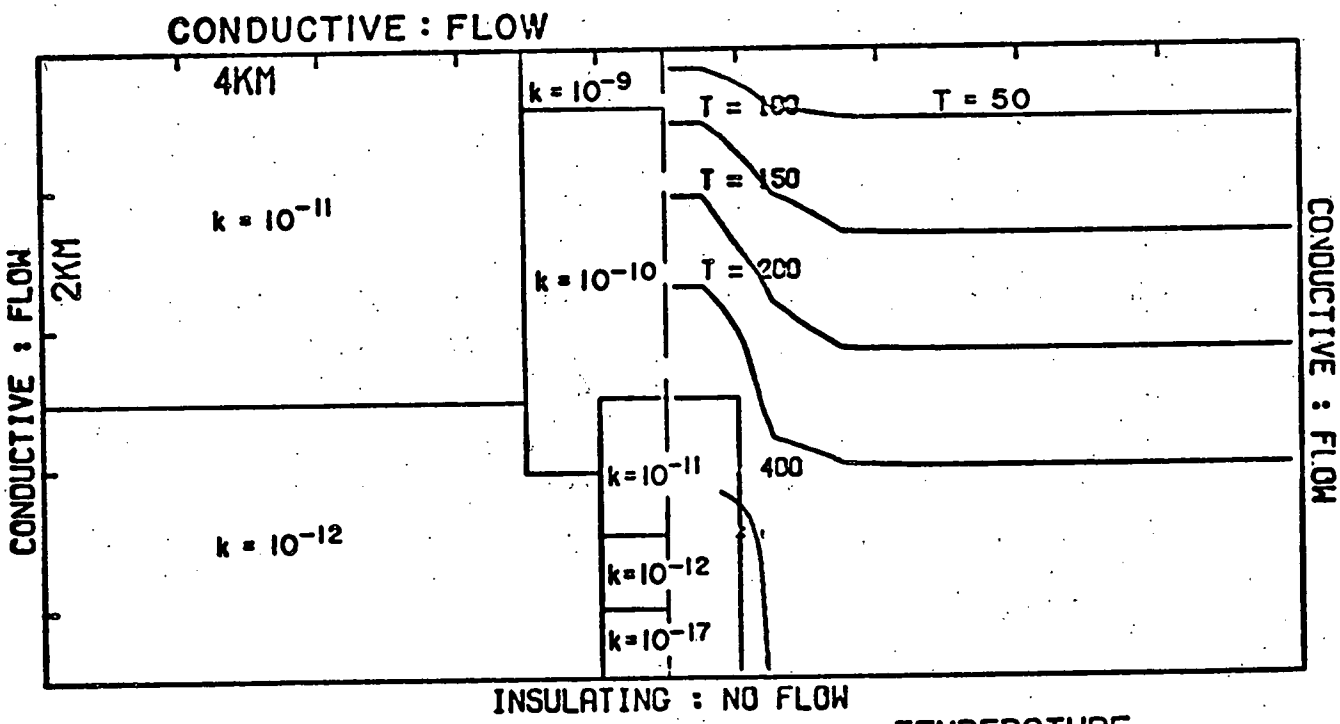

INITIAL & BOUNDARY CONDITIONS

TIME = 17,500 YRS.

TEMPERATURE

TIME = 19000 YEARS

Figure 3

COSO2 at 19,900 years.

LEFT

Contours of streamfunction in the domain. The gradient of the streamfunction is dimensionless mass flux.

RIGHT

Contours of temperature in the domain.

COSO2 at 29,900 years.

LEFT

Contours of streamfunction in the domain. The gradient of the streamfunction is dimensionless mass flux.

RIGHT

Contours of temperature in the domain.

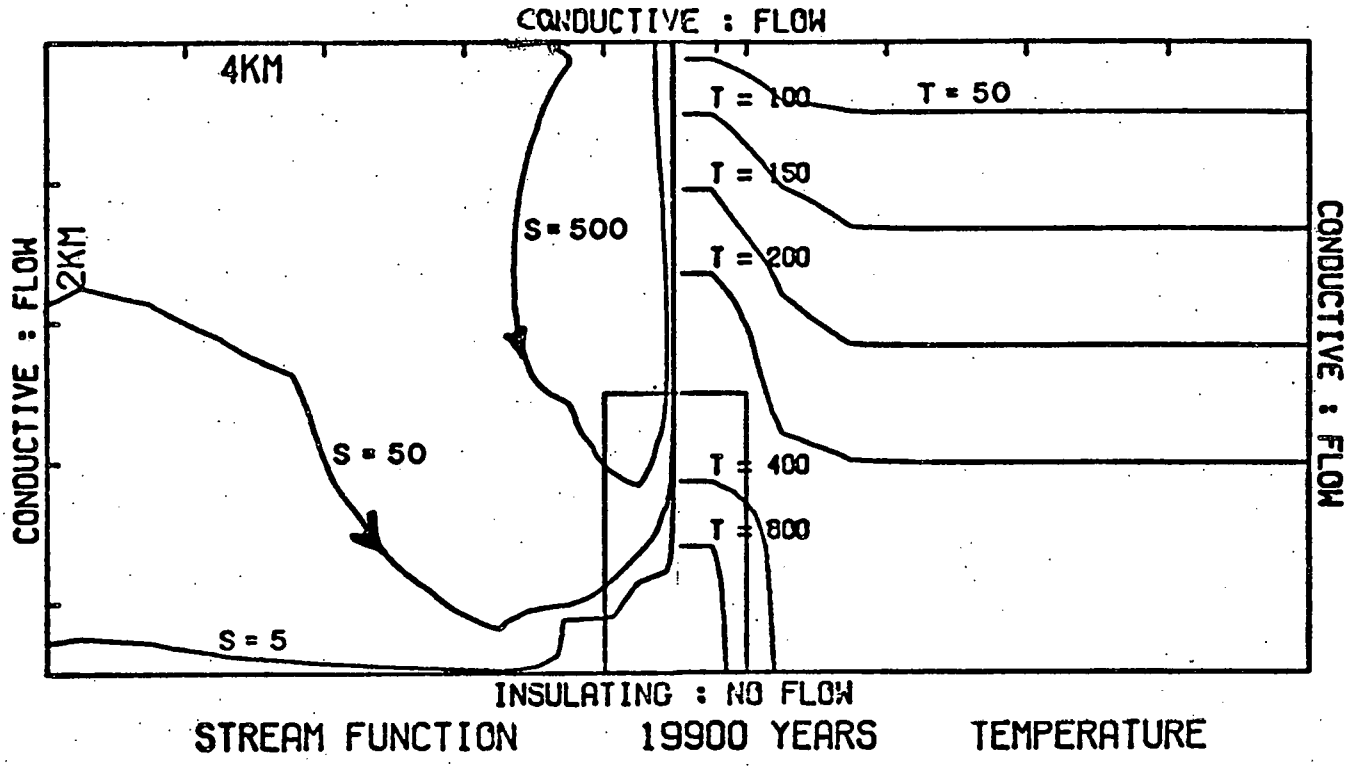

STREAM FUNCTION 19900 YEARS TEMPERATURE

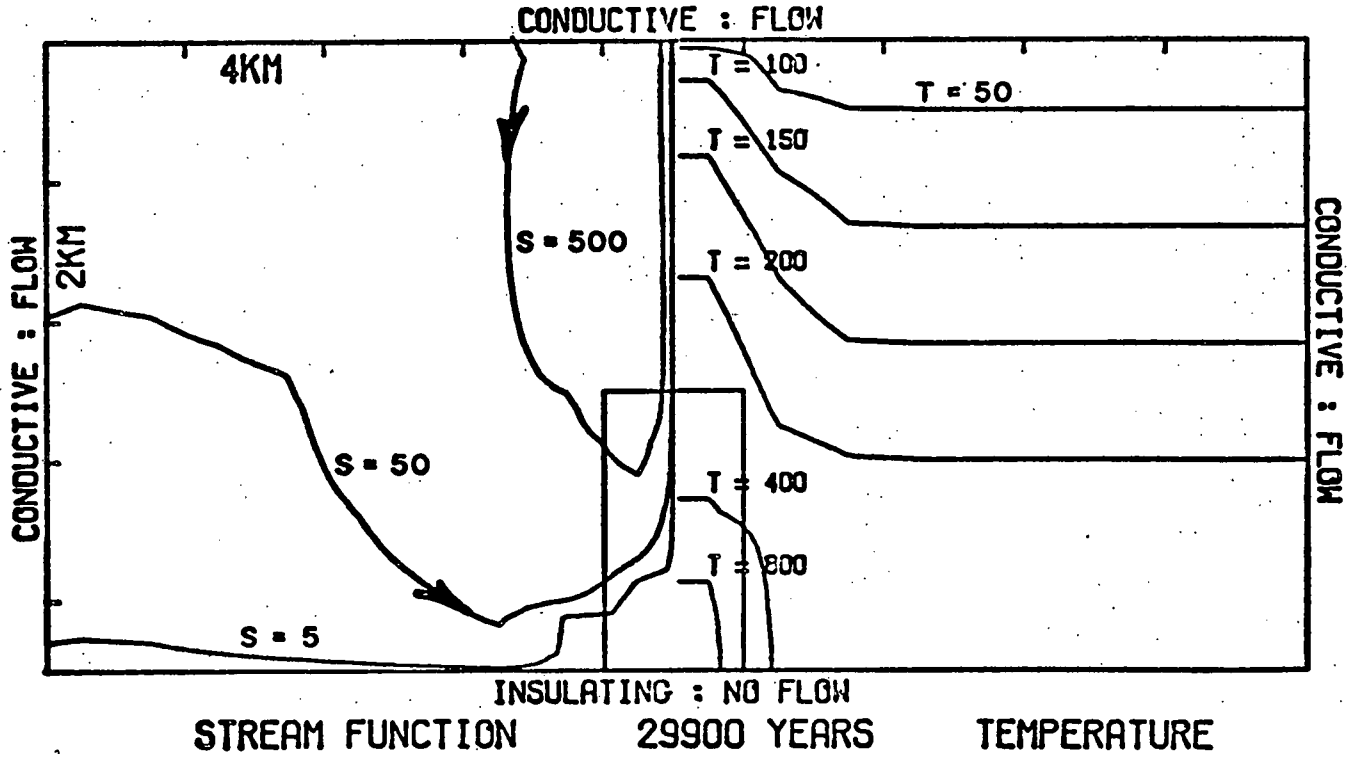

STREAM FUNCTION 29900 YEARS TEMPERATURE

Figure 4

COSO2 at 10,000 years.

Profiles of total heat flux versus distance from the domain edge. The pluton is 18.0 km from the domain edge and lies below the symmetrical anomaly. A thermal conductivity of 5 X 10^{-3} cal-(cm-sec-^{o}C)$^{-1}$ was used in the calculation. Depth below the surface for the profiles is: 1. 250 m, 2. 500 m, 3. 1,000 m. Profile 4 is the heat flux by conduction only at 250 m below the surface. Note the negative anomaly associated with the downflow zone in the convection system.

COSO2 at 15,000 years.

Profiles of total heat flux versus distance from the domain edge. The pluton is 18.0 km from the domain edge. A thermal conductivity of 5 X 10^{-3} cal-(cm-sec-^{o}C)$^{-1}$ was used in the calculation. Depth below the surface for the profiles is: 1. 250 m, 2. 500 m, 3. 1,000 m. Profile 4 is the heat flux by conduction only at 250 m below the surface.

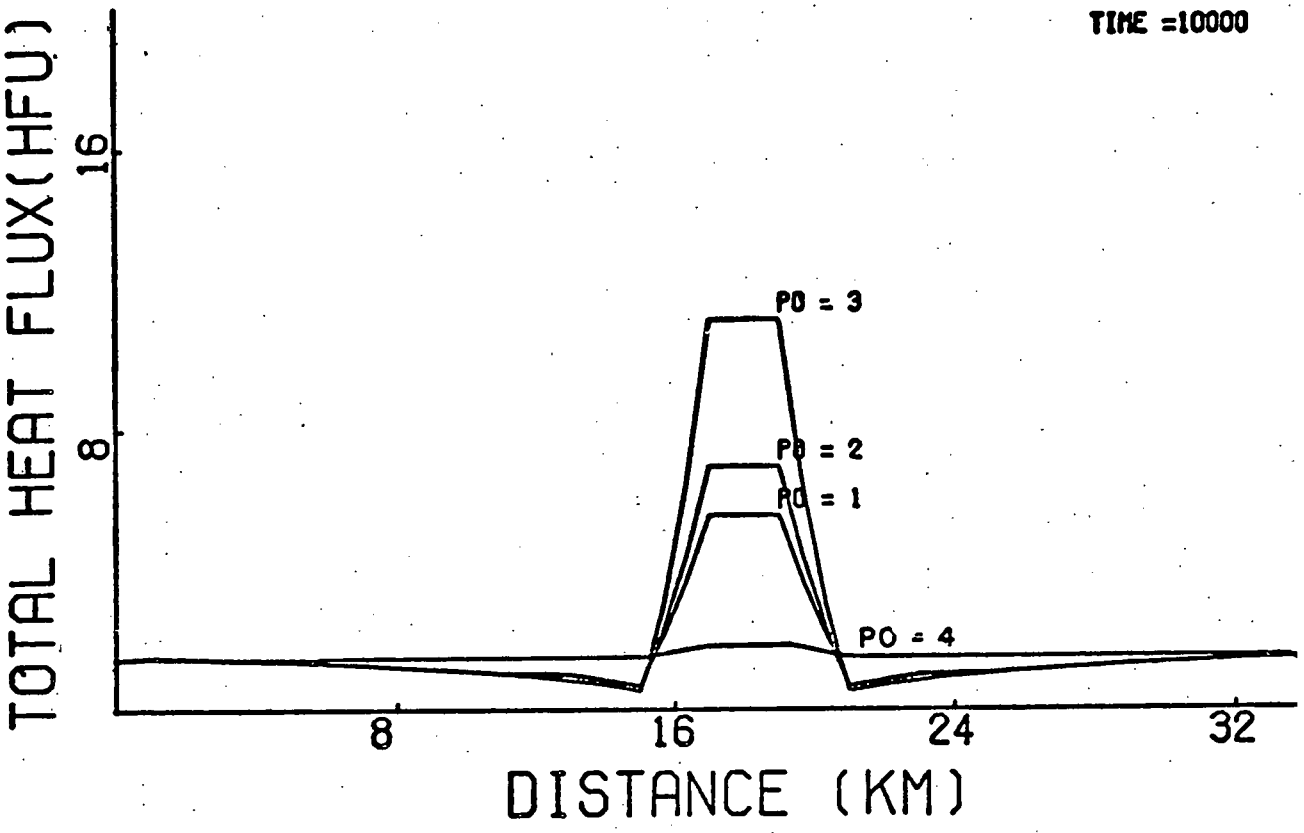
TIME =10000
TOTAL HEAT FLUX(HFU)
16
8
PO = 3
PO = 2
PO = 1
PO = 4
8
16
24
32
DISTANCE (KM)

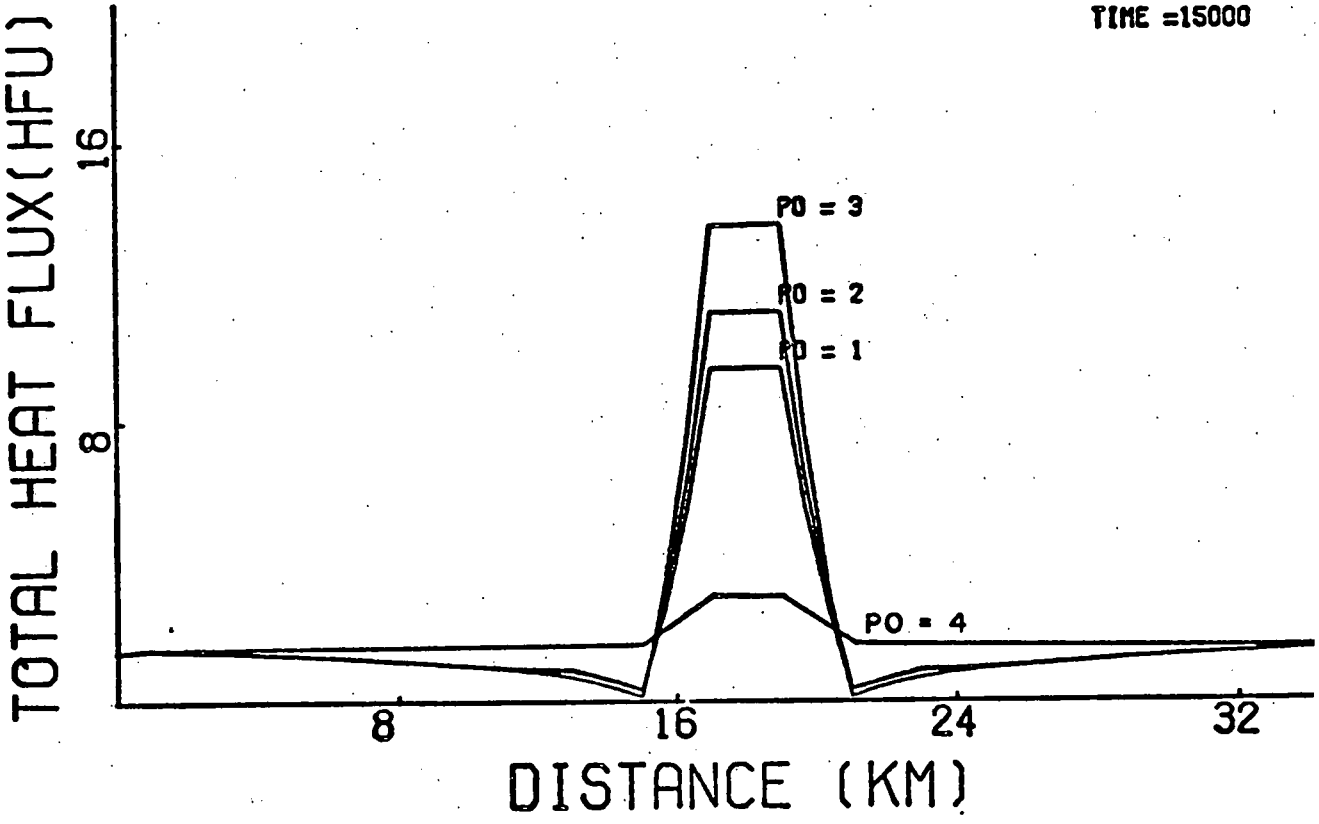
TIME =15000
TOTAL HEAT FLUX(HFU)
16
8
PO = 3
PO = 2
PO = 1
PO = 4
8
16
24
32
DISTANCE (KM)

Figure 5

COSO2 at 19,900 years.

Profiles of total heat flux versus distance from the domain edge. The pluton is 18.0 km from the domain edge. A thermal conductivity of 5×10^{-3} cal-(cm-sec-$^{\circ}$C)$^{-1}$ was used in the calculation. Depth below the surface for the profiles is: 1. 250 m, 2. 500 m, 3. 1,000 m. Profile 4 is the heat flux by conduction only at 250 m below the surface.

COSO2 at 29,900 years

Profiles of total heat flux versus distance from the domain edge. The pluton is 18.0 km from the domain edge. A thermal conductivity of 5×10^{-3} cal-(cm-sec-$^{\circ}$C)$^{-1}$ was used in the calculation. Depth below the surface for the profiles is: 1. 250 m, 2. 500 m, 3. 1,000 m. Profile 4 is the heat flux by conduction only at 250 m below the surface.

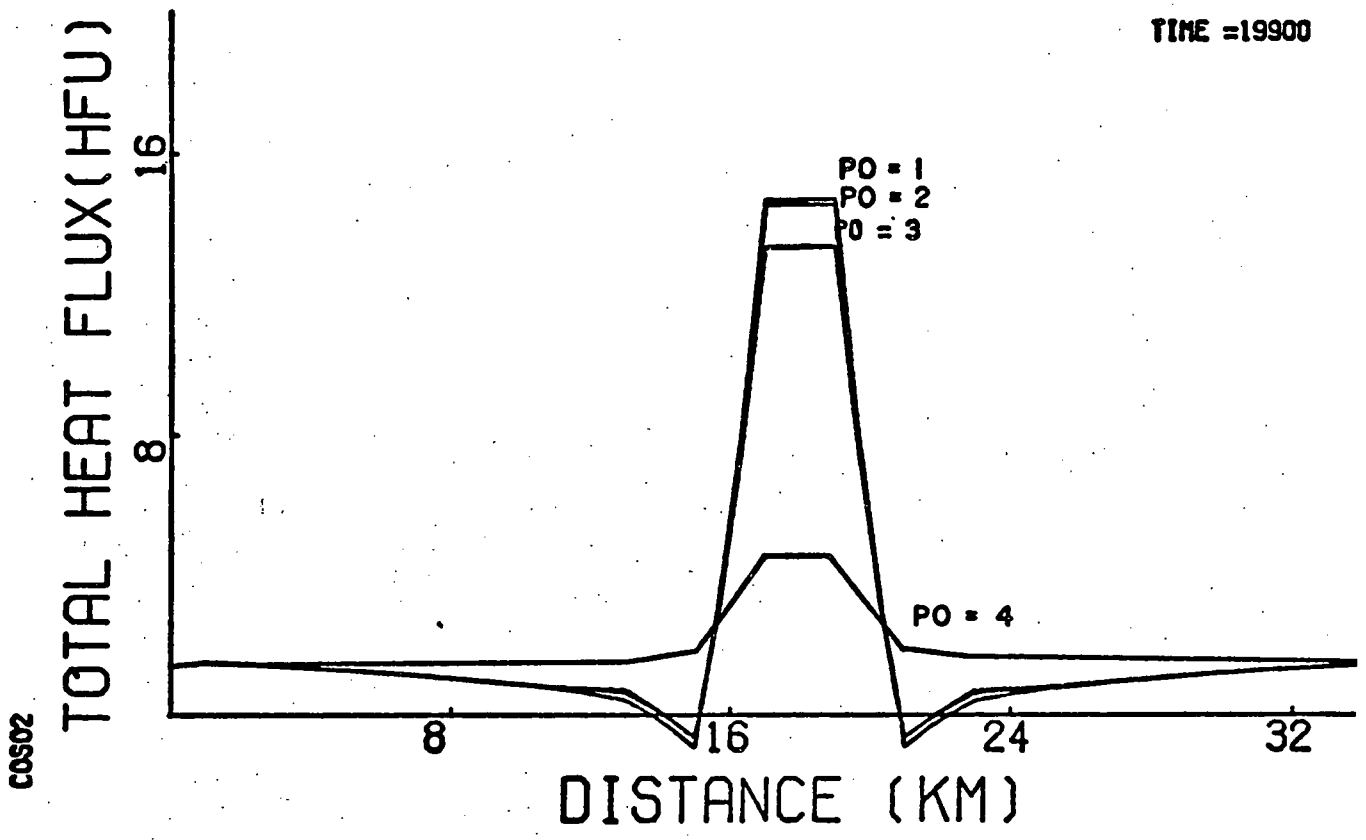
TIME =19900
TOTAL HEAT FLUX(HFU)
16
8
PO = 1
PO = 2
PO = 3
PO = 4
8
16
24
32
DISTANCE (KM)
COSO2

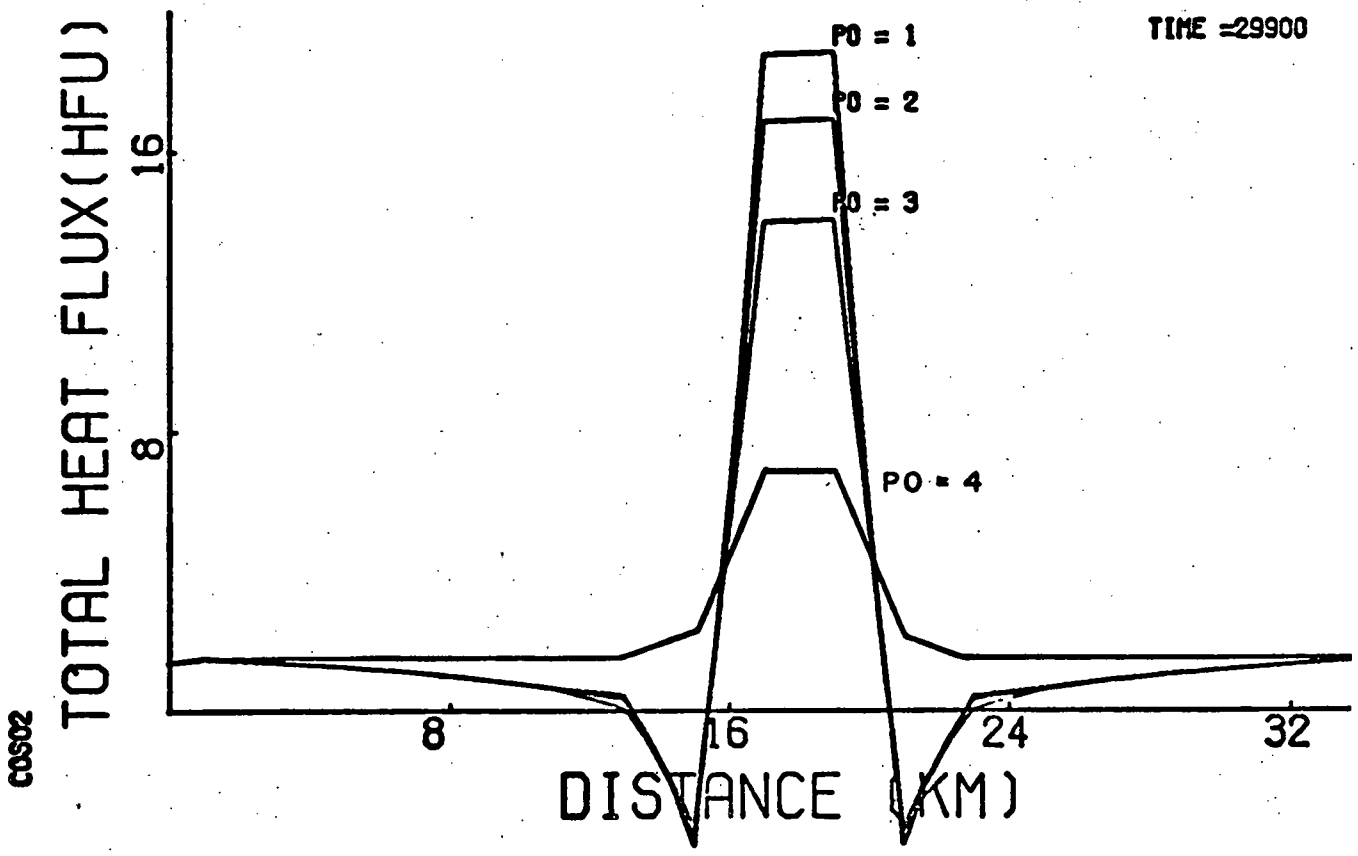
TIME =29900
TOTAL HEAT FLUX(HFU)
16
8
PO = 1
PO = 2
PO = 3
PO = 4
8
16
24
32
DISTANCE (KM)
COSO2

Figure 6

COSO2

Depth vs temperature profiles from surface to 4 km. Profiles are at 1 km from edge of pluton (leftmost profile) and down the symmetry plane of the system (rightmost profile). The upward migration of a large thermal gradient is particularly well illustrated by the symmetry plane profile. At 29,900 years the thermal gradient and, hence, the heat flux are still increasing.

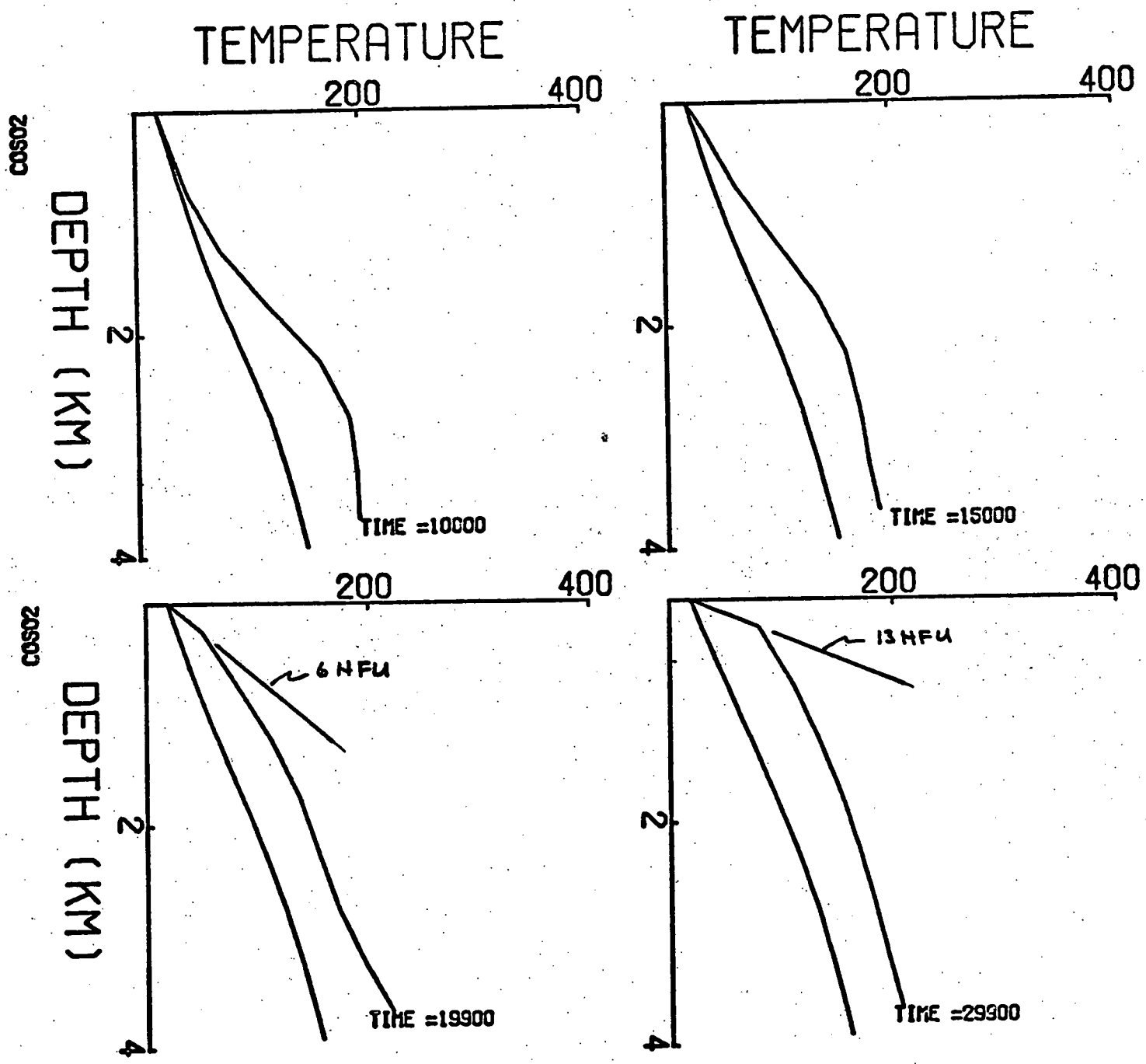
TEMPERATURE
200
400
COSO2
DEPTH (KM)
2
4
TIME =10000
TEMPERATURE
200
400
2
4
TIME =15000
200
400
COSO2
DEPTH (KM)
2
4
6 HFU
TIME =19900
200
400
13 HFU
2
4
TIME =29900

Figure 7

COSO2 at 10,000 and 15,000 years.

Energy content (cal/gr) along horizontal planes at: 1 = 250 m, 2 = 500 m, and 3 = 1,000 m depth below the surface. Computed on basis of C_p (rock) = .26 cal/gr^{o}C and a negligible fluid fraction.

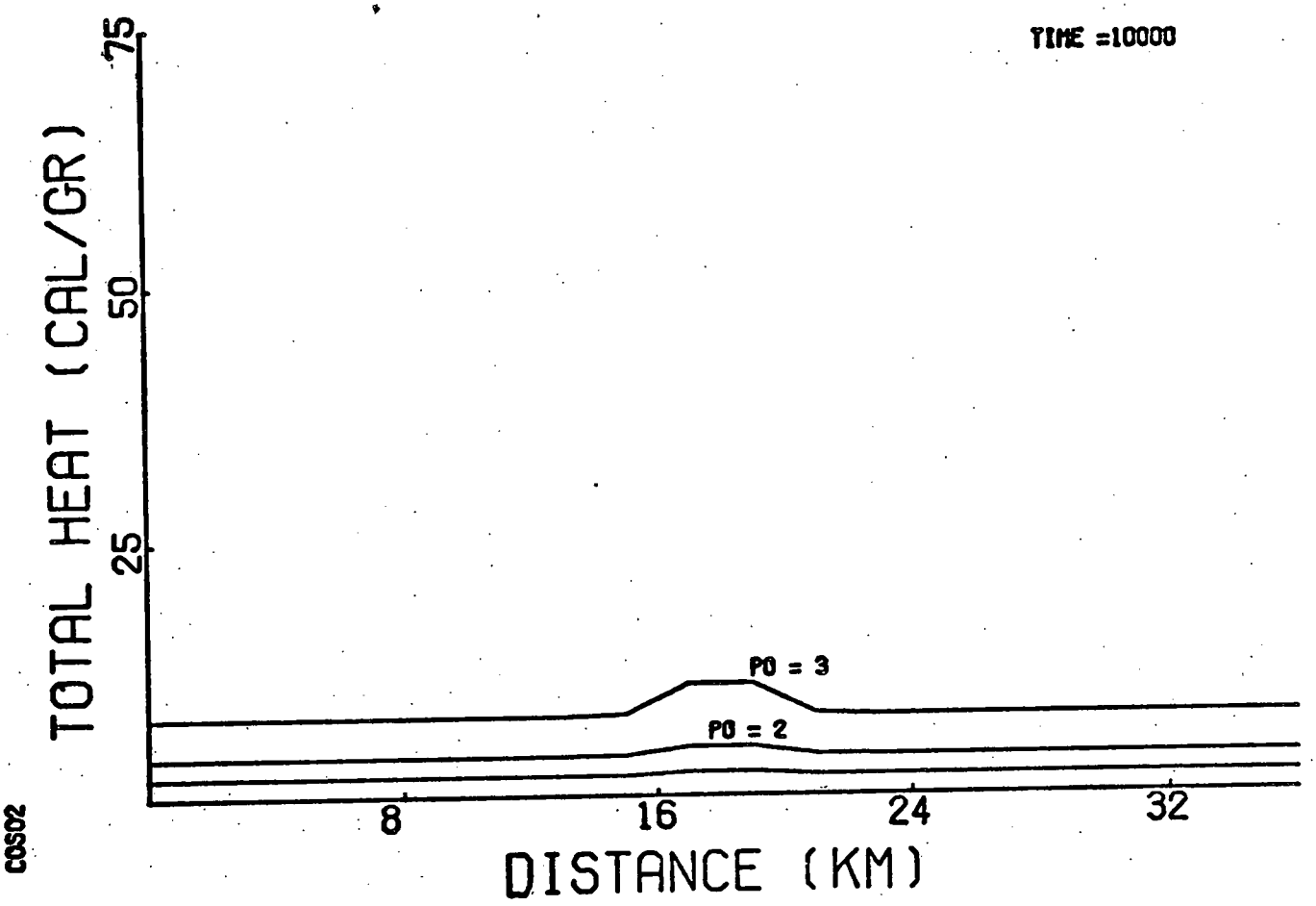
TIME =10000
TOTAL HEAT (CAL/GR)
75
50
25
PO = 3
PO = 2
8
16
24
32
DISTANCE (KM)
COSO2

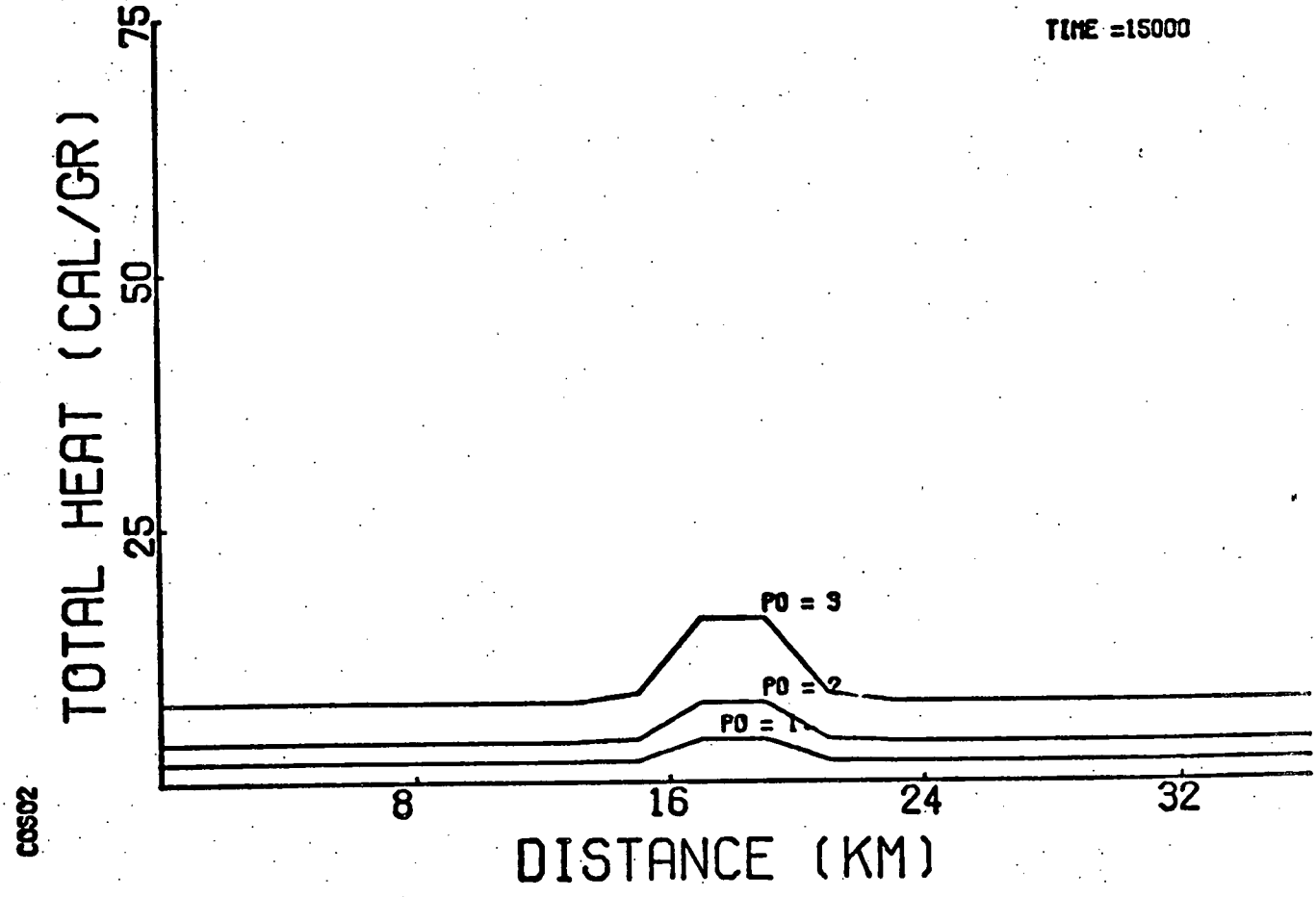
TIME =15000
TOTAL HEAT (CAL/GR)
75
50
25
PO = 3
PO = 2
PO = 1
8
16
24
32
DISTANCE (KM)
COSO2

Figure 8

COSO2 at 25,100 and 29,900 years.

Energy content (cal/gr) along horizontal planes at: 1 = 250 m, 2 = 500 m, and 3 = 1,000 m depth below the surface. Computed on basis of C_p (rock) = .26 cal/gr^{o}C and a negligible fluid fraction.

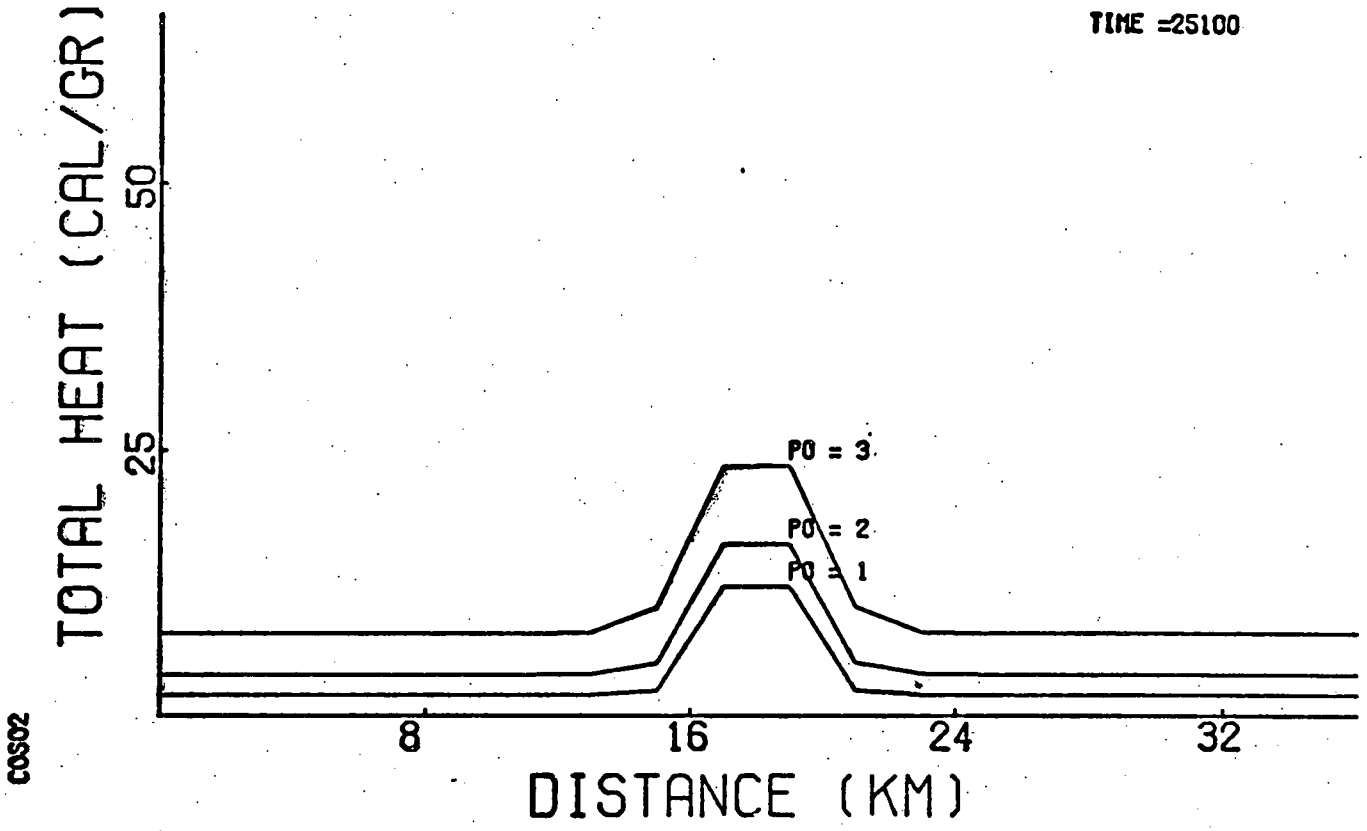
TIME =25100
TOTAL HEAT (CAL/GR)
50
25
PO = 3
PO = 2
PO = 1
8
16
24
32
DISTANCE (KM)
COS02

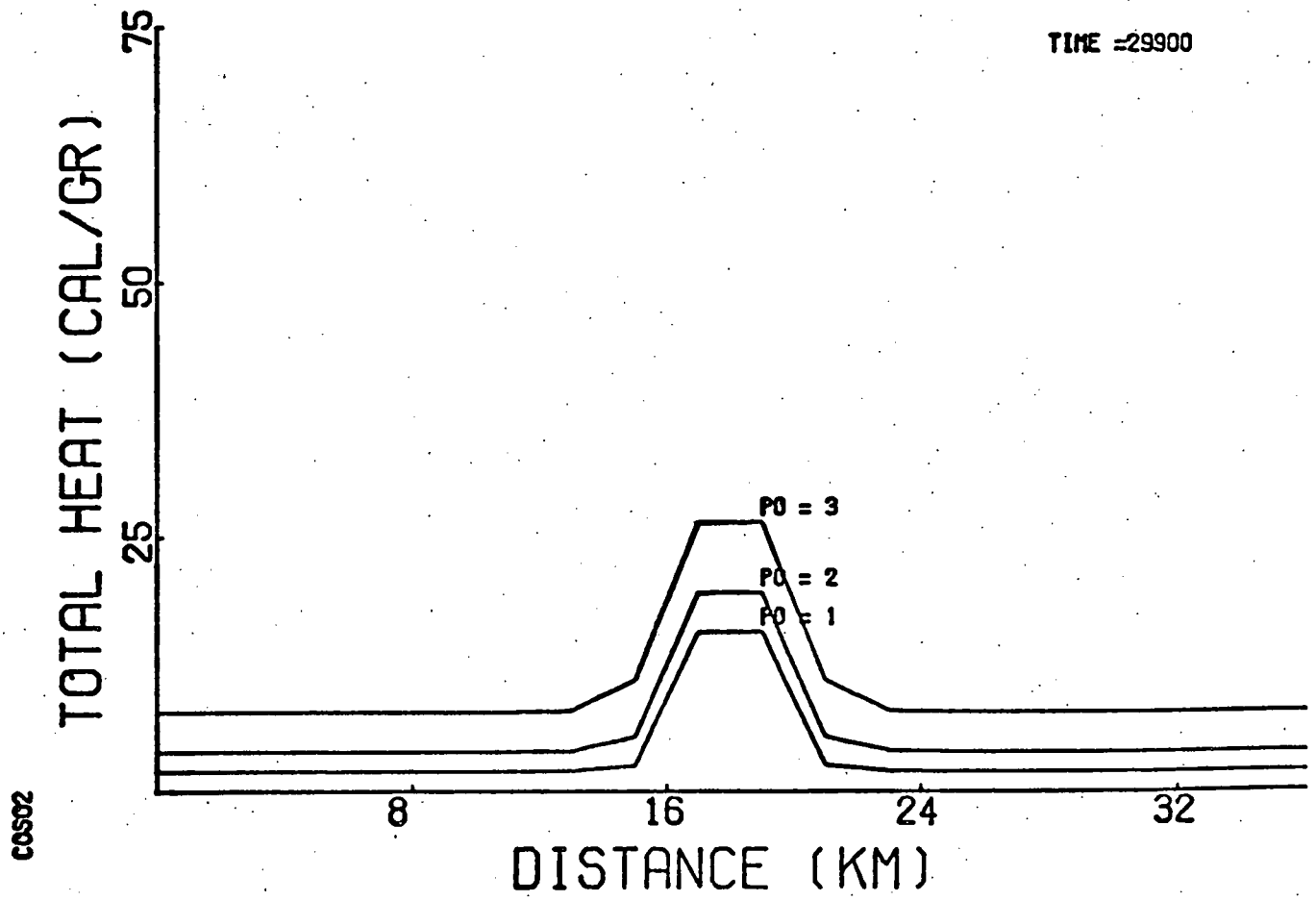
TIME =29900
TOTAL HEAT (CAL/GR)
75
50
25
PO = 3
PO = 2
PO = 1
8
16
24
32
DISTANCE (KM)
COS02

LONG VALLEY, CALIFORNIA

The Long Valley thermal system has been studied extensively by the U.S.G.S. We have completed a review of the considerable literature and have found the geological information on this system to be about the best available on any hydrothermal system, especially the data on the tectonic-volcanic history of the caldera, Bailey, R. A., 1976. Bailey's hypothetical cross sections provide excellent data with which to define an initial and boundary value numerical problem. We have abstracted data from Bailey's figure 8 to demonstrate how an analysis similar to the Coso study might be completed on the Long Valley system. The objective of the analysis would be to test various hypotheses expressed in the Long Valley Symposium papers regarding the nature of the present day subsurface conditions.

Bailey hypothesizes conditions at ∿ 0.7 m.y. ago in the following manner:

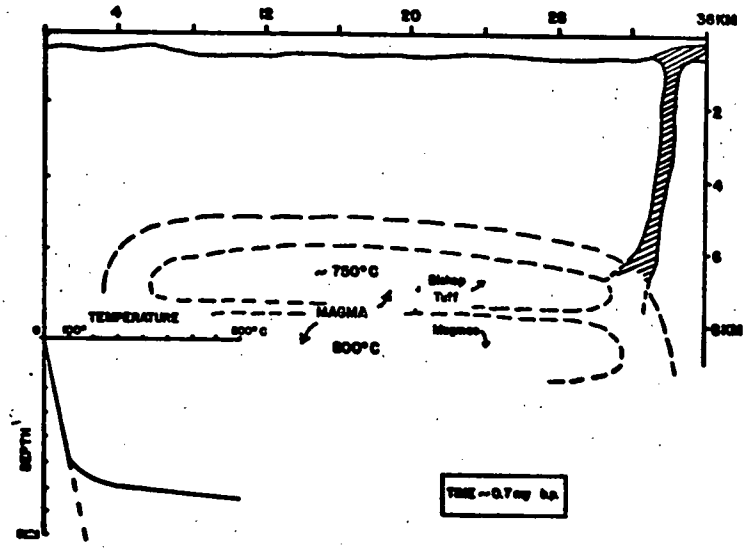

Figure 1

This would correspond to a Stage I type system having a normal temperature distribution above ∿ 5 km depth, as indicated in the T versus depth plot. Some 0.2 m.y. later, after some rhyolites were intruded, the reaction looked like:

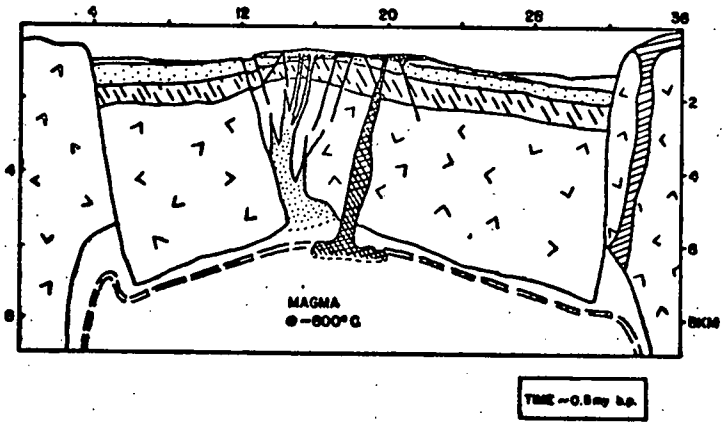

Figure 2

Note that a hypothetical magma is still present at depth. This hypothesis places constraints on the rate of heat lost from the chamber and on the size of the body. This system, then, evolves for approximately 0.2 m.y. longer to:

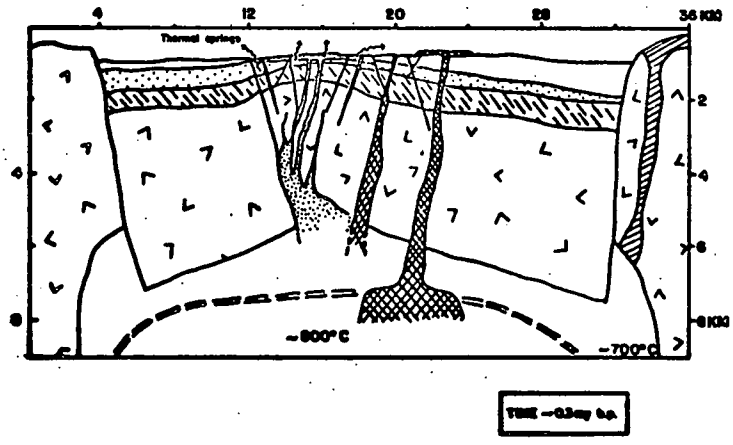

Figure 3

And finally to the present subsurface configurations:

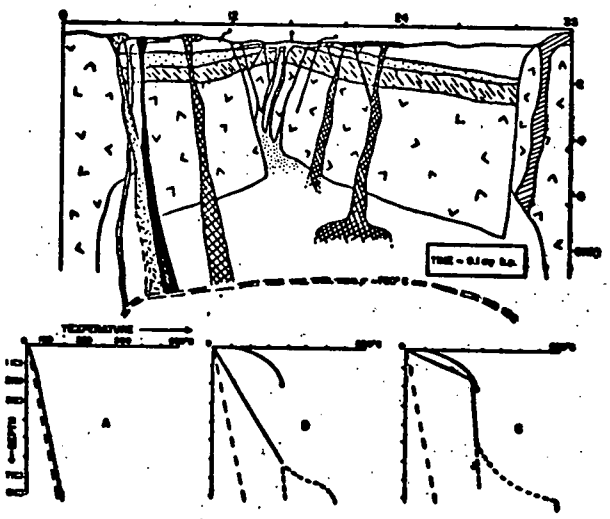

Figure 4

Relatively shallow drill hole data are available on this system, but the thermal profiles were inferred from the near-surface data and our experience with the model systems.

The profiles are partially based on temperature data from Lachenbruch, A. H. and others, 1976, solid lines, and on our extrapolations of data outside the caldera, A, normal gradient, inside the caldera in relatively unfractured rocks, B, and in fractured rocks, C. The "C" profile was linearly extrapolated to the liquid-vapor surface in the H_2O-system, then downward along an isochor in the H_2O-system, and finally to higher temperatures in the vicinity of the thermal source.

Data are not available which would be useful in estimating permeability of the rock units in the region, present transport of thermal energy in the subsurface (i.e., there

appears to be some uncertainty in the seismic noise data), or fluid circulation paths.

THIS PAGE
WAS INTENTIONALLY
LEFT BLANK

APPENDIX I-1

Operations procedures for interactive graphics programs developed during this study.

Program ETCHG (Developed under ERDA Contract)

Program ETCHG is a user-oriented interactive graphics program which permits the user to analyze the output from the heat and mass transfer simulations and prepare final copies of figures for publication. The program is written in FORTRAN IV and utilizes the PLOT10 FORTRAN IV Tektronix programs for routine operations. ETCHG accepts input files of variables computed at a sequence of elapsed times for the thermal anomaly. These variables include temperature, pressure, streamfunction, horizontal and vertical mass fluxes, permeability, and thermal conductivity. The following is an abstracted user's manual which documents the capabilities of the program.

```
C*** ETCHG.DOC
C*****************************************************************
C       PROGRAM ETCH    J. KNIGHT AND D. NORTON - 1976
C       INTERACTIVE GRAPHICS      B. MOSKOWITZ
C       UNIVERSITY OF ARIZONA
C
C       COMPATIBLE WITH VERSION 3 AND EARLIER VERSIONS OF
C       PROGRAM FLOW.
C
C       THIS PROGRAM USES ADVANCE GRAPHICS AS DESCRIBED IN THE
C       TEKTRONIX ADVANCE GRAPHICS AND TCS MANUALS.
C
C       VERSION 1.0      JULY 1976
C       VERSION 2.0      MULTIPLE EULERS,ENLARGMENTS,ERROR CHECKS
C                        REMOTE EXPONENTS ON DOMAIN PLOTS,RESCALE
C                        OPTION FOR DEPENDENT PLOTS      AUGUST 1976
C
C
C
C*****************************************************************
C       ETCH PRODUCES PLOTS OF DATA FROM FLOW DATA FILES.
C       IT WILL CONTOUR ANY OF 6 DATA BLOCKS IN THE FLOW FILE,
C       WILL COMPUTE PATHLINES AND STREAKLINES ORIGINATING AT
C       ANY POINT IN THE DOMAIN, WILL PLOT THE VARIATION
C       OF 21 VARIABLES AGAINST TIME OR AGAINST DISTANCE ALONG
C       VERTICAL OR HORIZONTAL SECTIONS CUT THROUGH THE DOMAIN.
C       RUN SWITCHES ARE INPUT AT THE TERMINAL
C
C       RAW DATA IS OBTAINED FROM A DISK OR TAPE FILE GENERATED BY
C       FLOW.  CONSULT THAT PROGRAM FOR THE STRUCTURE OF THE FILE.
C*****************************************************************
C*****************************************************************
C       FILES FOR RUNNING ARE
C              TAPE53  FLOW OUTPUT FILE
C
C
C       TO EXECUTE THE ADVANCE GRAPHICS PACKAGE:
C
C          SET THE TERMINAL TO GRAPHICS MODE
C
C          .R SETTTY
C          TYPE TERMINAL? 4010
C
C          TO EXECUTE THE PROGRAM TYPE
C
C          .EX@ETCHG[6130,636]
C
C       INPUT FOR ETCH IS CARRIED OUT BY TYPING OPTIONS
C       AT THE TERMINAL IN RESPONSE TO QUESTIONS.
C       FOR MULTIPLE ANSWERS SEPARATE BY COMMAS.
C       AFTER EACH ANSWER END WITH A CARRIAGE RETURN.
C
C
C       AFTER EACH DIAGRAM THE TERMINAL WILL WAIT FOR
```

```
C       TWO CARRIAGE RETURNS OR THE LETTER R(SEE BELOW).
C       AT THIS TIME A HARDCOPY CAN BE MADE.
C
C*****************************************************************


C       AT THE START OF EXECUTION THE SCREEN WILL BE ERASED
C       AND ONE OF THE FOLLOWING RESPONSES IS REQUIRIED:
C
C          CR      INRODUCTION TO ETCHG WILL BE DISPLAYED
C                  RETURN WITH TWO CARRIAGE RETURNS
C
C          S       SKIP INTRODUCTION AND CONTINUE TO OPTION INPUT
C
C
C
C
C..... INPUT THERMAL CONDUCTIVITY
C
C          THERMAL CONDUCTIVITY AT EACH GRID POINT IN DOMAIN.
C          (USED ONLY FOR PRE VERSION 3 FLOW DATA FILES)
C          ASSUMED CONSTANT AT EVERY GRID POINT.
C
C..... TOTAL POROSITY
C
C          PORTION OF ROCK WHICH IS FLUID.
C
C..... INPUT TIC INTERVAL(KM) FOR X AND Y DIRECTIONS FOR DOMAIN
C
C          SCALE FACTORS FOR X AND Y DIRECTIONS.
C          IF DOMAIN WIDTH IS 20 KM WITH A TIC INTERVAL OF 2.
C          WILL PRODUCE TICS AT 2 KM INTERVALS ACROSS DOMAIN.
C
C..... STARTING TIME IN YEARS
C
C          TIME TO START READING TIME BLOCKS FOR ACTUAL PLOTTING
C          (USUALLY 0.0 FOR IPLOT1-5).  FOR IPLOT=6, TMIN= FINAL TIME
C
C..... DO YOU WANT EULER, PATHLINE, STREAKLINE OR SOURCELINE
C       PLOTS?
C
C          SWITCHES TO DETERMINE TIME DEPENDENT OPTIONS.
C          0-NO
C          1-YES
C          MAY ONLY DO EULER + PATHLINES OR STREAKLINES OR
C          SOURCELINES.
C
C..... HOW MANY EULER PLOTS?
C
C          INPUT 1,2 OR 3 DEPENDIING ON THE NUMBER OF  DIFFERENT
C          VARIABLES YOU WISH TO PLOT
C
C
C..... INPUT OPTIONS FOR EULER PLOTS
C
C          INPUT OPTION NUMBERS(1-21) SEPARATED BY COMMAS
```

```
C
C
C..... TIC MARK INTERVAL
C
C          USED FOR PATHLINES, STREAKLINES, OR SOURCELINES
C          TICS WILL BE DRAWN IN INCREMENTS ON THIS TIME. IF
C          Ø.Ø NO TICS WILL BE DRAWN.
C
C..... FREQUENCY OF PARTICLES TRACED FROM SOURCE OR STREAK
C      LINES.
C
C          NEW POINTS ARE ADDED TO THE CALCULATION WITH
C          THE VALUE OF THIS OPTION. RUN TIME IS DIVIDED BY THIS
C          VALUE, BUT ACCURACY DECREASES.
C
C      INPUT OPTIONS(IPLOT,IXDEP,IYDEP):
C
C          IPLOT   SWITCH FOR PLOT TYPE
C                1       CONTOUR PLOT
C                2       PATHLINE PLOT
C                        THE PATHS TAKEN BY FLUID PACKETS STARTING
C                        AT ANY POINT IN THE DOMAIN ARE COMPUTED
C                3       STREAKLINE PLOT
C                        A LINE GOING THROUGH THE FINAL POSITIONS OF ALL
C                        FLUID PACKETS PASSING THROUGH A POINT IN THE
C                        DOMAIN IS COMPUTED
C                4       EULER PLOT
C                        VARIATION IN PARAMETER VALUE AT
C                        A FIXED LOCATION WITH TIME
C                5       PROFILE PLOTS
C                        VARIATION IN A FLUID OR ROCK PROPERTY WITH
C                        DEPTH OR DISTANCE FROM THE DOMAIN EDGE IS
C                        COMPUTED
C                6       SOURCELINES
C                        A LINE GOING THROUGH THE INITIAL POSITIONS OF
C                        ALL FLUID PACKETS PASSING THROUGH A POINT
C                        IN THE DOMAIN IS COMPUTED.
C                        THIS OPTION REQUIRES THE TIME BLOCKS
C                        IN THE FLOW DATA FILE BE ARRANGED IN ORDER
C                        OF DECREASING TIME.  FOR THIS OPTION TMIN
C                        IS GREATER THAN TMAX.(USE PROGRAM SHUF)
C
C          IXDEP IYDEP
C               THESE TWO SWITCHES ARE USED TO SPECIFIY THE DESIRED
C               OPTIONS.  THEY ARE USED AS FOLLOWS
C
C          IPLOT=1
C               IXDEP DETERMINES WHICH OPTION WILL BE CONTOURED
C               ONLY OPTIONS 1 TO 6 ARE AVAILABLE FOR CONTOURING
C
C          IPLOT=2
C               THESE TWO VARIABLES ARE USED TO CONTROL THE OPTIONS
C               FOR DEPENDENT PLOTS ALONG STREAMLINES.  IYDEP DETERMINES
C               THE VARIABLE TO BE PLOTTED ON THE Y-AXIS, IF IYDEP=Ø
C               NO DEPENDENT PLOT WILL BE MADE.  IXDEP DETERMINES THE
C               VARIABLE TO BE PLOTTED ON THE X-AXIS, IF IXDEP=Ø
```

```
C              AND IYDEP IS NONZERO THE IYDEP OPTION WILL BE PLOTTED
C              AGAINST DISTANCE ALONG THE PATHLINE (IN KM)
C
C          IPLOT=3
C               IXDEP AND IYDEP ARE NOT USED
C
C          IPLOT=4
C               IYDEP DETERMINES THE VARIABLE TO BE PLOTTED AGAINST
C               TIME IN EULER PLOTS.
C               IXDEP IS NOT USED.
C
C          IPLOT=5
C               IXDEP IS USED TO DETERMINE IF THE PROFILE WILL BE MADE
C               ALONG A VERTICAL OR HORIZONTAL SECTION.  IF IXDEP=0
C               THE HORIZONTAL SECTION WILL BE TAKEN, AND IYDEP
C               IS USED TO DETERMINE THE OPTION TO BE PLOTTED ON THE
C               Y-AXIS AGAINST DISTANCE FROM THE DOMAIN EDGE.
C               FOR VERTICAL SECTIONS IXDEP IS SET TO THE OPTION NUMBER
C               OF THE VARIABLE TO BE PLOTTED ON THE X-AXIS AGAINST
C               DEPTH.
C
C          IPLOT=6
C               IXDEP AND IYDEP ARE NOT USED
C
C
C          THE OPTION NUMBERS AND THEIR MEANINGS ARE
C
C                    1       STREAM FUNCTION
C                    2       PERMEABILITY
C                    3       HORIZONTAL MASS FLUX
C                    4       VERTICAL MASS FLUX
C                    5       TEMPERATURE
C                    6       PRESSURE
C                    7       DENSITY
C                    8       COEFFICIENT OF ISOBARIC THERMAL EXPANSION
C                    9       ENTHALPY
C                    10      HEAT CAPACITY
C                    11      VISCOSITY
C                    12      MASS FLUX
C                    13      CONDUCTIVE HEAT FLUX
C                    14      CONVECTIVE HEAT FLUX
C                    15      TOTAL HEAT FLUX
C                    16      ROCK HEAT
C                    17      FLUID HEAT
C                    18      TOTAL HEAT
C                    19      HORIZONTAL DARCY VELOCITY
C                    20      VERTICAL DARCY VELOCITY
C                    21      DARCY VELOCITY
C
C..... INPUT DEPENDENT PARAMETER FOR EULER PLOTS
C
C          SEE IXDEP,IYDEP ABOVE
C
C..... INPUT DEPENDENT PARAMETERS FOR PATHLINES
C
C          SEE IXDEP,IYDEP ABOVE
```

```
C
C..... NUMBER OF CURVES TO PLOT
C
C          USED FOR IPLOT=1,5
C          MAXIMUM NUMBER OF CURVES CAN BE 5.
C
C..... VALUE FOR EACH CONTOUR
C
C          USED ONLY FOR IPLOT=1
C
C..... INPUT SECOND OPTION TO CONTOUR
C
C          IF Ø ONLY ONE OPTION WILL BE CONTOURED ON DOMAIN.
C          IF 1-6 WILL CONTOUR THAT OPTION ON RIGHT SIDE OF
C          DOMAIN WHILE OTHER OPTION WILL BE ON LEFT SIDE.
C
C..... INPUT MIN. AND MAX. FOR DEPENDENT VARIABLE ON X AXIS
C..... INPUT MIN. AND MAX. FOR DEPENDENT VARIABLE ON Y AXIS
C
C          USED ONLY FOR IPLOT=2 AND IXDEP OR IYDEP
C          ARE NON ZERO.
C
C..... NUMBER OF INTERPOLATIONS BETWEEN DATA POINTS
C
C
C
C
C..... POSITION CURSOR AT MAXIMUM Y VALUE
C
C          USED ONLY FOR IPLOT=5 AND IYDEP=Ø
C          MAXIMUM DEPTH FOR VERTICAL PROFILES
C
C..... POSITION CURSOR AT X COORDINATE FOR VERTICAL SECTION
C
C          USED ONLY FOR IPLOT=5 AND IYDEP=Ø
C          POINT ON DOMAIN ON X DIRECTION FOR
C          VERTICAL PROFILE.
C
C..... POSITION CURSOR AT MAXIMUM X VALUE
C
C          USED ONLY FOR IPLOT=5 AND IXDEP=Ø
C          MAXIMUM DISTANCE FOR HORIZONTAL PROFILE
C
C..... POSITION CURSOR AT Y COORDINATE FOR HORIZONTAL SECTION
C
C          USED ONLY FOR IPLOT=5 AND IXDEP=Ø
C          POINT ON DOMAIN ON Y DIRECTION FOR HORIZONTAL SECTION
C
C..... POSITION CURSOR AT X-Y COORD
C
C          USED FOR IPLOT=2,3,4,6
C          POINT POSITION FOR TIME DEPENDENT PLOTS
C          MAXIMUM NUMBER OF POINTS IS 5
C          AFTER POSITIONING CURSOR INPUT ANY LETTER(EXCEPT SMALL e)
C          TO OBTAIN POINT. A SMALL e WILL EXIT FROM THIS OPTION.
C          (DO NOT INPUT A CARRIAGE RETURN)
```

```
C
C
C..... OPTIONS(GO, STAY, QUIT, RESCALE)
C
C          GO-       WILL PROCEED TO NEXT TIME
C          STAY-     CONTINUE AT PRESENT TIME WITH STEADY
C                    STATE PLOTTING
C          QUIT-     TERMINATION OF PROGRAM
C          RESCALE-  RESCALE DOMAIN TIC INTERVAL
C
C          IN ORDER TO DO TIME DEPENDENT PLOTTING PROCEED TO
C          FINAL TIME AND USE OPTION STAY
C
C..... ARE OPTIONS CORRECT
C
C          Y    YES AND CONTINUE
C          N    NO AND RETYPE OPTIONS
C
C..... RESCALE OPTION
C
C          USED ONLY FOR IPLOT=5,4
C          ONCE A DEPENDENT PLOT IS COMPLETED THE TERMINAL
C          WILL WAIT FOR A CAPTIAL R OR TWO CARRIAGE RETURNS.
C
C          R         RESCALE DEPENDENT VARIABLE
C          2-CR      PROCEED TO NEXT OPTION
C
C
C..... ENLARGEMENT OPTION
C
C          USED ONLY FOR IPLOT=1,2
C          ONCE A DOMAIN PLOT IS COMPLETED THE TERMINAL WILL
C          WAIT FOR A CARRIAGE RETURN OR A CAPTIAL B:
C
C             CR     PROCEED TO NEXT OPTION
C             B      ENLARGEMENT OPTION
C
C           IF B IS CHOSEN THE CROSSHAIRS WILL APPEAR. TO
C           ENLARGE AN AREA POSITION THE CROSSHAIR AT THE
C           LOWER LEFT HAND CORNER OF THE DESIRED AREA AND INPUT
C           A CAPTIAL P. THEN MOVE TO THE UPPER RIGHT HAND CORNER
C           OF THE AREA AND INPUT CAPITAL P AGAIN. A BOX WILL BE
C           DRAWN AROUND THE AREA FOR ENLARGEMENT.
C           ONCE THE BOX IS DRAWN, THE TERMINAL WILL WAIT
C           FOR A CARRIAGE RETURN, AT THIS TIME A HARD COPY
C           CAN BE GENERATED. AFTER THE CARRIAGE RETURN, THE OPTION
C           TO RESCALE THE DOMAIN WILL BE ASKED. ANOTHER CARRIAGE
C           RETURN IS REQUIRIED AFTER THIS OPTION
C
C..... INITIAL CONDITION DOMAIN
C
C          WHEN THIS DOMAIN IS DRAWN, THE USER MAY TURN
C          THE TERMINAL TO LOCAL AND WRITE ANYTHING UPON THIS
C          DIAGRAM. ONCE ON LINE, THE TERMINAL WILL WAIT
C          FOR EITHER:
C
```

```
C              CR   PROCEED
C              N    REDETERMINE POINTS AND REDRAW
C
C
C..... END OF FILE ENCOUNTERED
C..... FINAL TIME WILL BE USED
C
C          TIME EXCEEDS THE FINAL TIME IN THE DATA FILE.
C          A CARRIAGE RETURN WILL RETURN THE USER TO THE
C          OPTION SEQUENCE OF THE PROGRAM.
C          CAUTION A G OPTION WILL RESULT IN TERMINATION
C          OF THE PROGRAM.
C
C
C
C**********ERROR MESSAGES ARE FEW AND SELF EXPLANATORY.
C
C
C
C*****************************************************************
```

```
ETCHGR DOCUMENTION
C*************************************************************
C
C       ETCHGR VERSION (RESISTIVITY PLOTTING)
C
C
C       THIS VERSION CONTAINS OPTIONS TO:
C
C          1. CONTOUR PLOTTING OF RESISTIVITY
C          2. CONTOUR PLOTTING OF POROSITY
C          3. DEPENDENT PLOTTING OF RESISTIVITY,
C             POROSITY AND DIELECTRIC CONSTANT.
C
C       THIS VERSION ALSO CONTAINS CHARACTER
C       GENERATION CODE TO ROTATE LABELS
C
C       OPERATING PROCEDURES:
C
C*****  ETCHGR READS FROM A RESISTIVTY DATA FILE WHICH
C*****  CONTAINS FLUID RESISTIVITY DATA. THERE ARE
C*****  TWO DATA FILES CURRENTLY BEING USED:
C*****
C*****       1. RHO1      .Ø1 MOLAL NACL
C*****       2. RHO2       .1 MOLAL NACL
C*****
C*****  THESE DATA FILES INCLUDE DATA FOR T=25-625
C*****  AND P=1-1ØØØ BARS.
C
C       THE FOLLOWING IS A LIST OF OPTIONS
C       AVAILABLE FOR RESISTIVTY MODELING.
C
C       1. DO YOU WISH TO MODEL RESISTIVITY?
C
C          Y-YES
C          N-NO          REDUCES TO OLD VERSION OF ETCHG
C
C       2. NEW OR OLD MODEL?
C
C          N-NEW         NEW MODEL
C          O-OLD         PRIOR RESISTIVITY MODEL DATA WILL BE
C                        READ IN.
C
C       3. RESISTIVITY FILE?
C
C          USED ONLY FOR OLD MODEL. THIS FILE IS THE NAME
C          OF A PRIOR RESISTIVITY MODEL.
C
C       4. DO YOU WISH TO SAVE DATA?
C
C          Y-YES         WILL SAVE RESISTIVITY AND POROSITY
C                        DATA ON FOR5Ø.DAT. THIS FILE CAN BE USED
C                        TO RERUN A MODEL INSTEAD OF GENERATING
C                        NEW VALUES.
C          N-NO
```

```
C
C       5. DO YOU WISH TO MODEL POROSITY?
C          Y-YES        CALCULATE POROSITY AS A FUNCTION
C                       OF INCREASING TEMPERATURE.
C          N-NO        ASSUME CONSTANT POROSITY
C
C       6. RESISTIVITY INPUT FILE?
C
C          IF NEW MODEL IS BEING CALCULATED, THIS IS
C          THE NAME OF THE FLUID RESISTIVTY DATA FILE
C
C
C******* IMPORTANT    IF OLD MODEL IS BEING USED AN
C*******              EULER PLOT OPTION MUST BE
C*******.             USED ON RESISTIVITY.
C
C       PLOTTING OPTIONS
C
C       COMPLETE DESCRIPTION IS GIVEN IN THE MAIN
C       DOCUMENTAION FOR  ETCHGR
C
C       RESISTIVITY          OPTION =25
C       DIELECTRIC CONT.     OPTION =26
C       POROSITY             OPTION =27
C
C*************************************************************
```

APPENDIX II-1

The following preprint is currently in review at Jour. Geophys. Research. This contribution is the result of research supported by ERDA contract EY-76-S-02-2763.

A PRELIMINARY ANALYSIS OF INTRINSIC FLUID AND ROCK RESISTIVITY IN ACTIVE HYDROTHERMAL SYSTEMS

B. Moskowitz and D. Norton

Abstract

Electrical resistivity data are utilized in interpretations of subsurface environments and to explore for geothermal and mineral resources. Abnormally low resistivity data are alternatively interpreted to indicate the presence of high temperature fluids or conductive minerals (metal sulfides) at depth. The relative contributions of thermal, porosity, and fluid composition effects appear to be poorly known.

An analysis of intrinsic rock resistivities in active hydrothermal systems has been made using fluid resistivities, calculated electrical porosities, and two-dimensional heat and mass transfer computations.

The analyses indicate that the host rock resistivity distribution around igneous intrusives is primarily controlled by the mode of dispersion of thermal energy away from the pluton. Comparisons between numerical results and field observations in geothermal areas indicate that (1) low near-surface resistivity cannot be entirely accounted for by hot circulating saline water and (2) observations of high thermal gradients associated with low resistivity anomalies do not assure the existence of a high energy geothermal source at shallow crustal depths.

Introduction

The nature of rocks in the upper crust is often deduced from apparent electrical resistivity data. The relationship between these data and the intrinsic resistivities is poorly known, and, therefore, correlation of the electrical resistivity measurement of rocks with variations in rock and pore fluid properties is usually quite speculative. Although these interpretations are based on resistivity data measured in deep drill holes and laboratory measurements on rocks and fluids, the correlation of laboratory measurements, even in well-controlled laboratory experiments, with rock properties has not been satisfying. Better understanding of this correlation would facilitate mapping subsurface conditions with the aid of electrical survey data, and is particularly relevant in regions of active hydrothermal activity where there is considerable interest in energy resources.

The electrical resistivity variations in upper crustal rocks have been inferred from various electrical methods. The results of these surveys indicate average resistivity values in stable crustal regions range from 10^5 Ω-m to 10^2 Ω-m (Keller and Frischknecht, 1966; Keller et al., 1966). An analysis of laboratory experimental data on the resistivity of fluid saturated crustal rocks coupled with considerations of regional heat flow data predict similar ranges in resistivity to 40 km depth, Brace, 1971. Resistivity surveys in regions of geothermal activity indicate anomalously low

resistivities which range between 10 and 100 Ω-m (Sato, 1970; Cheng, 1970; Risk, McDonald, and Dawson, 1970; Zohdy et al., 1973; Keller, G. V., 1970). These anomalous values are often attributed to the presence of prospective thermal energy resources.

The properties and conditions in geothermal systems which contribute to resistivity values are fluid and mineral composition, porosity, temperature, and pressure (Brace, 1971; Brace and Orange, 1968; Brace, Orange, and Madden, 1965; Keller and Firschknecht, 1966). The effect of porosity and fluid resistivity on the bulk rock resistivity of sedimentary rocks was deduced by Archie (1942), and extended to fractured crystalline rocks by Brace, Orange, and Madden (1965). The empirical relationship derived by Archie defines bulk rock resistivity, ρ_r,

$$(1) \quad \rho_r = a\rho_f\phi^{-n},$$

in terms of pore fluid resistivity, ρ_f, a proportionality constant, a, porosity, ϕ, and a factor which depends on the degree of rock consolidation, n. Experimental data by Brace (1965) suggest that for fractured media a = 1 and n = 2, which apparently agrees with theoretical electrical network models of Greenberg and Brace (1969) and Shankland and Waff (1974). The porosity value normally used in equation (1) is that of total rock porosity. However, only those pores which contribute to current flow should be included in this term. In fractured media the total porosity may not be totally composed of

interconnected pores, as indicated by studies of ion transport in these types of rocks, Norton and Knapp (1977). Ranges in rock resistivity of six orders of magnitude may be realized for reasonable variations in the abundance of interconnected pores in fractured media, Moskowitz (1977). There does not appear to be a reasonable physical model or theory which adequately defines ϕ in equation (1).

The transient thermal history of rocks in hydrothermal systems related to cooling igneous bodies has been simulated by numerical methods, Norton and Knight (1977). Their heuristic models simulate both temperature and pressure variation over large regions and for long time periods. Since the variation in resistivity of rocks relates directly to subsurface temperature and pressure conditions, their numerical models provide a basis with which to analyze intrinsic resistivity of hydrothermal systems. The purpose of this communication is to present the results of a first order approximation to the nature of intrinsic resistivity in such systems. The study considered variations in permeability and porosity, heat sources, rock and fluid properties, including variation in pore fluid resistivity as a function of temperature, pressure, and concentration of components in solution, as well as the time dependence of these parameters in a two-dimensional domain.

Porosity

The distribution of porosity in the crust varies in

response to changes in pore fluid pressure. Effective pressure, P_e, is the difference between confining pressure (P_c) and pore fluid pressure (P_f),

$$(2) \quad P_e = P_c - P_f .$$

A recent study of the variation of effective pressure with depth in the crust, by Knapp and Knight (1977), shows that in many geologic environments increases in pore fluid pressure, as a result of temperature increases, will cause the effective pressure to decrease. As a consequence of the low tensile strength of rocks, when effective pressure is reduced to zero the rock will fracture. Thus, an increase in porosity is expected at zero effective pressure.

The concept presented by Knapp and Knight (1977) can be used to relate porosity change at zero effective pressure to temperature. The total derivative of the rock-pore volume at constant composition is

$$(3) \quad dV = \left(\frac{\partial V}{\partial T}\right)_P dT + \left(\frac{\partial V}{\partial P}\right)_T dP,$$

where $V = V_r + V_f$, V_r is rock volume, and V_f is pore volume. The coefficients of isobaric thermal expansion (α) and isothermal compressibility (β) for the bulk rock are defined as

$$(4a) \quad \alpha \equiv \frac{1}{V}\left(\frac{\partial V}{\partial T}\right)_P$$

$$(4b) \quad \beta \equiv -\frac{1}{V}\left(\frac{\partial V}{\partial P}\right)_T .$$

Substitution of equations (4a,b) into equation (3) defines the total volume change in terms of α and β:

(5) $dV = V\alpha dT - V\beta dP.$

This total derivative can also be expressed in terms of the individual thermal expansions and compressibilities of pore fluid and rock:

(6) $dV = [V_f\alpha_f + V_r\alpha_r]dT - [V_f\beta_f + V_r\beta_r]dP.$

However, when rocks fracture as a consequence of pore fluid expansion, infinitesimal increases in pore fluid pressure will produce further fracturing. Therefore, $dP \tilde{=} 0$, and equation (6) may be simplified to

(7) $dV = [V_f\alpha_f + V_r\alpha_r]dT.$

Typical values for α_r, for common silicate minerals, over a temperature range of 0 - 800°C, are on the order of $10^{-6}/°C$ (Clark, 1966). The thermal expansion coefficient for pure water, over the same temperature span, is on the order of $10^{-3}/°C$. As long as pore volume, V_f, is .01 or greater, $V_f\alpha_f >> V_r\alpha_r$, and equation (7) becomes

(8) $dV = V_f\alpha_f dT.$

The total volume change, according to equation (8), occurs as a result of pore volume changes, with rock volume remaining essentially constant. Rearranging equation (8) with the approximation that $dV \tilde{=} dV_f$ yields an integral equation relating pore volume and temperature:

(9) $$\int_{V_f^o}^{V_f} \frac{dV_f}{V_f} = \int_{T_b}^{T} \alpha_f(T)dT.$$

In equation (9), V_f^o is the initial residual pore volume, and T_b is the temperature at which the rock fractures. Integrating equation (9) gives the pore volume as a function of temperature:

$$(10) \quad V_f = V_f^o \exp\left[\int_{T_b}^{T} \alpha_f(T)dT\right],$$

where $T > T_b$. The initial residual porosity, ϕ^o, is defined as

$$(11) \quad \phi^o = \frac{V_f^o}{V^o} = \frac{V_f^o}{V_r + V_f^o}$$

and the fluid and rock volumes are, respectively:

$$(12) \quad V_f^o = \phi^o V^o \; ; \quad V_r = (1 - \phi^o)V^o.$$

Substituting equations (11) and (12) into equation (10) defines a porosity temperature function, in terms of the initial residual porosity:

$$(13) \quad \phi = \frac{\phi^o F(T)}{(1 - \phi^o) + \phi^o F(T)} \; ,$$

where

$$(14) \quad F(T) = \exp\left[\int_{T_b}^{T} \alpha_f(T)dT\right].$$

For the purposes of this discussion, we will consider that equation (13) defines increases in the effective electrical porosity. That is, all porosity increases due to thermal effects are assumed to contribute to increased

electrical current flow in the rocks.

The temperature at which the rocks initially fracture, T_b, may be defined as

$$(15) \quad T_b = T_a + \Delta T,$$

where T_a is the ambient temperature, and ΔT is the temperature increment necessary to reduce effective pressure to zero. The value of ΔT depends on the geothermal gradient (Knapp and Knight, 1977), where its maximum value along a geothermal gradient of $20^{\circ}C/km$ is $20^{\circ}C$.

Porosity, defined by equation (13), was computed for 1, 2, 3, and 4 km below the earth's surface, figure 1. At depths of 1 km and initial temperature of $40^{\circ}C$, large increases in porosity are predicted for temperature changes on the order of $300^{\circ}C$. However, the porosity increases are small for changes in temperatures $< 100^{\circ}C$ at this same depth. At greater depths, e.g., 4 km, much smaller increases in porosity are predicted for these same temperature conditions, due to increased confining pressure.

The relationship between bulk rock resistivity, fluid resistivity, and electrical porosity is poorly known. A commonly used empirical relationship is Archie's Law, equation (1). For our study, we have assumed this relationship is an adequate first approximation to rock resistivity. Therefore, the important parameter in predicting resistivity from equation (1) is ϕ^{-2}, and, therefore, small increases in porosity

will result in a significant decrease in ρ_R, figure 2.

Fluid Resistivity

The resistivity of natural groundwaters varies as a function of temperature, pressure, and composition. Since the dissolved constituents in natural waters are often dominated by sodium and chloride, and the variation in resistivity due to different components is less than a factor of 2.5, the compositional affects of fluid resistivity may be approximated by the system NaCl-H_2O (Quist and Marshall, 1968; Chambers, 1958; Gunning and Gordon, 1942). Variations in resistivity for a 0.1 molal NaCl solution are shown in figure 3. The variation in resistivity with temperature and pressure exhibits a steady, pressure independent decrease in resistivity to approximately 300°C. The dominant pressure effect is to shift the resistivity minima to higher temperatures with increasing pressure. Also, increasing the NaCl concentration will result in a decrease in resistivity. This decrease may vary from 100 Ω-m to 0.01 Ω-m for concentrations ranging from 10^4 to 2 molal.

Fluid temperatures in geothermal systems range up to 300°C, and pressures to 1 kb. Total ionic strength of these fluids ranges from 1 molal, such as observed in the Imperial Valley system (Meidev and Furgerson, 1972) to 10^{-2} molal, such as observed in the Broadlands, New Zealand system, Brown and Ellis, 1970. Typical resistivities of geothermal reservoir fluids range from 0.01 ohm-meters to 10 Ω-m, Cheng, 1970, which is similar to the range in resistivity of pore fluids in a variety of geologic environments, Keller and Frischknecht,

1966.

Temperature-Pressure Distribution

Notions of temperatures and pressures in geothermal systems are primarily derived from production or exploration wells, which are usually restricted to small portions of the total system. Knowledge of these parameters over the entire hydrothermal system is necessary in order to analyze the time dependence of resistivity in the region of a cooling pluton. Simulation of cooling plutons by numerical methods is one method by which these parameters can be defined for an idealized geothermal system.

Fluid flow caused by thermal anomalies related to igneous plutons is effectively scaled and represented in two-dimensions by partial differential equations which describe the conservation of mass, momentum, and energy for the fluid-rock system, Norton and Knight, 1977:

$$(16) \quad \gamma \frac{\partial T}{\partial t} + q\nabla H = \nabla \cdot \kappa \nabla T \qquad \text{(conservation of energy)}$$

and

$$(17) \quad \frac{\nu \nabla \cdot \nu}{k} \nabla \Psi = R \frac{\partial \rho}{\partial y}, \qquad \text{(conservation of momentum)}$$

where T is the temperature, Ψ the streamfunction, q the fluid flux, t the time, H, ρ, and ν are the enthalpy, density, and viscosity of the fluid, k is the permeability of the rock, κ the thermal conductivity and γ the volumetric heat capacity of the fluid saturated media, R the Rayleigh number, ∇ the gradient operator, and y the horizontal distance in the

two-dimensional section to which these equations apply.

Equations (16) and (17) are approximated by finite difference numerical equations which permit computation of the values of the dependent variables at discrete points in the domain from initial and boundary values specified for the system. The numerical analysis provides the option to include variable transport properties of the fluid (H_2O-system) and rock, general boundary and initial conditions, and radioactive and volumetric heat sources in a two-dimensional domain. The transport process related to the transient thermal anomaly is approximated by a time sequence of steady state numerical solutions to (16) and (17), computed at explicitly stable time intervals. An alternating-direction-implicit finite difference method is used to approximate the spatial derivatives at discrete intervals on the order of 0.1 to 0.5 of the system height. Fluid pressure in the system is computed at each steady state step by integration of Darcy's Law in which the fluid properties, viscosity and density, are expressed as a function of temperature and pressure.

The methods used by Norton and Knight, 1977, were used to define the temperature variation in the environment of a cooling pluton as a function of time. The hypothetical system is characterized by a dominance of convective heat transport over conductive heat transport as a result of relatively large host rock permeabilities, figure 4. As a consequence of fluid circulation, the temperature distribution in the

host rocks evolves into a plumose pattern at $\sim 10^5$ years, figure 5, and results in broad regions of uniform temperature above the pluton.

Before emplacement of the pluton at 4.5 km depth, the initial temperature at this depth was 110°C (defined by the 20°C/km geothermal gradient). At 190,000 years after pluton emplacement, the 200°C isotherm is at approximately 0.5 km depth (figure 5), and the temperatures between the top of the pluton and the 200°C isotherm have increased by at least 90°C. The pore fluid resistivity will reach a minimum at temperatures between 200°C - 300°C (figure 3). The porosity increase defined by equation (13) will be approximately 10% for temperature increases of 100° - 200°C. Therefore, the zone between the 200°C isotherm and the top of the pluton in the system will be characterized by maximum porosity increase and the maximum decrease in pore fluid resistivity.

Porosities in host rocks at depths < 2 km directly over the pluton have significantly increased, approximately 20%, at 190,000 years after pluton emplacement. This porosity increase persists uniformly to 4 km depth. Time variations in porosity, calculated at fixed points 4, 2.5, and .5 km above the top of the pluton, predict a maxima 0.5 km above the pluton at 4×10^4 and 10^5 years after emplacement, figure 6. However, as a result of convective transport of thermal energy to the surface, a porosity maxima is observed at depths < 2 km.

The spatial and temporal distribution of temperature in the system will directly determine the host rock resistivity distribution. The resistivity isopleths closely parallel the isotherms at 50,000 and 190,000 years, respectively, figures 7 and 8, which also illustrate the displacement in the resistivity isopleths between 50,000 and 190,000 years. By 190,000 years, the lateral extent of the isopleth displacement at 1 km depth spans the entire width of the system ($\sim$ 22 km).

The time variation of resistivity for fixed points 4, 2.5, and 0.5 km above the top of the pluton is directly affected by the porosity, temperature, and pore-fluid resistivity changes occurring over the pluton. At 0.5 km above the pluton a resistivity minima occurs at 20,000 years. By 110,000 years, the resistivities calculated at 2.5 and 4 km depths are nearly equal. The convective transport of thermal energy away from the pluton results in an order of magnitude decrease in resistivity at depths < 2 km by 100,000 years after pluton emplacement.

In summary, the calculations indicate that the dispersion of thermal energy away from a pluton will directly affect the host rock resistivity. When pluton emplacement is into permeable host rocks, significant decreases in resistivity between the surface and depths < 0.5 km are predicted. These resistivity values then persist uniformly in a vertical zone,

extending from 0.5 km to approximately 4 km above the pluton by 190,000 years after pluton emplacement. The maximum decrease in resistivity is less than a factor of 10, as compared to surface values. The range in host rock resistivity is from 10^4 - 10^5 ohm-m. These values are quite high with respect to values obtained on real rocks. However, our calculations only account for a conductive fluid in a nonconductive matrix.

Discussion

The temperature variations in hydrothermal systems account for changes in electrical porosity and electrical resistivity of pore fluids. The results of our analysis suggest resistivity anomalies caused by thermal events are several times broader in extent than the thermal source, and the lateral resistivity gradients at the margins of the anomaly are much lower than the vertical resistivity gradients directly above the pluton. The side and top margins of the resistivity anomaly correspond closely to 200^{o} isotherm, as a consequence of the fluid properties. The resistivity minima occurs at relatively shallow depths, 0.5 km, and extends to 4 km. However, the magnitude of these resistivities is considerably greater than values measured in geothermal systems.

The magnitude of ρ_R is defined by the pore-fluid concentration and initial host rock porosity while the distribution of ρ_R is defined by the temperature distribution. To determine the change in magnitude of ρ_R, due to varying molality

of pore-fluids and host rock porosities, a series of calculations was made with different initial values of porosity and NaCl molalities. The isopleths of resistivity as a function of porosity and NaCl molality at constant temperature are defined by equation (1) and shown for T = 300°C in figure 9. The results of the calculations are summarized as the minimum resistivities predicted for the cooling pluton environment, are comparable to actual values realized in geothermal systems and in saline groundwater systems. In order to explain the observed resistivities in geothermal areas (< 10 ohm-m), high molality pore-fluids and/or high porosity host rocks must occur for large vertical and horizontal zones within the geothermal system.

The results of this study indicate that rock resistivities in active hydrothermal systems are considerably less than can be accounted for by simple changes in fluid resistivity or rock porosity. The discrepancies between the numerical resistivity models and the field resistivity observations in geothermal systems may be accounted for by the presence of conducting minerals since pyrite and conductive clay minerals are typically found in the region of hydrothermal systems over the top of the thermal anomaly. If one uses a conservative estimate of a factor of 10 decrease in host rock resistivities resulting from conducting minerals, a geologically reasonable range in porosity and fluid composition can produce the anomalously low resistivity values observed in geothermal areas.

Therefore, except in anomalously high salinity and high porosity environments, the presence of hot fluids alone is not sufficient to generate the low resistivity values observed in geothermal areas.

Considerable interest has been given to exploration techniques that might be useful in detecting high energy geothermal systems. Commonly used techniques include measurements of heat flow and electrical resistivity. High heat flow in combination with anomalously low electrical resistivity data have been used as a justification for drilling of exploratory wells. Sedimentary basins and young, old, and mature geothermal systems in fractured rocks constitute a set of geologic environments within which the correlation of high thermal gradients, low near-surface resistivities, and surface thermal effects may lead to non-unique interpretations of the potential for geothermal energy resources at moderate depths. In the basin and range province of the western United States, concentrated brines associated with evaporite deposits in the high porosity basins can produce lateral density gradients which cause fluid circulation. Exothermal hydration reactions that produce local thermal anomalies, coupled with the fluid circulation, are often sufficient to cause high surface heat flux and surface thermal springs. The high salinity and high porosity in these sedimentary basins would result in anomalously low near-surface resistivity. This particular environment appears to occur in the Safford Basin, southeastern

Arizona (Norton et al., 1977).

Geothermal systems which have nearly cooled to regional background temperatures may be characterized by large conductive heat fluxes, Norton, 1977, as a result of remnant thermal energy that has been transported from the heat source to near-surface environments. Conducting minerals will undoubtedly have been formed above the pluton, and thermal springs will still be prevalent on the surface. In this environment low resistivity would be associated with the conducting minerals and, in part, with the remnant thermal circulating saline fluids.

Geothermal systems in their early stages of formation have not been studied; however, their characteristics have been simulated numerically. The transport of thermal energy away from a pluton may be rapid with respect to the mass flux of reactive components in solution to the surface. This means that hot saline fluids will dominate changes in host rock resistivities because not enough time has elapsed to produce significant quantities of conducting minerals. High heat flux and surface thermal effects will probably form relatively early in the life cycle of a geothermal system. The calculated resistivity values resulting from increased temperatures are anomalous with respect to background values but are relatively high (10^4 - 10^5 ohm-m). Therefore, this environment is characterized by high heat flux, thermal surface effects, but probably an undetectable resistivity anomaly,

even though there is a high energy thermal source at depth.

Active, mature geothermal systems are abundant world-wide where high heat flux, thermal surface effects, and low resistivities are associated with a productive thermal source at depth. However, low resistivity anomalies, < 100 Ω-m, are probably caused by the presence of conductive minerals which may be coincident with hot thermal fluids.

The four geologic environments presented serve to illustrate the problems which can be encountered when attempting to interpret near-surface resistivity anomalies. Also, a combination of heat flux measurements, surface thermal effects, and low resistivity can be characteristic of both productive high energy geothermal systems as well as unproductive, low energy geothermal environments. The observations are also manifested in the fact that electrical methods are used in prospecting for both sulfide mineral deposits and thermal energy.

Acknowledgements

We wish to acknowledge the Energy Research and Development Administration for support of this study through contract E-11-1-2763. We thank R. Knapp and J. Knight who contributed discussions and questions which greatly improved the concepts, and L. McLean for editing and typing the manuscript.

References

Archie, G. E., 1942, The electrical resistivity log as an aid in determining some reservoir characteristics: Trans. AIME, Petrol. Br., v. 146, p. 54-62.

Brace, W. F., 1971, Resistivity of saturated crustal rocks to 40 km based on laboratory studies, in Heacock, J. G., ed.: The Structure and Physical Properties of the Earth's Crust: Am. Geophys. Union Mon. 14, p. 243-257.

Brace, W. F., and Orange, A. S., 1968b, Further studies of the effect of pressure on electrical resistivity of rocks: Jour. Geophys. Res., v. 73, p. 5407-5420.

Brace, W. F., Orange, A. S., and Madden, T. R., 1965, The effect of pressure on the electrical resistivity of water saturated crystalline rocks: Jour. Geophys. Res., v. 70, p. 5669-5678.

Browne, P. R. L., and Ellis, A. J., 1970, The Ohaki-Broadlands hydrothermal area, New Zealand: Mineralogy and related geochemistry: Am. Jour. Sci., v. 269, p. 97-131.

Chambers, J. F., 1958, The conductance of concentrated aqueous solutions of potassium iodide at 25°C and of potassium and sodium chlorides at 50°C: Jour. Phys. Chem., v. 62, p. 1136.

Cheng, W. T., 1970, Geophysical exploration in the Tatun volcanic region, Taiwan: Geothermics Spec. Issue 2, U. N. Symp. on the Development and Utilization of Geothermal Resources, Pisa, v. 2, part 1, p. 910-917.

Greenberg, R. J., and Brace, W. F., 1969, Archie's Law for rocks modeled by simple networks: Jour. Geophys. Res., v. 74, p. 2099-2102.

Gunning, H. E., and Gordon, A. R., 1942, The conductance and ionic mobilities for aqueous solutions of K and NaCl at T = 15°C - 45°C: Jour. Chem. Phys., v. 10.

Keller, G. V., 1970, Induction methods in prospecting for hot water: Geothermics Spec. Issue 2, U. N. Sump. on the Development and Utilization of Geothermal Resources, Pisa, v. 2, part 1, p. 318-332.

Keller, G. V., Anderson, L. A., and Pritchard, J. I., 1966, Geological survey investigations of the electrical properties of the crust and upper mantle: Geophysics, v. 31, p. 1078-1087.

Keller, G. V., and Frischknecht, F. C., 1966, Electrical Methods in Geophysical Prospecting: Pergamon Press, Oxford.

Knapp, R., and Knight, J., 1977, Decrease in effective pressure by differential thermal expansion of pore fluids: Jour. Geophys. Res., accepted for publication.

Meidav, T., and Furgerson, R., 1972, Resistivity studies of the Imperial Valley geothermal area, California: Geothermics, v. 1, p. 47-62.

Mitchell, B. J., and Landisman, M., 1971, Geophysical measurements in the southern great plains, in Heacock, J. G., ed.: The Structure and Physical Properties of the Earth's Crust: Am. Geophys. Union Mon. 14, p. 77-95.

Moskowitz, Bruce M., 1976, Numerical analysis of electrical resistivity in hydrothermal systems: Unpublished M.S. Thesis, University of Arizona, Tucson, Arizona.

Norton, D., Gerlach, T., DeCook, K. J., and Sumner, J. S., 1975, Geothermal water resources in Arizona: Feasibility study: Technical Completion Rept., Office of Water Research and Technology, Project A-054-ARIZ.

Norton, D., 1977, Fluid circulation in the earth's crust, in Heacock, J. G., ed.: The Structure and Physical Properties of the Earth's Crust: Am. Geophys. Union Mon. 20, in press.

Norton, D., and Knapp, R., 1977, Transport phenomena in hydrothermal systems: The nature of porosity: Am. Jour. Sci., v. 277, p.

Norton, D., and Knight, J., 1977, Transport phenomena in hydrothermal systems: Cooling plutons: Am. Jour. Sci., v. 277, p.

Quist, A. S., and Marshal, W. L., 1968, Electrical conductances of aqueous sodium chloride solutions from 0°C to 200°C and at pressures to 4000 bars: Jour. Phys. Chem., v. 72, p. 684-703.

Risk, G. F., MacDonald, W. J. P., and Dawson, G. B., 1970, D.C. resistivity surveys of the Broadlands geothermal region, New Zealand: Geothermics Spec. Issue 2, U. N. Symp. on the Development and Utilization of Geothermal Resources, Pisa, v. 2, part 1, p. 287-294.

Sato, K., 1970, The present state of geothermal development in Japan: Geothermics Spec. Issue 2, U. N. Symp. on the Development and Utilization of Geothermal Resources, Pisa, v. 2, part 1, p. 155-184.

Shankland, T. J., and Waff, H. S., 1974, Conductivity in fluid bearing rocks: Jour. Geophys. Res., v. 79, p. 4863-4868.

Zohdy, A. A. R., Anderson, L. A., and Muffler, L. J. P., 1973, Resistivity, self potential, and induced polarization surveys of a vapor-dominated geothermal system: Geophysics, v. 38, p. 1130-1144.

Figure Captions

Figure 1. Porosity as a function of temperature at 1, 2, 3, and 4 km depth, as computed from equation (13). Initial porosity, $\phi_o = 0.1$, background temperatures are consistent with a surface temperature of 20°C and a temperature gradient of 20°C/km. Pressures were computed for a rock density of 2.75 g/cm^3. Insert shows porosity values consistent with temperatures up to 1200°C.

Figure 2. ϕ^{-2} as a function of temperature at 1, 2, 3, and 4 km depth. Parameters used are same as in figure 1.

Figure 3. Temperature-pressure projection of the two-phase surface (liquid-vapor) in the NaCl H_2O system at 0.01 m NaCl concentration depicting fluid resistivity isopleths.

Figure 4. Two-dimensional cross section of a pluton intruded into uniform permeability host rocks depicting initial and boundary conditions for numerical simulation of heat and mass transfer. Domain was discretized into 120 grid points such that $\Delta z = 0.9$ km and $\Delta y = 1.75$ km. The initial conditions include a background temperature consistent with a surface temperature of 20°C and a thermal gradient, $\nabla_z T =$ 20°C/km. The pluton's initial temperature is 960°C. Permeabilities are 10^{-15} m^2 and 10^{-18} m^2 for the host and pluton rocks, respectively.

Figure 5. Temperature distribution in idealized hydrothermal system, defined by figure 4, for 5 x 10^4 yrs (left half) and 1.9 x 10^5 yrs elapsed time (right half).

Figure 6. Porosity as a function of time resulting from thermal energy transport into host rocks from pluton at positions directly over pluton, 0.5, 2, and 4 km below the surface, figure 4.

Figure 7. Resistivity and temperature values in hydrothermal system at 5 x 10^4 yrs elapsed time, depicting the temperature control on intrinsic resistivities.

Figure 8. Resistivity and temperature values in hydrothermal systems at 1.9 x 10^5 yrs elapsed time, depicting the temperature control on intrinsic resistivities.

Figure 9. Concentration of NaCl in pore fluids and electrical porosity effect on intrinsic rock resistivities, 10, 10^2, 10^3, and 10^4 ohm-m isopleths. Values are for T = 300°C, at which the minimum in fluid resistivity occurs, and for P = 500 bars. Note the minimum in fluid resistivity is nearly independent of pressures, figure 3.

Regions delimited by dashed lines represent ranges in values of porosity and fluid compositions observed in the respective geologic environments and for idealized systems considered in this study. The latter are labeled "fractured igneous systems."

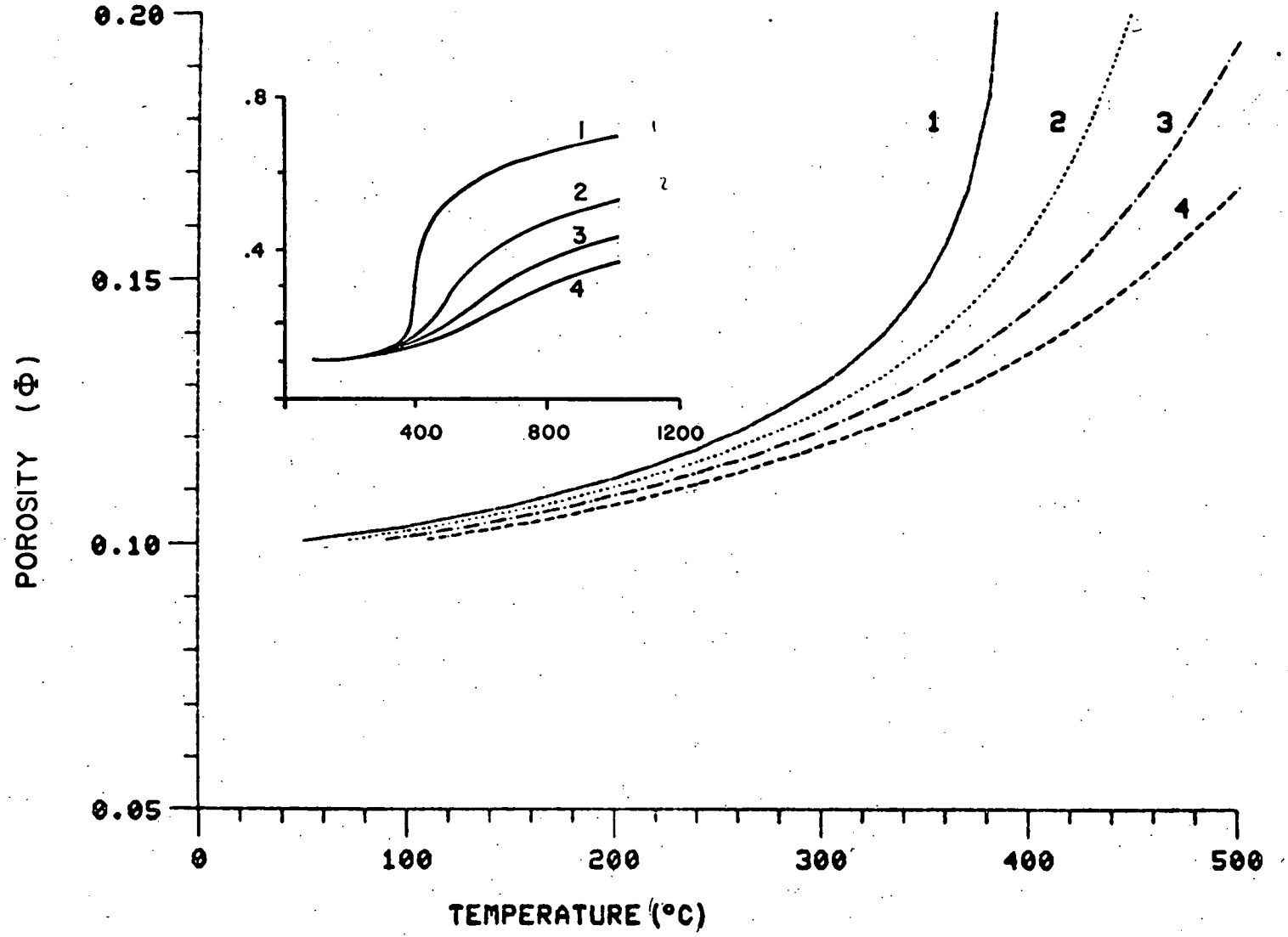
0.20
0.15
0.10
0.05
POROSITY (Φ)
0
100
200
300
400
500
TEMPERATURE (°C)
1
2
3
4
.8
.4
400
800
1200

Figure 1

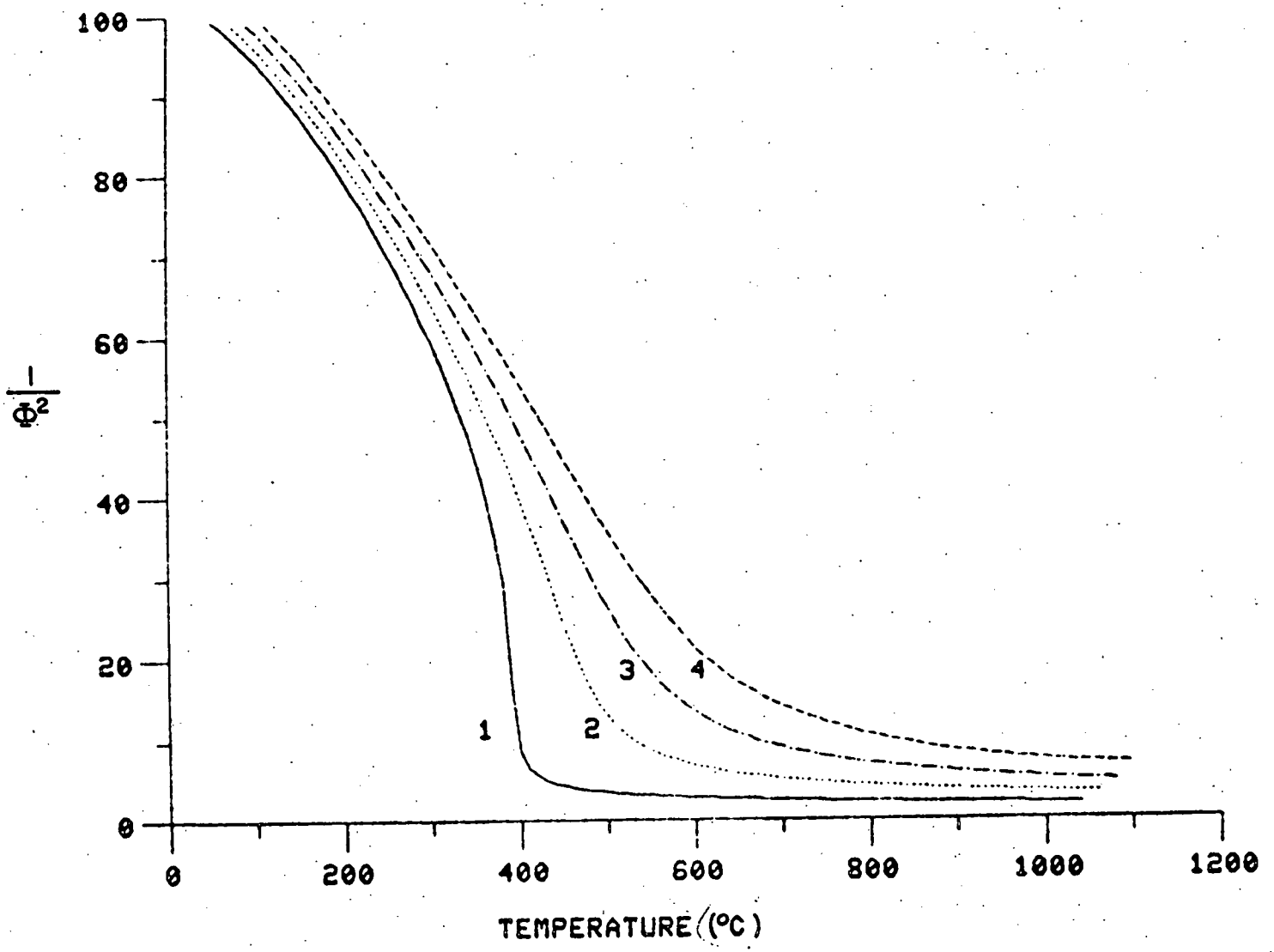
100
80
60
40
20
0
$\frac{1}{\Phi^2}$
0
200
400
600
800
1000
1200
TEMPERATURE (°C)
1
2
3
4

Figure 2

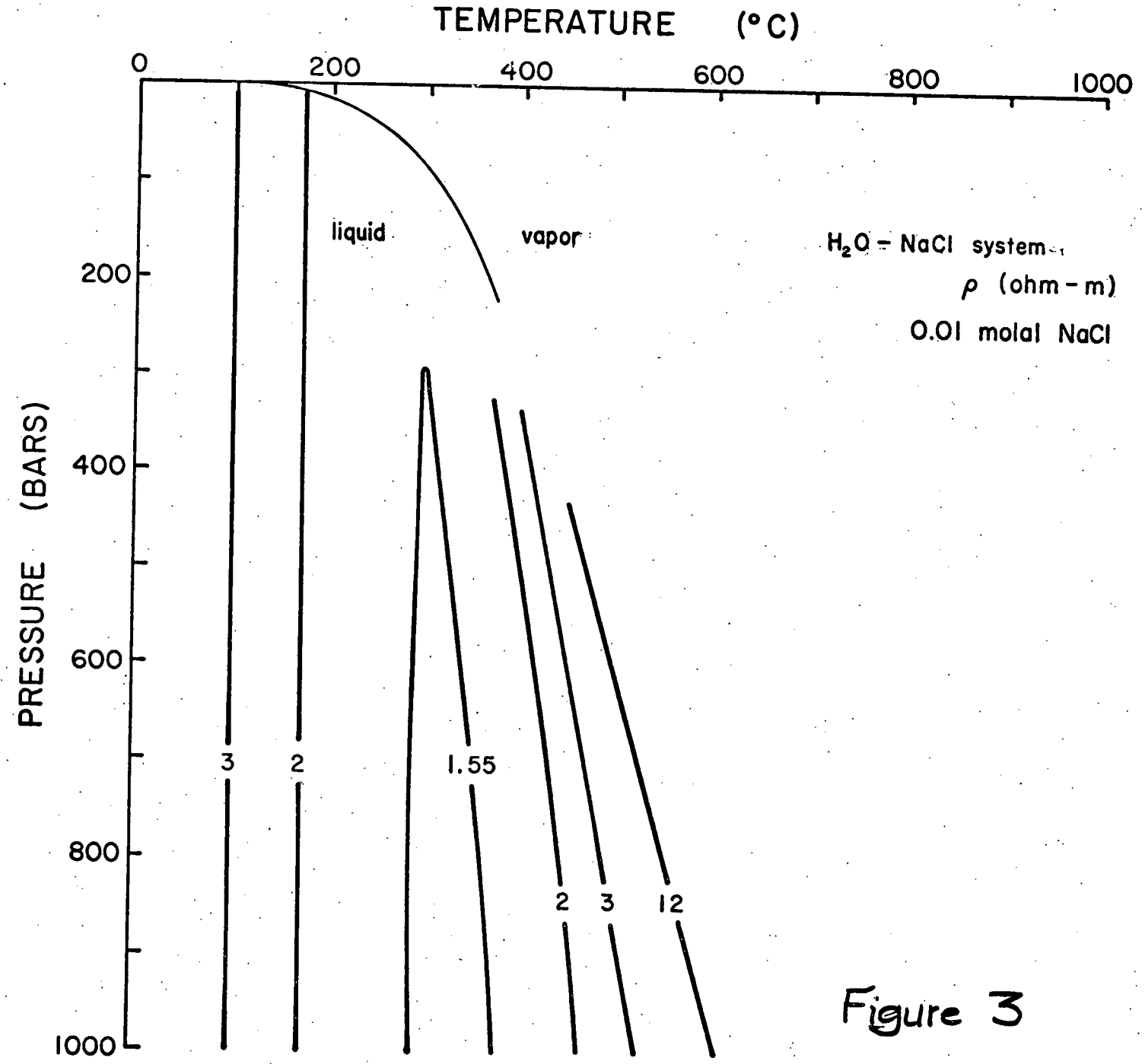
TEMPERATURE (°C)
0
200
400
600
800
1000
PRESSURE (BARS)
200
400
600
800
1000
liquid
vapor
H_2O - NaCl system
ρ (ohm - m)
0.01 molal NaCl
3
2
1.55
2
3
12

Figure 3

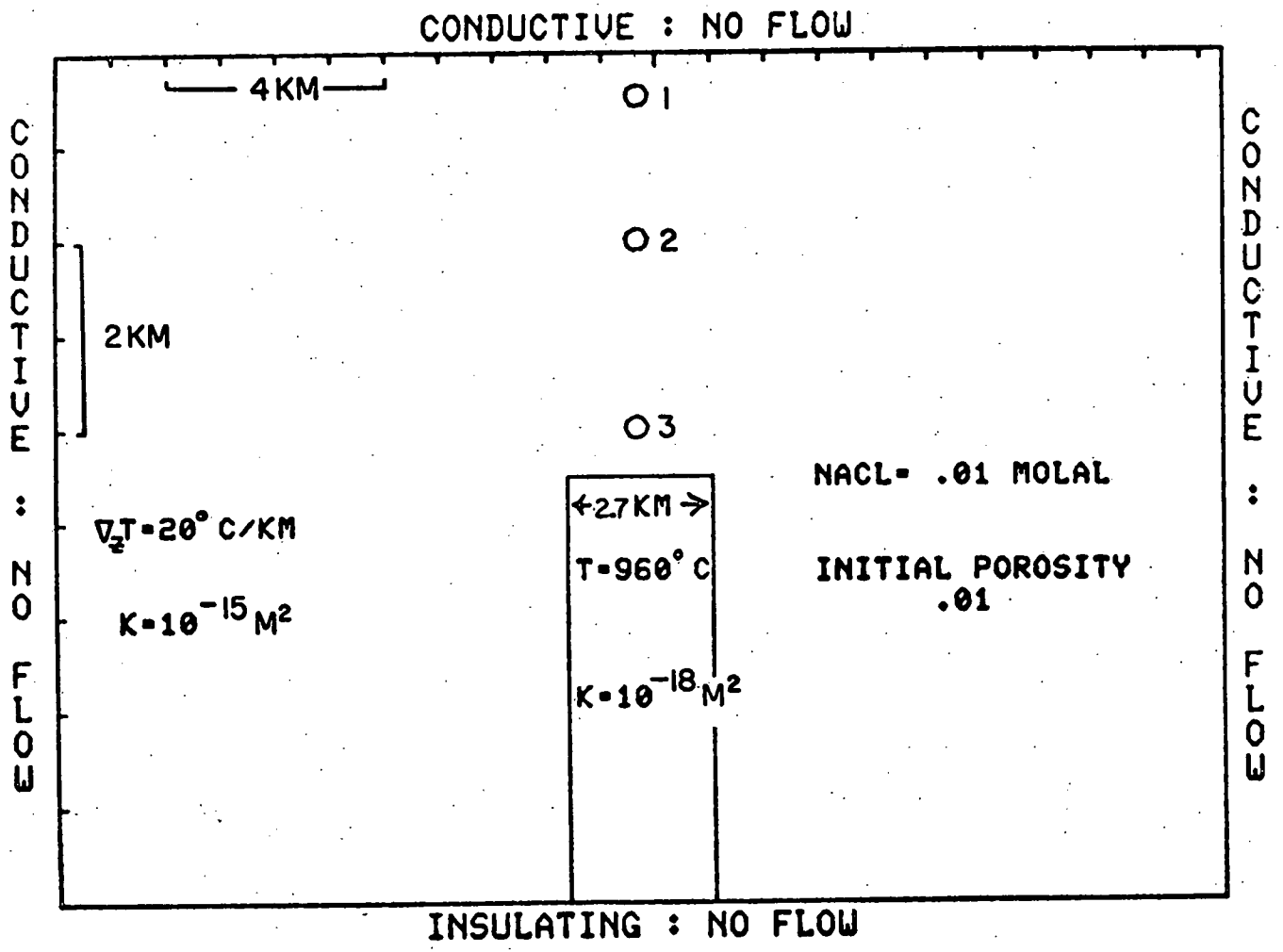
CONDUCTIVE : NO FLOW
4KM
O1
O2
O3
2KM
CONDUCTIVE : NO FLOW
CONDUCTIVE : NO FLOW
$\nabla_z T = 20^\circ$ C/KM
$K = 10^{-15}$ M²
2.7KM
T = 960° C
$K = 10^{-18}$ M²
NACL = .01 MOLAL
INITIAL POROSITY
.01
INSULATING : NO FLOW

Figure 4

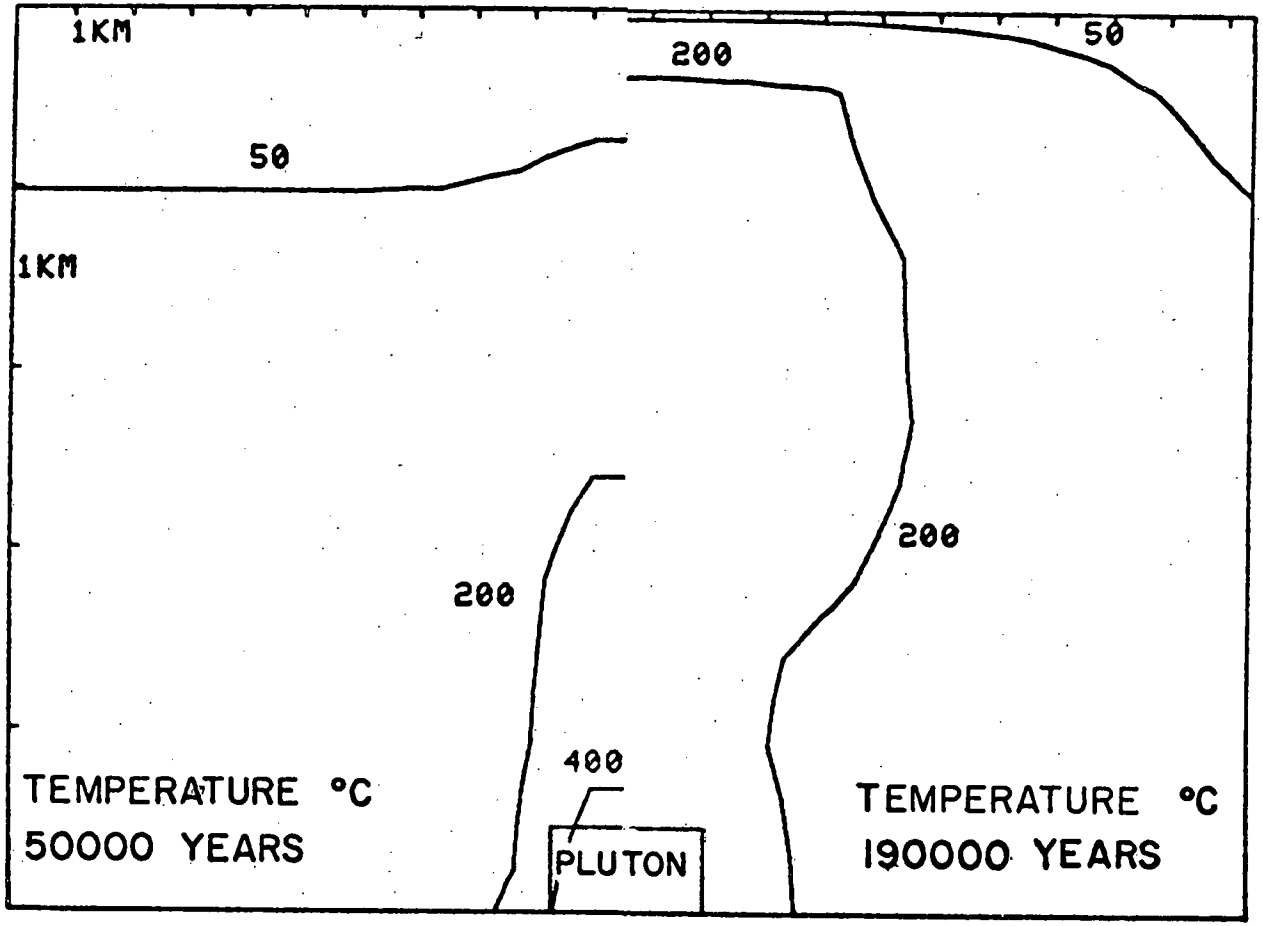
1KM
50
200
50
1KM
200
200
400
PLUTON
TEMPERATURE °C
50000 YEARS
TEMPERATURE °C
190000 YEARS

Figure 5

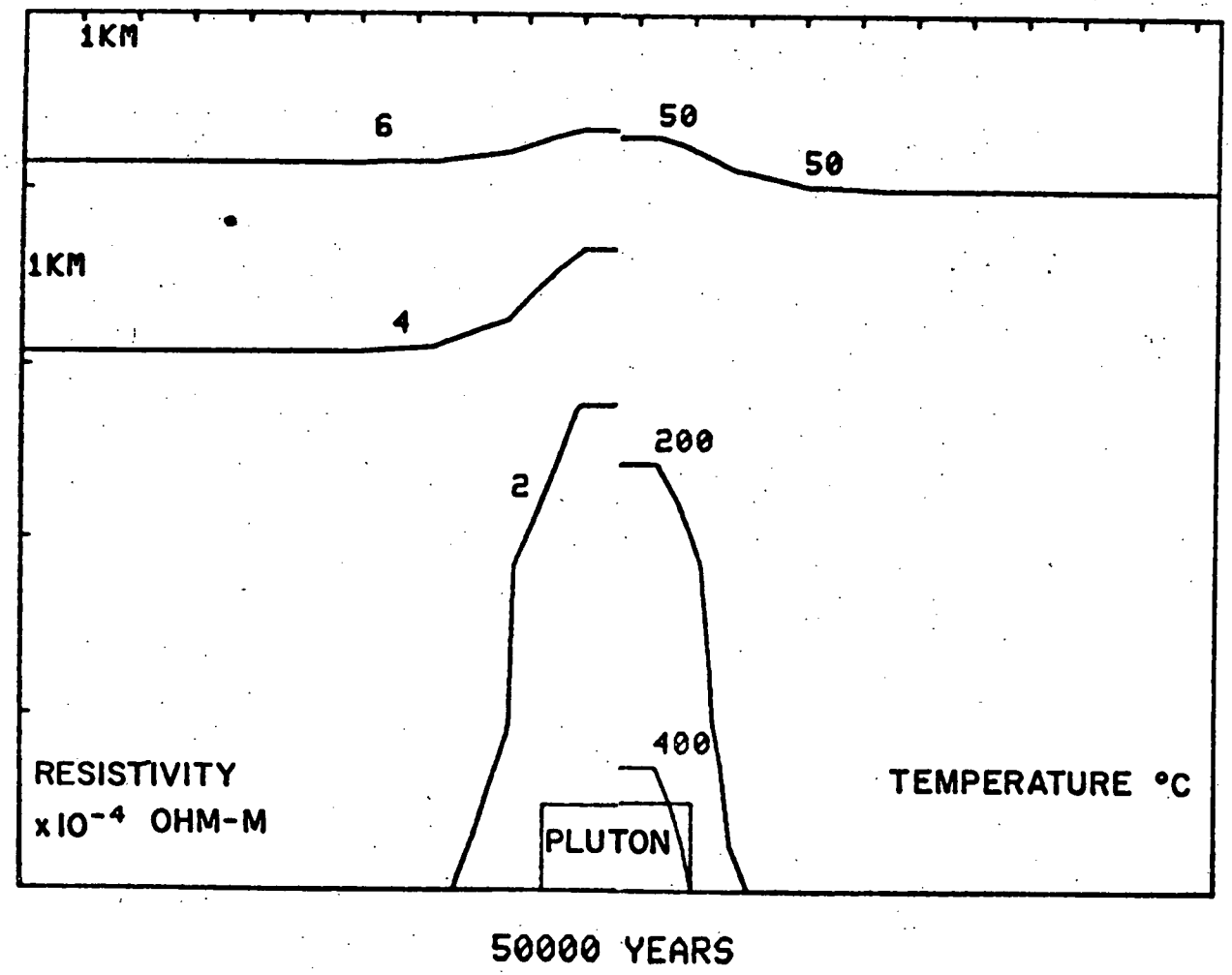
1KM
6
50
50
1KM
4
2
200
400
RESISTIVITY
x10⁻⁴ OHM-M
PLUTON
TEMPERATURE °C
50000 YEARS

Figure 6

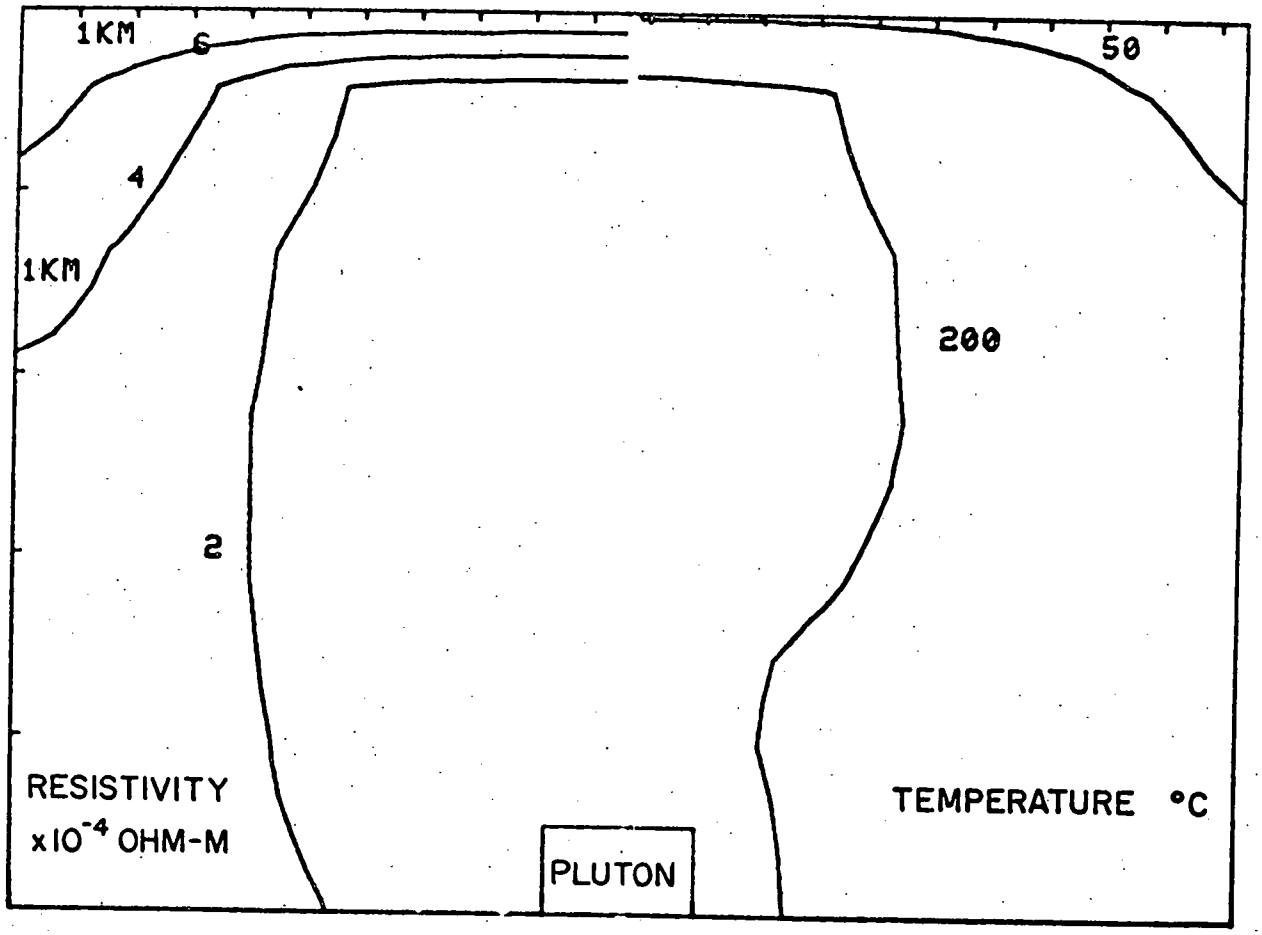

1.9×10^5 YEARS

Figure 7

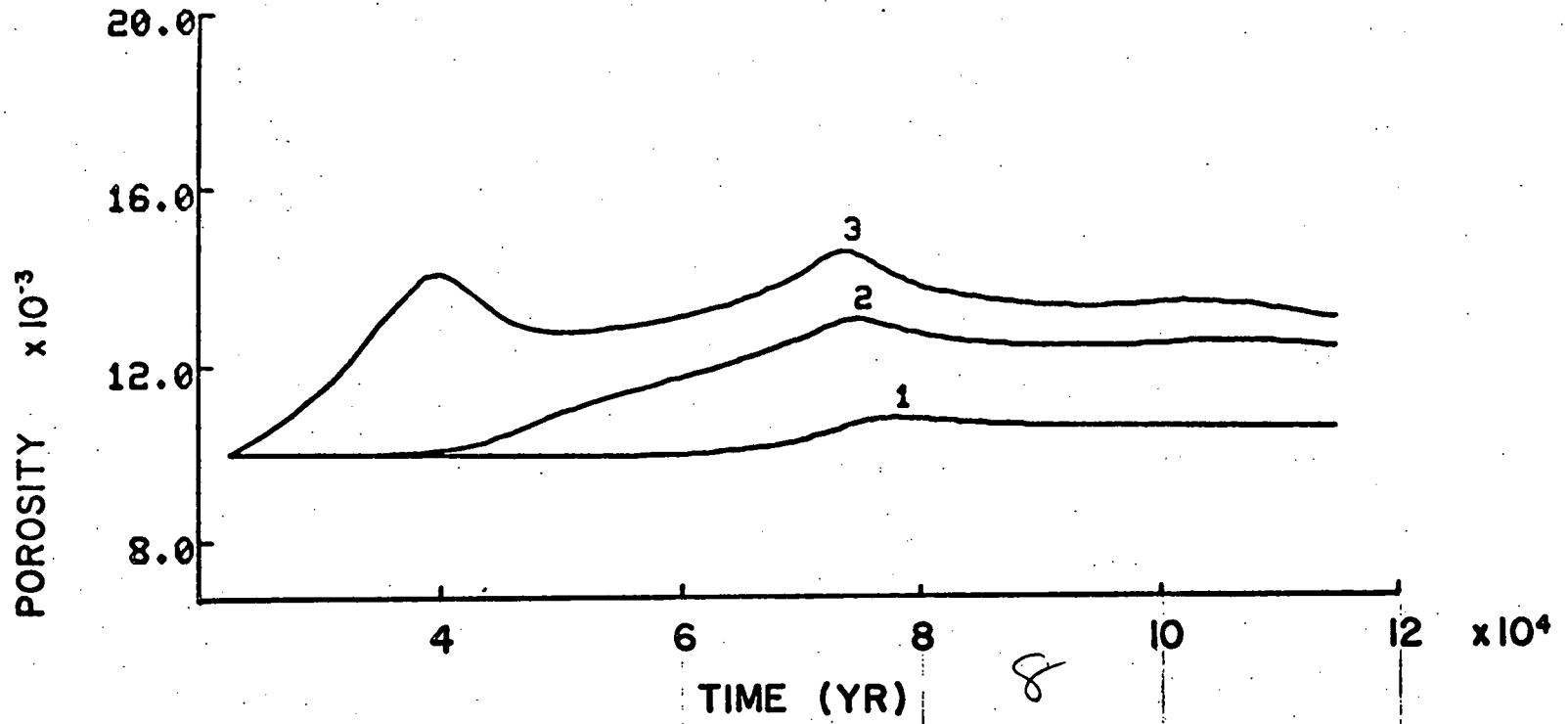

Figure 8

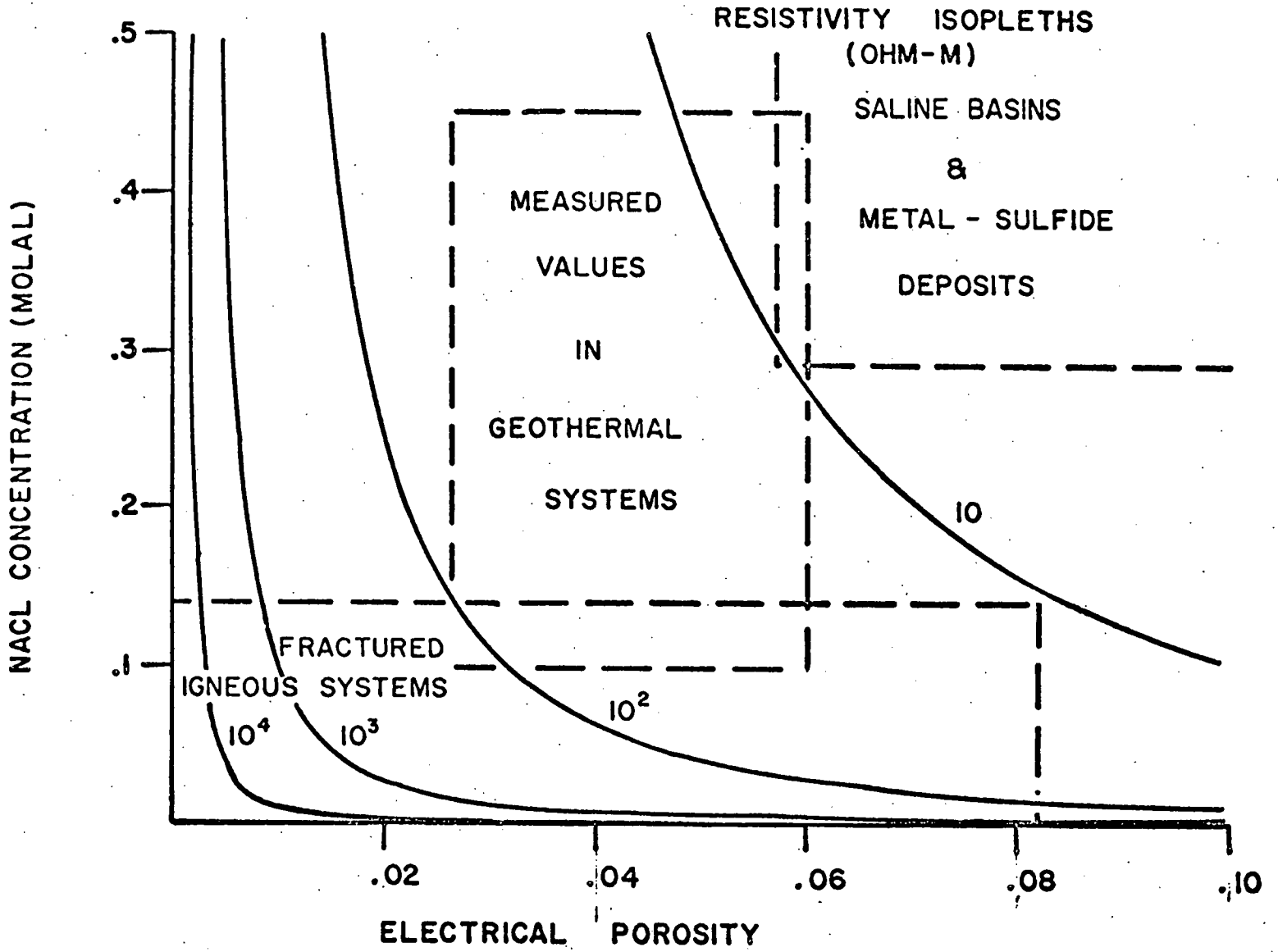
RESISTIVITY ISOPLETHS
(OHM-M)
SALINE BASINS
&
METAL - SULFIDE
DEPOSITS
MEASURED
VALUES
IN
GEOTHERMAL
SYSTEMS
FRACTURED
IGNEOUS SYSTEMS
10
10²
10³
10⁴
.5
.4
.3
.2
.1
.02
.04
.06
.08
.10
NACL CONCENTRATION (MOLAL)
ELECTRICAL POROSITY

Figure 9

THIS PAGE
WAS INTENTIONALLY
LEFT BLANK

APPENDIX II-2

The following is a preprint of a paper which is to appear in Am. Geophys. Union Mon. #20 on the Earth's Crust. This contribution is the result of research supported in part by the ERDA contract EY-76-S-02-2763.

THIS PAGE
WAS INTENTIONALLY
LEFT BLANK

FLUID CIRCULATION IN THE EARTH'S CRUST

Denis Norton
Department of Geosciences
University of Arizona, Tucson, Arizona 85721

Abstract

Numerical simulation of thermally driven fluid flow caused by igneous intrusives in the upper crust indicates that fluid circulation is an inevitable consequence of lateral density gradients in pore fluids characteristic of these environments. Thermal perturbations associated with igneous plutons are predicted to be sufficiently large to generate hydrothermal systems in which the magnitude of convective heat transport exceeds that of conductive heat transport for rock permeabilities greater than 10^{-18} m^2, Norton and Knight, 1977. Furthermore, the style of the heat transfer is significantly different from systems in which conduction is the dominant heat transfer mechanism, particularly when the transport and thermodynamic properties of the fluid phase are taken into account. As a consequence of the critical end-point which exists in the H_2O and related systems, the region above plutons is predicted to contain extensive vertical zones of nearly constant temperature.

These first order approximations of fluid circulation reveal several points relevant to predicting the thermal regime of the crust: (1) thermal gradients above convection dominated systems are very nonlinear and cannot uniquely predict subsurface temperatures within out present scope of

of knowledge and data, and (2) since fluid circulation may extend through a considerable portion of the upper crust in tectonically active regions, the thermal regime of these crustal regions is poorly understood.

Introduction

Temperature conditions in the earth's crust are normally predicted on the basis of extrapolated temperature-gradient data, petrologic arguments, and numerical approximations of conductive heat transfer processes in which various thermal energy sources, as well as rock properties, are considered. Analyses of thermal convection have usually indicated fluid circulation to be an important heat transport process, at least in geothermal areas (Elder, 1965; Ribando et al., 1976; Lister, 1974; Lowell, 1975). However, the consequences of fluid circulation on the thermal conditions in the crust have only recently been analyzed for situations in which (1) the transport and thermodynamic properties of the fluid phase are allowed to vary with temperature and pressure changes and (2) an igneous intrusive body is present in the upper crust.

The unique characteristics of fluid systems for which H_2O is a principal component suggest that the properties of these types of fluids should contribute significantly to the heat transport process in convection dominated systems, Norton and Knight, 1977. Enthalpy, density, and viscosity of phases in the pure H_2O-system and in SALT-H_2O stystems are very dependent on temperature and pressure in a temperature-pressure

region which starts at the critical end-point and extends to higher pressures. As a consequence of this dependence, natural systems are predicted to have thermal characteristics distinctly different from those predicted on the basis of constant fluid properties or even those predicted on the basis of properties approximated by simplistic equations of state. Most equations of state that have been previously used merely predict fluid properties along the two-phase surface in the H_2O or SALT-H_2O systems.

Crustal environments which contain hot igneous bodies inevitably cause fluid circulation, and, if the intrinsic host rock permeability is greater than 10^{-18} m^2, heat transfer by convection accounts for at least 10% of the total heat transfer, and at permeabilities greater than 10^{-18} m^2 convection greatly predominates over conduction, Norton and Knight, 1977. Fluid driving forces are generated as a natural consequence of the near-vertical side contact of intrusives, which cause lateral perturbations in the density of pore fluids. Instability of the fluids and the onset of convection is, therefore, instantaneous in these systems; the magnitude of the initial fluid flux depends principally on permeability of host intrusive rocks.

The purpose of this communication is to review the nature of fluid circulation related to transient thermal anomalies in the crust and to consider the consequences this fluid circulation might have on our concepts of the thermal environment in the crust.

Numerical Simulation of Fluid Circulation

Lateral density perturbations in fluids contained in the flow porosity of rocks cause fluid flow. The magnitude of this flow in natural systems can be determined by Darcy's Law:

$$(1) \quad \bar{q} = \frac{k}{\nu} (\nabla P + \rho \bar{g}),$$

where the mass flux, $\bar{q}$, is a function of intrinsic rock permeability, k, fluid viscosity, ν, and density, ρ, the gradient in pressure, ∇P, and the gravitational vector, $\bar{g}$. Density gradients, which may be the result of concentrations as well as thermal gradients on the fluid, give rise to $\nabla_x P$ and $\nabla_y P$ terms in the horizontal plane. Although both types of density gradients are ubiquitous in the crust, only those resulting from anomalies are included in the computations.

Thermal anomalies often cause and are coincident with extensive fracture zones and, therefore, probably represent the most significant contribution to fluid circulation in the crust, except in sedimentary basin environments where large concentration gradients are common. The inferred association of permeable fractured rocks with thermal anomalies in the upper 10 - 15 km of the crust suggests that fluid circulation is a characteristic feature in these environments.

Fluid flow caused by thermal anomalies related to igneous plutons are effectively scaled and represented in two dimensions by partial differential equations which describe the conservation of mass, momentum, and energy for the fluid-rock system, Norton and Knight, 1977:

$$(2) \quad \gamma \frac{\partial T}{\partial t} + q\nabla H = \nabla \cdot \kappa \nabla T$$

and

$$(3) \quad \frac{\nu \nabla \cdot \nu}{k \; k} \nabla \Psi = R \frac{\partial \rho}{\partial y},$$

where T is the temperature, Ψ the streamfunction, q the fluid flux, t the time, H, ρ, and ν are the enthalpy, density, and viscosity of the fluid, k is the permeability of the rock, κ the thermal conductivity and γ the volumetric heat capacity of the fluid saturated media, R the Rayleigh number, t the time, ∇ the gradient operator, and y the horizontal distance in the two-dimensional section to which these equations apply.

The physical meaning of equations (2) and (3) is apparent if one considers that the fluid density gradients, right-hand side of equation (3), resulting from a thermal anomaly cause fluid circulation, e.g., define gradient values of the streamfunction and, therefore, fluid flux, since $q_z = -\frac{\partial \Psi}{\partial y}$ and $q_y = \frac{\partial \Psi}{\partial z}$. The fluid flux, q, in turn transports heat away from the thermal anomaly, second term on left of equation (1); at the same time, thermal energy is conducted away from the thermal anomaly, right-hand side in equation (2). Both of these processes give rise to a decrease in temperature with respect to time and, therefore, decrease the horizontal fluid density gradients. And, consequently, the thermal anomaly is decreased by combined convective and conductive heat transfer. Equations (2) and (3) are approximated by finite difference numerical equations which permit computation of the values of the dependent variables at discrete points in the domain from initial

and boundary values specified for the system. The numerical analysis provides the option to include variable transport properties of the fluid (H_2O-system) and rock, general boundary and initial conditions, and radioactive and volumetric heat sources in a two-dimensional domain. The transport processes related to the transient thermal anomaly are approximated by a time sequence of steady state numerical solutions to (2) and (3), computed at explicitly stable time intervals. An alternating-direction-implicit finite difference method is used to approximate the spatial derivatives at discrete intervals on the order of 0.1 to 0.5 of the system height. Fluid pressure in the system is computed at each steady state step by integration of equation (2) in which the fluid properties, viscosity and density, are expressed as a function of temperature and pressure. The following discussion relies on computations and analyses using these methods.

The Nature of Fluid Circulation Related to Thermal Anomalies

The style of fluid circulation in the upper 10 km of crust and the nature of pluton cooling has been simulated, Norton and Knight, 1977, for a variety of host rock permeability values and geometries.

Convection dominates heat transfer in hot igneous pluton environments if rock permeabilities are on the order of 10^{-18} m^2 or greater, resulting in a significantly different spatial redistribution of thermal energy than in similar environments in which conductive heat transfer predominates. Although the time duration of convection dominated thermal anomalies is

similar to conduction dominated systems when the pluton itself is impermeable, the cooling time is significantly shortened by increases in permeability, such as might accompany extensive fracturing of the pluton. The direct application of these modeling results to actual systems must be made with caution since the in-situ values of rock permeability are virtually unknown. However, analogies drawn between rocks for which permeability data are available and estimates of permeability suggest that permeability values exceeding the 10^{-18} m^2 minima may characterize a substantial portion of the upper crust, Norton and Knapp, 1977.

A numerical model of a system which illustrates the convective transfer of heat around igneous plutons is presented. A basaltic magma at $\sim$ 1300°C is presumed to be emplaced relatively rapidly with respect to the rate of heat transfer away from the magma body, into host rocks whose permeability increases upward from 10^{-18} m^2 to 10^{-14} m^2, figure 1. The relatively rapid intrusion rate only requires magma flow velocities on the order of a few cm/yr, which seems to be reasonable. Since cooling of magmas is normally accompanied by fracture development resulting from reactions that increase or decrease the pluton volume, the pluton permeability is changed from effectively zero to 10^{-17} m^2 as the temperature of discrete grid points in the pluton decreases to < 700°C, thereby simulating fracture development and permitting fluid circulation through the pluton.

Boundary conditions selected for this system are analogous

to natural systems where thermal energy is conducted through all the boundaries. The bottom and top boundary temperatures are set to 220°C and 20°C, respectively. Thermal conductivity of the domain is assumed to be constant, 0.6 cal/ms°C, and, since the bottom boundary is conductive, the domain has a constant regional flux of 1.2 HFU and the host rocks have an initial background thermal gradient of 20°C/km. The relative permeability values within the domain are set to simulate the decrease in continuous fractures with depth, and the magnitude of the permeability is set to illustrate the effects of fluid circulation. The side and top boundaries are permeable, but the base is impermeable in order to further simulate decrease in permeability with depth. The permeable top boundary condition does not, however, permit convection of thermal energy out of the system. This latter condition simulates natural systems which do not have hot springs emerging at the top boundary, e.g., the fluids flow through and thermally equilibrate with the rocks at the top boundary. This system was then simulated using a spatial discretization of 160 points, which results in an 0.1 vertical increment and an 0.06 horizontal increment. The numerical approximations represent the partial differential equations to within a truncation error on the order of 0.05 of the value of the dependent variable. Discrete time increments are computed on the basis of stability criteria, which results in convergence errors on the order of 0.005 of the dependent variable.

The thermal anomaly, introduced by the pluton, causes pore

fluids in the host rocks to circulate from the sides and top boundaries of the domain toward the pluton then upward along its side margins and out the top of the domain, figures 2 - 4. This circulation pattern significantly increases the heat flux over the pluton top, with respect to a purely conductive process. As a consequence of the convective heat transfer, thermal gradients in the domain directly over the pluton are relatively steep near the surface, i.e., 0 - 0.5 km, decrease sharply and remain constant over several km, then gradually increase toward the pluton top, figures 5a - c. The conductive heat flux at the surface directly above the pluton varies from 1.2 HFU at the initial time to 15 HFU at 8×10^4 years, whereas the vertical component of convective flux at 0.5 km depth ranges from 0.5 HFU at 2×10^4 years to 20 HFU at 8×10^4 years and then gradually decreases to 10 HFU at 1.5×10^5 years.

The caveat about these values at the surface is that they are arbitrary to the extent that they are a function of the numerical discretization. However, the relative comparison between the values in the same system at various times is a reasonable approximation of what can be expected in nature. Finer discretization merely results in a nonlinear thermal gradient and predicts it to better precision. Progressive fracturing of the pluton contributes to the persistence of large convective heat fluxes over a long time period. The estimated time duration for which convective fluxes will be greater than the regional heat flux in the upper 2 km of the system is about 5×10^5 years.

Laterally away from the pluton, thermal gradients in the fluid down-flow zone are depressed below the regional gradients as a result of the convective heat flux of -3 HFU. In these regions, at cooling times $\sim 1.2 \times 10^5$ years, the isotherms are depressed downward with respect to their regional position, cf. 200°C isotherm. The portion of the anomaly, at temperatures > 100°C, in the upper 3 km is dispersed over an area equivalent to the pluton top.

The several kilometer vertical extent of relatively constant thermal gradients in the host rocks overlying the pluton and the corresponding temperature values, 100 - 400°C, is characteristic of convection dominated systems which we have analyzed, Norton and Knight, 1977. Transport and thermodynamic properties of supercritical fluid in the H_2O-system and SALT-H_2O systems are characterized by extremes which contribute to these thermal gradient features, figure 6. In the region which extends from the critical end-point, $\sim$ 375°C and 220 bars for the H_2O-system, derivatives of fluid density and enthalpy with respect to temperature at constant pressure are maximums and fluid viscosity is a minimum. Therefore, thermal perturbations at these conditions result in the largest fluid density gradients which together with the minimum in the fluid viscosity tend to maximize the fluid fluxes. The heat capacity of the fluid is also a maximum of these conditions, and, hence, the convective heat transport is maximized in this temperature-pressure region. As a point of interest, these extremes tend to decrease in magnitude from the region near the critical

end-point to lesser extremes at higher pressures. The critical end-point and related extremes in fluid properties are displaced to higher temperatures and pressures for SALT-H_2O systems, figure 6. Fluids which contain dissolved components equivalent to a 3 molal NaCl solution have a critical end-point at 590°C and 850 bars, and the extremes in fluid properties extend into a region analogous in position to the pure H_2O-system, figure 6.

The nature of the thermal gradients within permeable rocks overlying thermal anomalies in a natural system is clearly predicated on the values of fluid properties and permeability. Since the fluid properties, at least for the H_2O-system, are relatively well known, one can reasonably assume these thermal gradients will at least be characteristic of environments where rock permeabilities are $\geq 10^{-18}$ m^2 and anomaly temperatures are $\geq$ 375°C, at depths where pressures are greater than 220 bars, i.e., $\sim$ 2.2 km. In natural environments where dissolved components are relatively more concentrated, these effects will be realized at progressively greater depths and slightly higher temperatures.

The example system discussed above contains relatively high values of rock permeabilities with respect to our current best guesses of conditions in the crust. However, fluid circulation effects have been observed in models where the pluton tops are 12 km deep, within low permeability rocks, 10^{-20} m^2, but are overlain by higher permeability, 10^{-18} m^2, zones which simulate vertical fractures. Thermal gradients are more linear

in these systems than in the system discussed above, but only a few percent contribution to the heat flux by convection has significant effect on our interpretations of the thermal environment in the crust. The most significant feature of the simulated system is that vertical thermal gradients in systems where convective heat transfer occurs do not provide a unique set of data with which subsurface temperatures can be predicted.

Fluid Circulation in the Crust

Fluid circulation in the upper crust is predicted to be more extensive than previously thought; its magnitude may be large enough to contribute significantly to the redistribution of thermal energy in this environment. The magnitude of the contribution of fluid circulation to heat transport depends entirely on the magnitude of permeability in crustal rocks and the distribution, with respect to thermal anomalies, of fluid saturated rocks with permeabilities $\geq 10^{-18}$ m^2. Minimum permeability value is realized in rocks which have continuously open-planar fractures spaced 0.1 km apart with an effective aperture $\sim$ 20 μm, Norton and Knapp, 1977; Snow, D., 1970. This abundance of continuous fractures is easily realized in tectonically active regions and in pluton environments, Villas, 1975, but apertures and continuity of fractures with respect to depth are unknown. In tectonically quiescent regions neither abundance nor aperture of fractures have been documented. However, indirect evidence suggests that permeabilities sufficient to permit significant heat transfer by convection may be realized in the upper crust. First, in tectonically active

regions continuous fractures develop to considerable depths, as indicated by earthquake hypocenter data, and, second, igneous intrusive processes contribute to development of fracture sets in the rocks they intrude. The extent and magnitude of the permeability resulting from combined tectonic and igneous intrusive events is clearly conducive to extensive fluid circulation, as evidenced by eroded equivalents to these environments which show abundant mineral alteration, as well as large gains and losses of chemical components in and adjacent to fractures. Transport of thermal energy into the crust by magma or simple conduction also produces fractures due to the differential thermal expansion of pore fluids and rocks, Knapp and Knight, 1977. In tectonically less active regions, permeability values can be inferred from electrical and, perhaps, seismic properties, empirical relationships between pore continuity, and electrical resistivity, Brace, 1971, or variations in seismic wave velocity, Nur and Simmons, 1969. These indirect lines of evidence suggest that crustal rocks contain a fluid phase, which may be relatively concentrated in dissolved components, and are sufficiently permeable to warrant further efforts toward quantitative determination of bulk rock permeability.

Analyses of transport phenomena in permeable media suggest that fluid circulation through fractured rocks may contribute significantly to heat transfer through the crust, at least to depths of 10 - 15 km. As a consequence of fluid circulation, several effects may be realized in nature: lower than normal

thermal gradients over several kilometer vertical distances in the upper crust; abnormally low conductive thermal values coincident with fluid down-flow zones; and gross errors in predicting subsurface temperatures by downward extrapolation of thermal gradients. These effects are undoubtedly present in active geothermal systems and can be predicted, with reasonable confidence, to occur in the vicinity of virtually all igneous bodies emplaced into the upper crust. The more widespread realization of the effects in more normal crust is mere speculation at this time, and many questions remain that will require more precise numerical models and data acquisition. However, this first approximation suggests that the nature of the upper crustal environment may indeed be the result of dynamic fluid systems, the extent of which are unknown.

Acknowledgments

This work was supported by funds provided by ERDA, contract E-11-1-2763, and NSF Grant EAR74-03515 A01 for which the author is grateful. Discussions with numerous colleagues have contributed extensively to the author's current concept of the physical properties of rocks at depth. I am grateful for discussions with W. F. Brace, and for his published work that provided the incentive to consider the problem of permeability distribution in the crust, and to L. McLean for her editorial assistance in preparing the manuscript.

References

Brace, W. F., 1971, Resistivity of saturated crustal rocks to 40 km based on laboratory measurements: Am. Geophys. Union Mon. #14, p. 243-255.

Elder, J. W., 1965, Physical processes in geothermal areas: Am. Geophys. Union Mon. #8, p. 211-239.

Knapp, R., and Knight, J., 1977, Permeability of rocks in hydrothermal systems: Fracture propagation by pore fluid expansion: Jour. Geophys. Res., in press.

Lister, C. R. B., 1974, On the penetration of water into hot rock: Geophys. Jour. Royal Astr. Soc., v. 39, p. 465-509.

Lowell, R. P., 1975, Circulation in fractures, hot springs, and convective heat transport on mid-ocean ridge crests: Geophys. Jour. Royal Astr. Soc., v. 40, p. 351-365.

Norton, D., and Knight, J., 1977, Transport phenomena in hydrothermal systems: Cooling plutons: Am. Jour. Sci., v. 277, in press.

Norton, D., and Knapp, R., 1977, Transport phenomena in hydrothermal systems: The nature of porosity: Am. Jour. Sci., v. 277, in press.

Nur, A., and Simmons, G., 1969, The effect of saturation on velocity in low porosity rocks: Earth and Planet. Sci. Letts., v. 17, p. 183-193.

Ribando, R. J. et al., 1976, Numerical models for hydrothermal circulation in the oceanic coast: Jour. Geophys. Res., v. 81, no. 17, p. 3007-3012.

Snow, D. T., 1970, The frequency and aperture of fractures in rocks: Jour. Rock Mech., v. 7, p. 23-40.

Villas, R. N., 1975, Fracture analysis, hydrodynamic properties, and mineral abundances in altered igneous rocks at the Mayflower Mine, Park City District, Utah: Unpublished Ph.D. dissertation, University of Utah, 254 p.

Figure Captions

Figure 1. Two-dimensional cross section of crust 10 km deep and 24 km wide containing igneous pluton 4 km high and 6 km wide. Initial value and boundary conditions for magma body emplaced instantaneously at 6 km below surface. Pluton permeability is effectively zero until temperature of discrete points in body decreases to 700°C, then permeability at those points is set to 10^{-17} m^2. Regional heat flux is set at 1.2 HFU for the duration of the system, and the initial thermal gradient is 20°C/km, whereas the magma is homogeneous and is connected to a magma reservoir below base of pluton at T = 1300°C for the initial 50,000 years. Thermal conductivity is constant at 0.6 cal/°C ms; the circulating fluid is pure H_2O and does not react with the enclosing rocks.

Figure 2. Scalar streamfunction (g/ms) and temperature (°C) distributions after 2 x 10^4 years elapsed time, illustrating steady state fluid circulation and temperature, respectively. Vertical fluid fluxes on the order of 5 x 10^{-5} g/m^2s are realized 3 km directly above pluton, which, together with conductive heat transfer, causes 100°C isotherm to migrate upward at about 0.05 m/yr.

Figure 3. Scalar streamfunction and isotherm distributions after 8×10^4 years elapsed time. Vertical fluid fluxes on the order of 10^{-3} g/m^2s are realized 3 km directly above pluton, and, 8 km laterally away from this up-flow zone, downward fluid fluxes, $\sim 10^{-14}$ g/m^2s, occur.

Figure 4. Scalar streamfunction and isotherm distributions after 1.5×10^5 years elapsed time. Vertical fluid fluxes at comparable positions in previous times have decreased to about 50 percent of the fluxes at 8×10^4 years. The 100^oC and 200^oC isotherms have moved to slightly deeper portions in response to the decreasing convecture flux. The outer 1.5 km of the upper 2 km of pluton fractured at 10^5 years, thereby increasing the cooling rate of the body. The average pluton temperature is 800^oC at this time.

Figure 5. Vertical thermal gradients from surface to base of system at elapsed times of (a) 2×10^4, (b) 8×10^4, and (c) 1.5×10^5 years. Vertical sections are located along the (1) center line of the pluton, (2) 1 kilometer away from the side wall of the pluton, and (3) 5 kilometers away from the side wall of the pluton, cf. figure 1 for positions.

Figure 6. Temperature-pressure sections through the NaCl-H_2O systems depicting the two-phase surface, liquid-vapor, and critical end-point for 0 and 3 molal NaCl concentrations. The approximate region of anomalous extreme in transport properties of supercritical fluid is depicted for 0 molal and 3 molal solution. Note the shift of the critical end-point and associated anomalous regions to higher temperatures and pressures as a result of adding NaCl to the system.

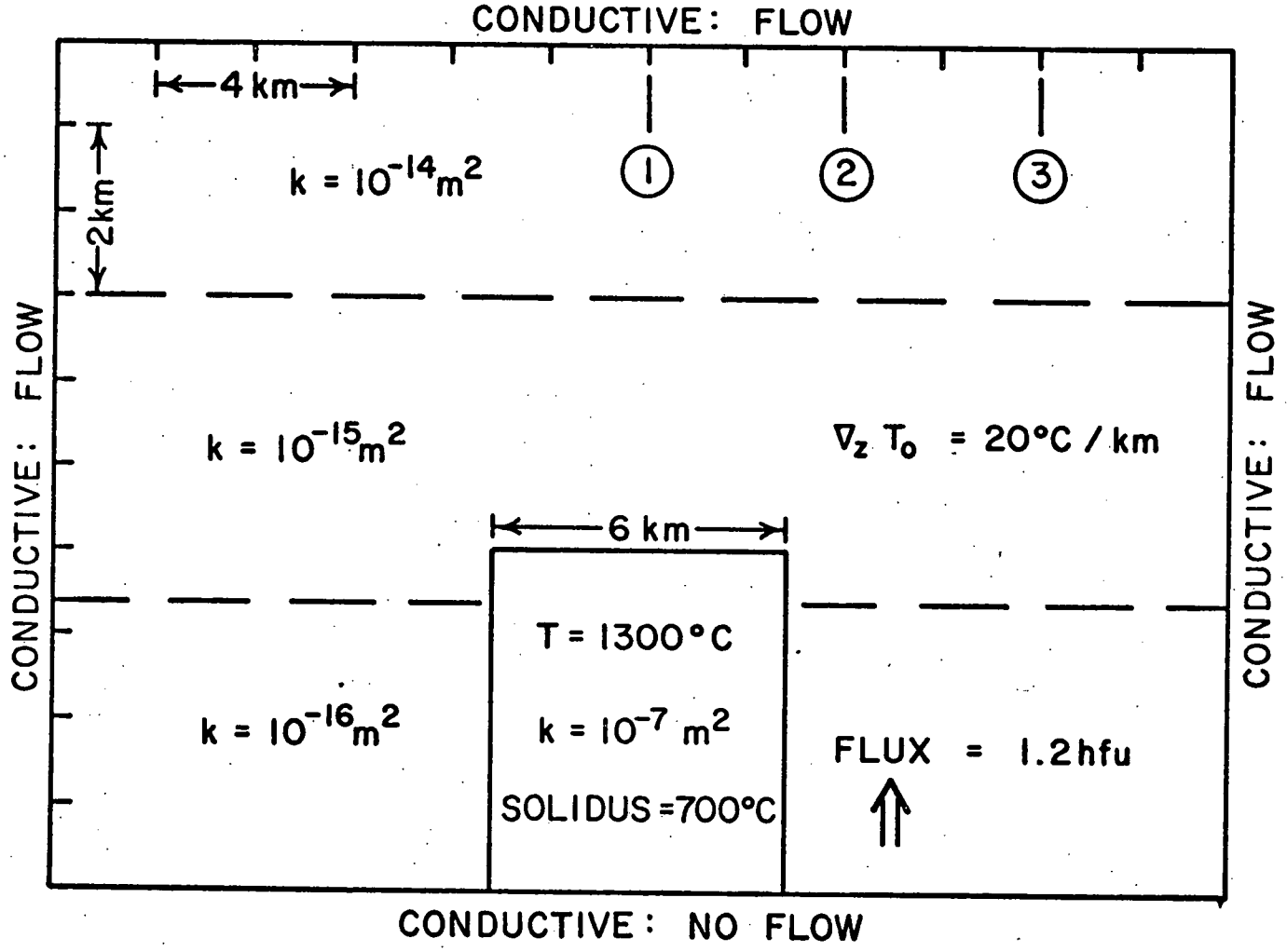
CONDUCTIVE: FLOW
4 km
2km
k = 10^-14 m^2
1
2
3
CONDUCTIVE: FLOW
CONDUCTIVE: FLOW
k = 10^-15 m^2
∇z To = 20°C / km
6 km
T = 1300°C
k = 10^-16 m^2
k = 10^-7 m^2
SOLIDUS = 700°C
FLUX = 1.2 hfu
CONDUCTIVE: NO FLOW

Figure 1

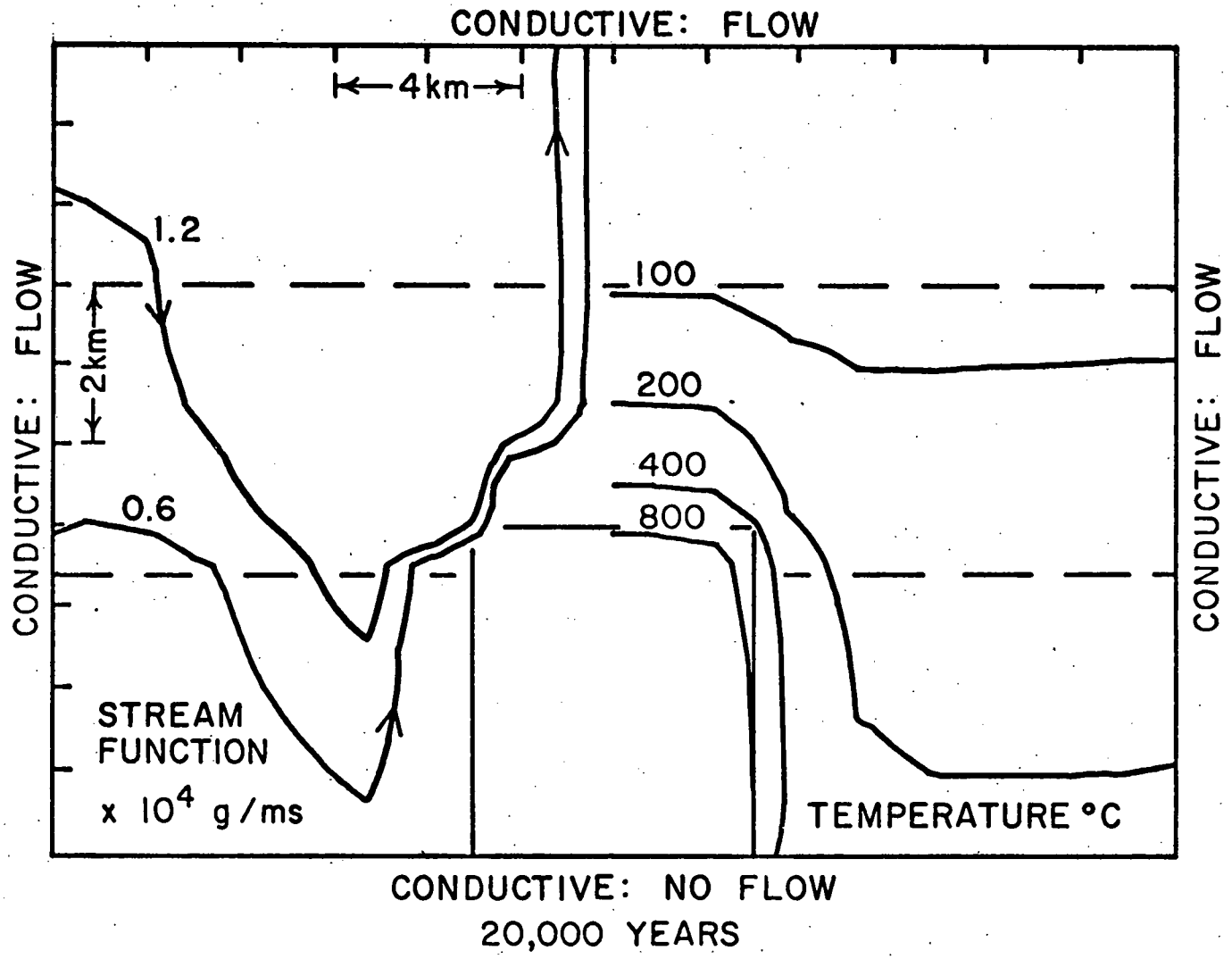
CONDUCTIVE: FLOW
4km
1.2
100
2km
200
400
0.6
800
CONDUCTIVE: FLOW
CONDUCTIVE: FLOW
STREAM
FUNCTION
x 10^4 g/ms
TEMPERATURE °C
CONDUCTIVE: NO FLOW
20,000 YEARS

Figure 2

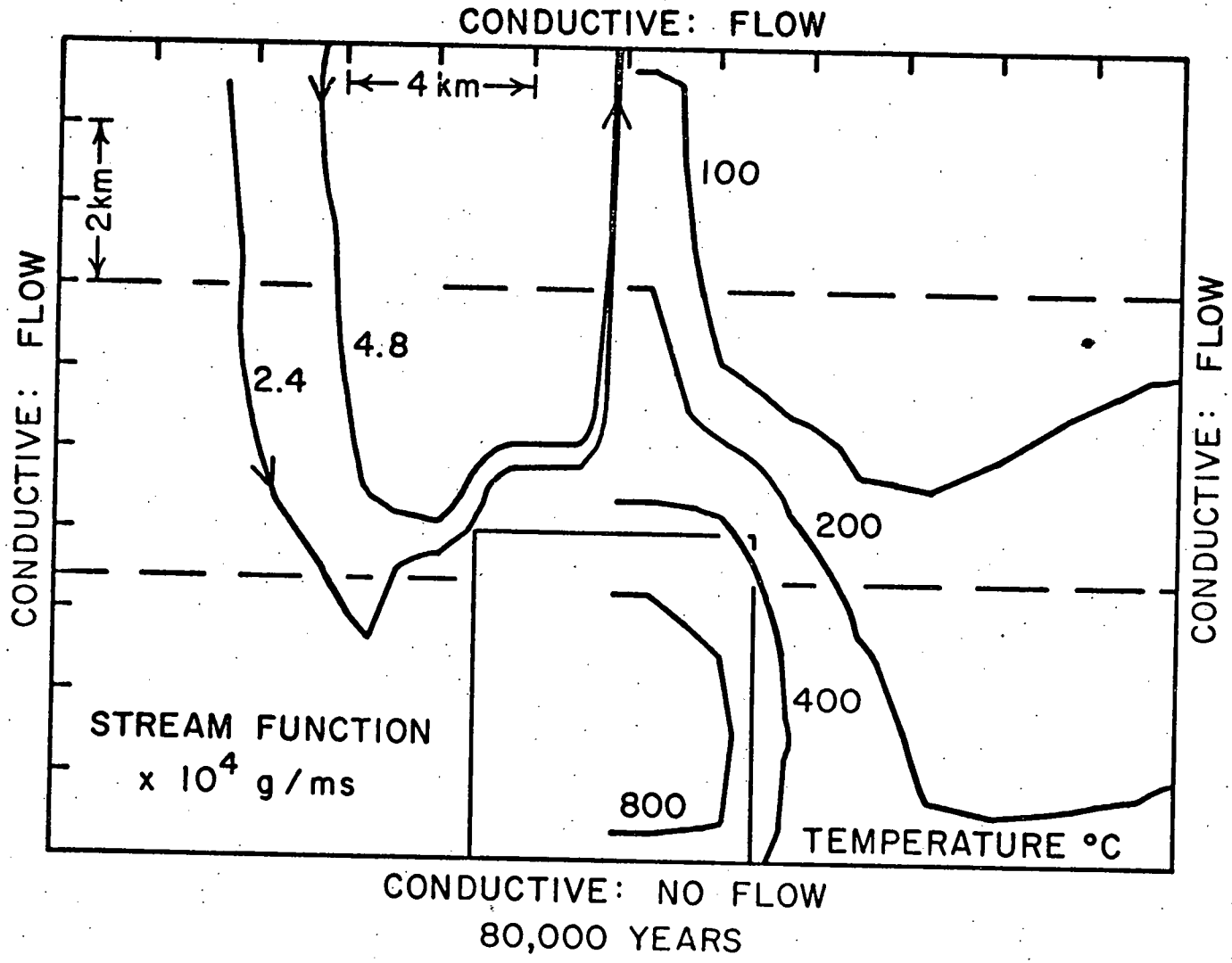
CONDUCTIVE: FLOW
4 km
2km
100
4.8
2.4
200
400
800
STREAM FUNCTION
x 10^4 g/ms
TEMPERATURE °C
CONDUCTIVE: FLOW
CONDUCTIVE: FLOW
CONDUCTIVE: NO FLOW
80,000 YEARS

Figure 3

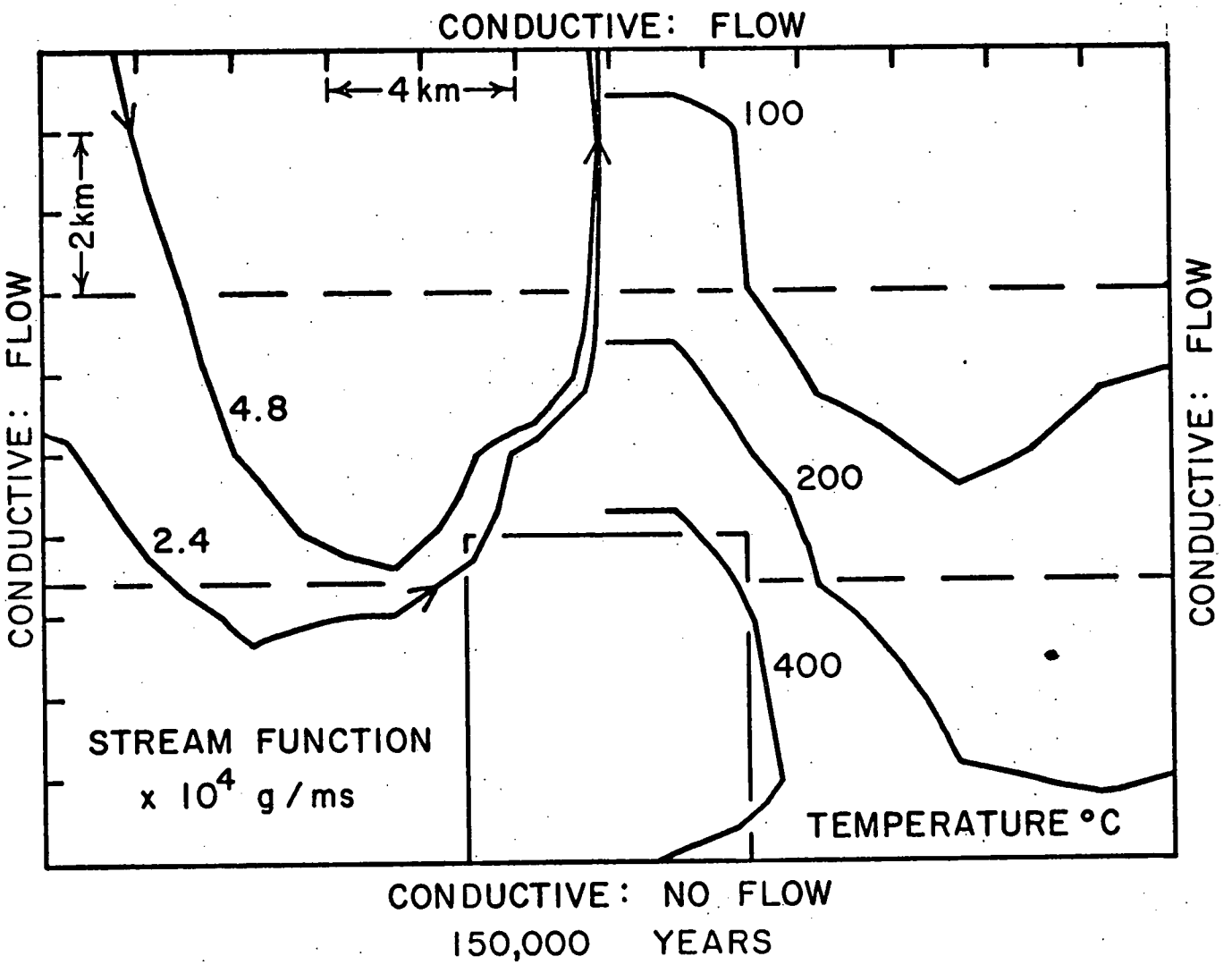
CONDUCTIVE: FLOW
4 km
2 km
100
4.8
200
2.4
400
CONDUCTIVE: FLOW
CONDUCTIVE: FLOW
STREAM FUNCTION
x 10^4 g/ms
TEMPERATURE °C
CONDUCTIVE: NO FLOW
150,000 YEARS

Figure 4

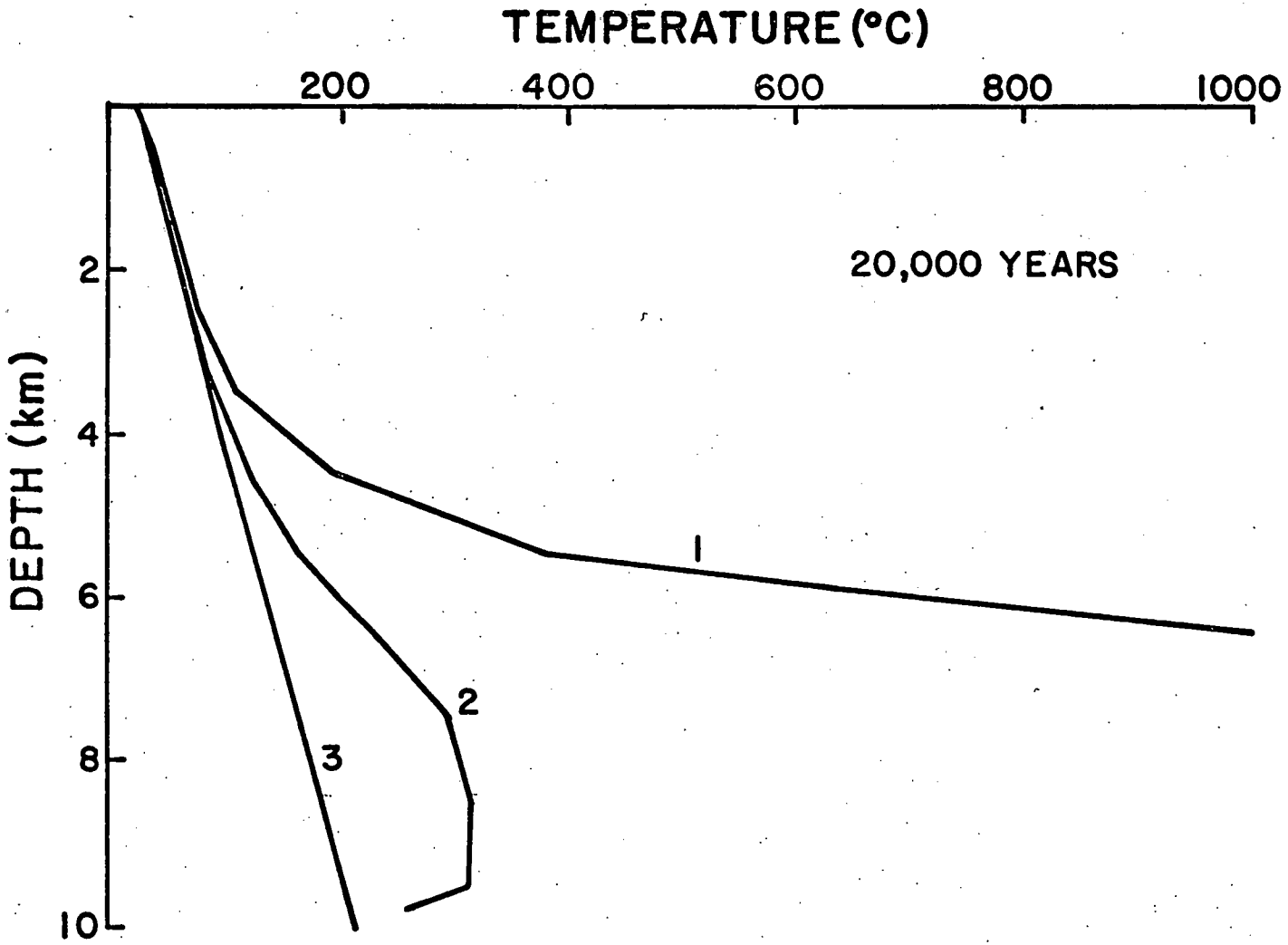
TEMPERATURE (°C)
200
400
600
800
1000
DEPTH (km)
2
4
6
8
10
20,000 YEARS
1
2
3

Figure 5a

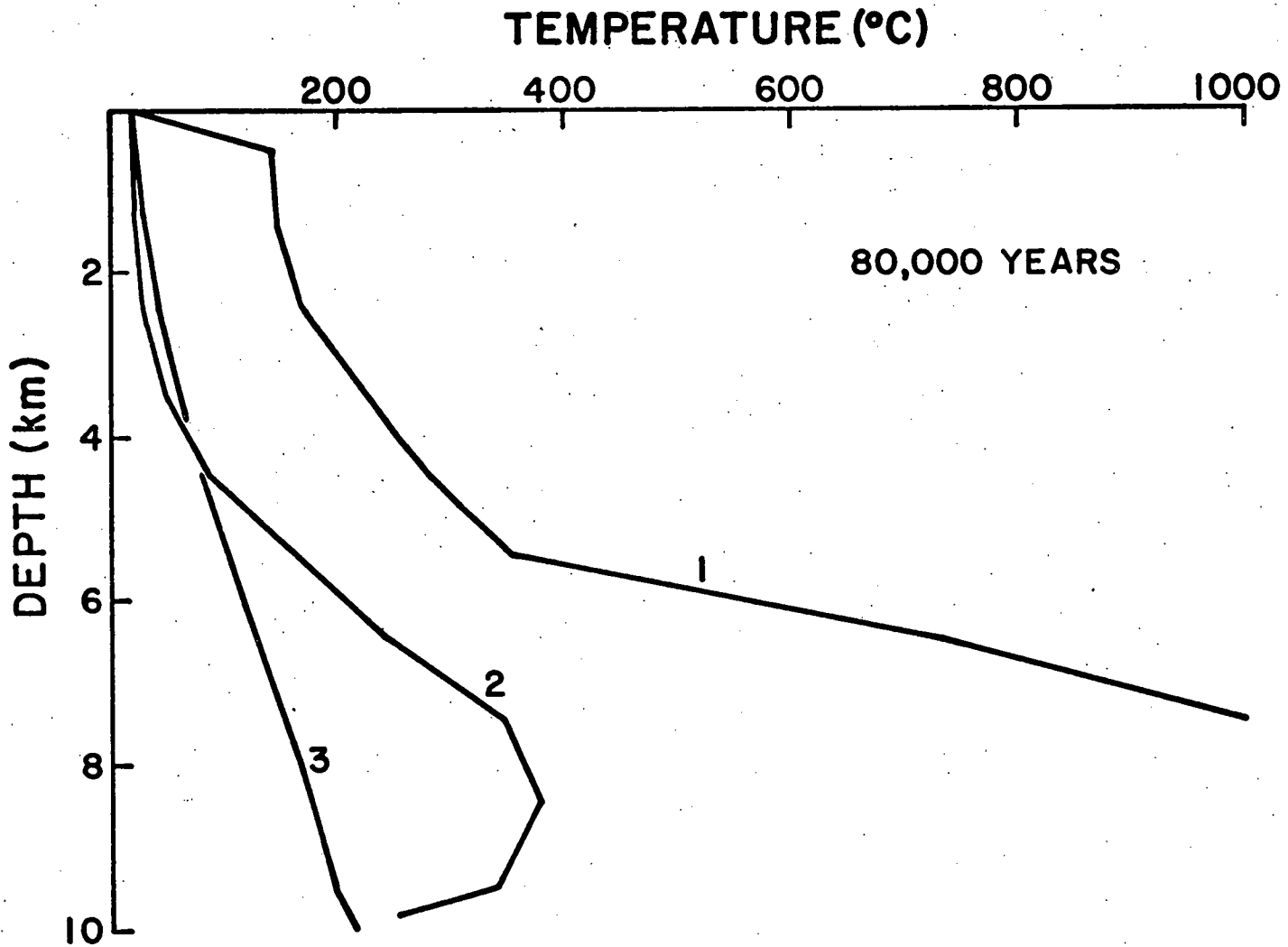
TEMPERATURE (°C)
200
400
600
800
1000
80,000 YEARS
DEPTH (km)
2
4
6
8
10
1
2
3

Figure 5 b

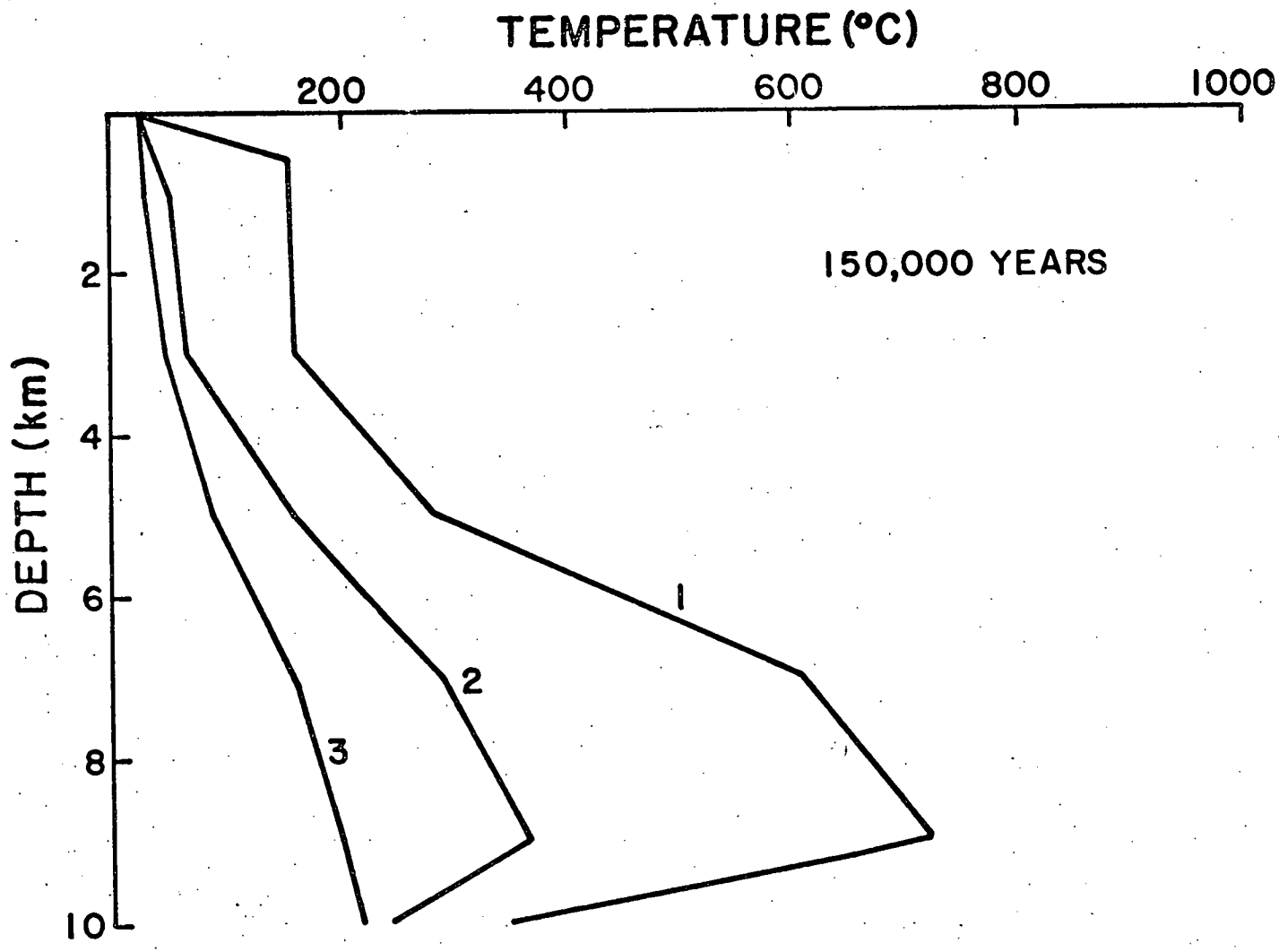
TEMPERATURE (°C)
200
400
600
800
1000
150,000 YEARS
DEPTH (km)
2
4
6
8
10
1
2
3

Figure 5c

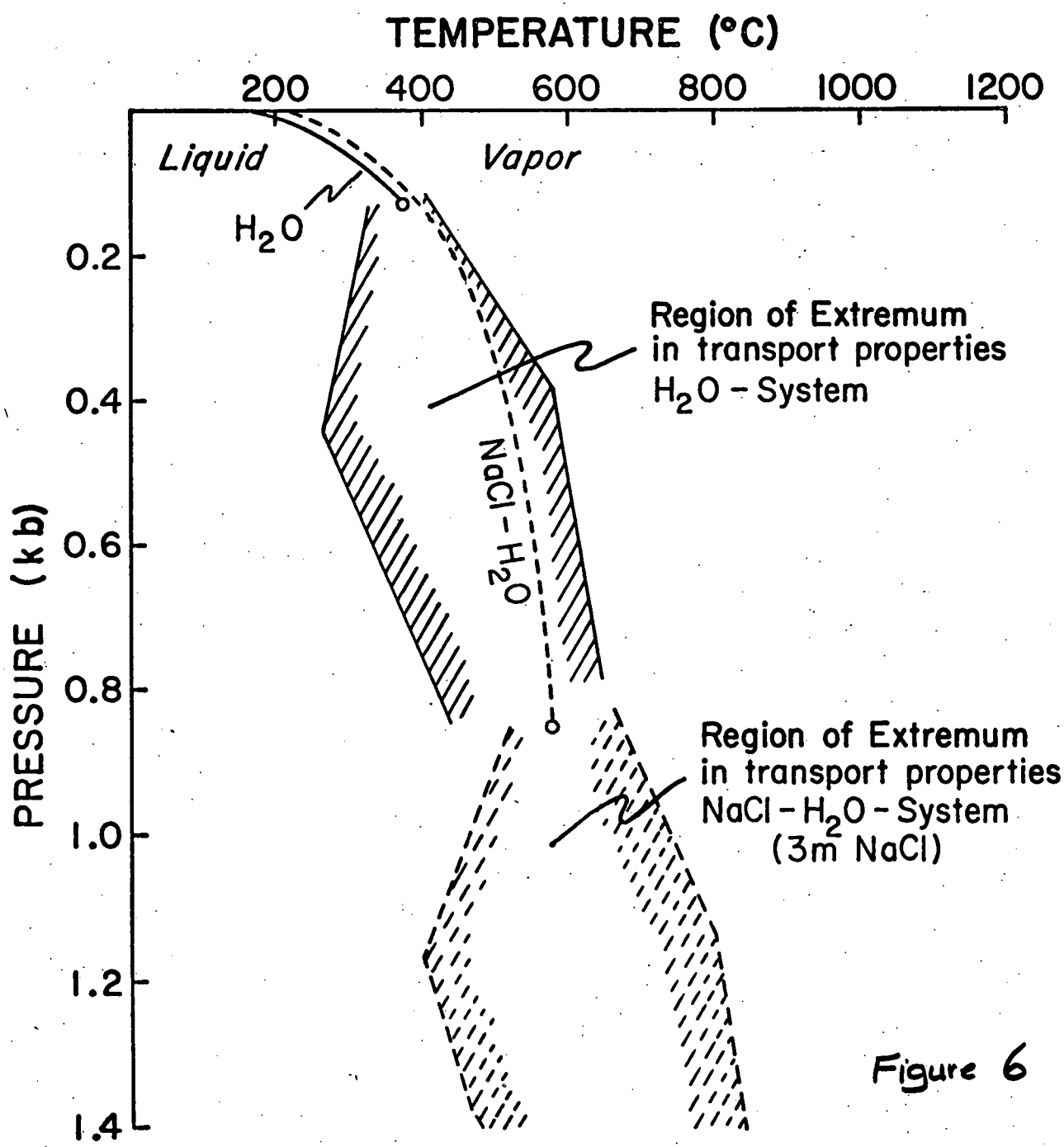
TEMPERATURE (°C)
200
400
600
800
1000
1200
Liquid
Vapor
H_2O
0.2
0.4
0.6
0.8
1.0
1.2
1.4
PRESSURE (kb)
Region of Extremum
in transport properties
H_2O - System
NaCl - H_2O
Region of Extremum
in transport properties
NaCl - H_2O - System
(3m NaCl)

Figure 6

APPENDIX II-3

The following preprint is a paper currently in review at Geochim. et Cosmochim. Acta. The research was supported entirely by other agencies (NSF and Ist. Res. Geoth.). The manuscript is included here as an indication of the state-of-the-art in utilizing geochemical transport theory in analyzing geothermal systems. As can be seen, the transport theory for reactive fluids is poorly developed, but this analysis suggests it should be better developed.

THIS PAGE
WAS INTENTIONALLY
LEFT BLANK

SOURCES AND CIRCULATION PATHS OF THERMAL FLUIDS IN THE ABANO REGION, NORTHERN ITALY

by

D. Norton[1] and C. Panichi[2]

Abstract

Water samples from natural springs and artesian wells in the Abano region of northern Italy are characterized by anomalous temperatures and compositions. Concentrations of major components, aqueous ion activities, and oxygen isotopes in samples of these fluids have been interpreted in the context of regional geologic features and fluid-rock reactions in an attempt to define the source regions and pathlines of these fluids.

The circulation of fluids in the Abano region is interpreted to be the result of meteoric water infiltration into the Permian and Mesozoic aquifers in the pre-Alps. This aquifer geometry results in forced convection of aqueous ions derived from the evaporite, limestone, and dolomite bearing formations and thermal energy along flow paths, approximately 60 km in length, which extend to depths of 2 km below the Abano region. Local variation in compositions of samples is consistent with local meteoric waters and formation fluids mixing with the fluids derived from Alpine sources.

---

[1]Geosciences Department, University of Arizona, Tucson, Arizona 85721.

[2]Istituto Internazionale per la Richerche Geotermiche, Pisa, Italy.

Introduction

The Abano region in northern Italy contains numerous occurrences of saline thermal waters which are utilized in the local termes. These thermal waters flow from springs and artesian wells located around the Berici and Euganei hills and in the valley separating these hills. The Abano thermal area lies at the northern edge of the Po River Valley and at the southern edge of the pre-Alps. Calcareous mudstones of Cretaceous age, pyroclastic volcanic rocks of Tertiary age, and alluvium outcrop in the area.

The presence of a complex hydrothermal system in the subsurface rocks beneath the Abano region has been hypothesized by Piccoli et al., 1973. On the basis of positive correlations between salinity and temperature of spring samples, they postulated a regional circulation system and further concluded that the systematic variation in salinity and correlations between major dissolved components were the result of subsurface fluids flowing along different circulation paths. In particular, they noted samples that contain relatively large concentrations of chloride are also characterized by high temperatures. These samples were inferred to represent fluids derived from evaporite bearing formations at depths below the region.

Oxygen isotope data on samples from the region indicate these fluids were originally of meteoric origin, Panichi et al., 1976. However, they observed that some of the samples are depleted in ^{18}O with respect to the local meteoric waters and are

more representative of precipitation which falls at high elevation, such as realized to the north of Abano in the pre-Alps. Variations in the ^{18}O content of samples were, therefore, attributed to mixing of meteoric waters from the pre-Alps with local meteoric waters. The correlation between high salinity and low ^{18}O values was also observed, and this Panichi et al. suggested to be evidence for a deep circulation path through the subsurface rocks, as hypothesized by Piccoli et al., 1973. However, Panichi et al. pointed out that these waters were probably meteoric in origin avd were derived from the pre-Alps. Calculation of mixing ratios confirmed this hypothesis for many of the samples, Panichi et al., 1976.

Fluid-rock reactions along fluid circulation paths occur in response to changes in temperature, pressure, and composition of the environment through which the fluids flow, Norton, 1977. In general these are overall irreversible reactions, but they can be represented by a series of equilibrium diagrams if we hypothesize homogeneous equilibrium exists in the aqueous phase and heterogeneous equilibrium exists between the aqueous phase and product mineral phases, which form as a consequence of the reaction, Helgeson, 1969. On the basis of this premise, a sample of the aqueous fluid at some point along its flow path should have a composition characteristic of the product mineral phases which are present at that point. Furthermore, a sequence of samples along the flow path should define a reaction path which passes through the product mineral stability fields and trends toward overall equilibrium between

the solution and initial reactant phases present along the flow path. Then, from an inverse point of view, since the composition of fluid along a circulation path is the result of reactions which occurred further "upstream," the chemical and mineralogical composition of the upstream environment can be predicted. Fluid composition should reflect composition of this "upstream" environment. Obviously, for very complex flow paths, or in systems characterized by flow fluxes which are small relative to reaction fluxes, this may be practically impossible. However, if independent data are available which define the original fluid source, then the reliability of the interpretation is enhanced.

Samples from the Abano region are well suited for this type of analysis since the original fluid sources are defined by oxygen isotope data, the possible fluid pathlines are defined by the regional hydrology, and the rock compositions along the pathlines are known from geologic mapping. The purpose of this communication is to reinterpret the Abano data on the basis of the concept that fluid compositions are diagnostic of the geologic environment which occurs upstream along the flow paths.

Data

Water samples from the Abano region, figure 1, were collected from artesian wells and springs and were analyzed for their major element and oxygen isotope content, using methods described by Panichi et al., 1976. Samples of spring waters

were collected during dry and rainy seasons to ascertain the effect of seasonal variations as a result of local meteoric waters. Replicate analyses were also made to ascertain the reliability of both oxygen isotope and major element determinations. The precision is ± .1°/oo for oxygen isotope determinations and is found to be ± 5% for major element determinations.

Geologic data on the surface and subsurface environments was taken from the summary discussion and geologic sections in Piccoli et al., 1973. The true ionic strength of the samples ranges between .01 and .2 molal. The electrical balance for water analyses was found to be < .005. Mineral stability data for equilibrium diagrams were taken from Helgeson, 1969. From approximately 200 of these samples, 88 were selected for which the analytical data were complete and most reliable.

The activities of ions and aqueous complexes were computed from the major component concentrations and temperatures of each sample, using program DIST, Knight, 1976. These computations were based on equilibrium stability constants for aqueous complexes from Helgeson, 1969, and a modified Debye-Hückel expression from Helgeson and James, 1968.

Bulk Chemical Composition of Samples

The concentration of major components in the water samples indicates there are five principal types of spring waters in the region. These types are referred to as Abano, Euganei-A, Euganei-B, Euganei-C, Berici, and shallow groundwater, and they are distinctly different in both their bulk composition temperature

and isotopic composition, figures 2, 3, and 4. The relative composition diagram for these waters indicates the Abano samples are relatively concentrated in Na + K and SO_4 + Cl relative to the other cations and anions, figure 2. These same samples represent fluids which have an average temperature of 75°C, figure 3, and which are used in the Abano, Battaglia, and Montegrotto termes. They also have larger ionic strengths, ∿ 0.2 molal, than the other samples. Euganei-B samples have similar compositions, but trend toward relatively higher Ca + Mg and SO_4 + Cl, and their temperatures range from 50°C down to ∿ 20°C. They also have corresponding lower ionic strength, ∿ 0.15 to 0.1 molal. Several samples from springs which occur in the valley at the base of the Berici Hills are similar to the Abano and Euganei-B groups of samples, with respect to their relatively high SO_4 + Cl and moderately anomalous temperatures. They also tend to contain relatively larger amounts of Ca, figure 2. These three groups of samples are clearly the most anomalous with respect to temperature and bulk composition of all the samples in the Abano region.

The other extremes in bulk compositions are represented by sample groups: Euganei-A, Euganei-C, and local groundwaters, figures 2 and 3. These samples are relatively concentrated in HCO_3 and Ca, figure 2, and represent springs along the base of Euganei Hills, in the valley between the Euganei and Berici hills, and in the Berici Hills, figure 1.

Oxygen isotope composition of the water samples in this

region varies from -11.8°/oo to -7.5°/oo, figure 4. The very low values are typical of samples which are from Berici and Abano, Montegrotto and Battaglia termes, figure 4. An area, characterized by slightly higher values, -10°/oo, extends into the Euganei region adjacent to the south end of the Euganei Hills. Samples from the valley between the Euganei and Berici hills contain the highest $\delta^{18}O$ values, -7.5°/oo, whereas samples containg the lowest $\delta^{18}O$ values are from springs or artesian wells along fracture zones in the bedrock. These high δO^{18} samples also tend to have relatively high SO_4 + Cl and Ca + Mg concentrations, figure 2.

Variations are also observed between the oxygen isotopic composition and total chloride concentration, figure 5. These three linear correlations for different sample groups were defined by Panichi et al., 1976. These trends suggest that the Euganei, Berici, and Abano waters are a result of mixing between low ^{18}O-content high salinity waters and lower salinity high ^{18}O waters. The isotopic values obtained by extrapolation of these functions to zero salinity might be expected to coincide with isotopic values of the respective local meteoric waters. In the case of Berici and Euganei-A samples, there is a reasonable agreement between the local meteoric and groundwater values with the extrapolated functions, whereas the Euganei-B and Abano functions extrapolate to a $\delta^{18}O$, $\leq$ -9°/oo. All three of the sample groups have similar $\delta^{18}O$ maximum values, $\sim$ -11°/oo. These relationships imply that fluid circulation giving rise to the two isotopic types of water may

originate in the same source region, and their different bulk chemical characteristics are related to differences in the reservoir rocks through which they flowed. The $\delta^{18}O$ value predicted for meteoric water in the Berici area is $8^{o}/oo$ and in the Euganei area is $-9^{o}/oo$. These values agree with measured values of local meteoric waters in the Berici and Euganei hills, figure 1. Isotopic values which lie between the extremes of local meteoric water values and the $-11^{o}/oo$ water values derived from springs are apparently the result of mixing of meteoric or shallow groundwater and subsurface waters.

The seasonal variations in composition of the water samples further confirm that local meteoric waters are mixing with waters from another source. The springs belonging to the two families also show two clear linear correlations between the oxygen isotopic composition and total salinity, but in each case they extrapolate to $\delta^{18}O$ values at zero salinity which are notably more positive than those obtained from January to June. During this same time period, the salinity values are higher, thus confirming the hypothesis that there is a smaller contribution to the mixtures from the surface waters with very low salinity and relatively higher ^{18}O contents. This is particularly clear for the Berici area and Euganei-A families whose salinity variations range from values of about 30% for the less saline waters to about 10% for the more saline waters, with isotopic variations of 0.7 and 0.4%, respectively.

The chemical characteristics of the water from some boreholes in the low elevation plain lying between the Berici Hills and Euganei Hills indicate that none of the samples in this group have a high chloride ion content. There are some waters whose chemical composition is identical to the Berici samples, whether they be sulphate or carbonate-types, and to the Euganei-C samples. Therefore, these are mainly wells that draw, at shallow depths, from very shallow circulation waters characterized by the bicarbonate ion and by a varying percentage of the Ca and Na + K ions, depending on the presence in greater or smaller quantities of volcanics in the cap rock.

The source region for the waters characterized by $-11^{o}/oo$ $\delta^{18}O$ values must be from aquifer recharge areas at much higher elevations, such as realized to the north in the Alpine region. Elevations of $\sim$ 1.5 km in the latter region are sufficient to account for the relatively low $\delta^{18}O$ values.

Representation of the sample compositions on mineral equilibrium diagrams depict the relationship between the natural waters and the stability of common rock forming minerals, figures 6 - 8. Although the precise relationship between the samples and the aluminum silicate phases is unknown because aluminum was not determined on most of the samples, the compositions clearly project onto kaolinite and montmorillonite stability fields. Compositional trends are apparent for each of the sample groups, suggesting an overall rock-solution reaction or mixing of different solutions.

The Abano sample compositions plot along the Ca-montmorillonite--Mg-montmorillonite--saturated solution phase boundary, but they are also related to the calcite-dolomite saturation surface for $P_{CO_2} = 10^{-2}$, figure 6, whereas the Berici and Euganei sample compositions, figures 7 and 8, plot entirely within the kaolinite-saturated solution stability field and appear to be undersaturated with both calcite and dolomite at $P_{CO_2} = 10^{-2}$. The sample compositions generally plot along a 1:1 slope on the activity-activity diagrams. These types of trends have been recognized in other groups of natural waters, Norton, 1974; Garrels and MacKenzie, 1967; Paces, 1972, and occur consistently in numerical simulations of irreversible solution-rock reactions. These trends normally depict irreversible reaction paths between minerals and solutions along which there is a simple consumption of hydrogen ions as the solution composition evolves toward equilibration with the bulk mineralogy of the rocks. However, as a consequence of the variations in temperature and concentrations of components within each sample group, these isothermal projects are inadequate to fully interpret the nature of the reaction paths.

The samples all appear to be saturated or slightly supersaturated with respect to quartz at their collection temperatures, figure 9. Samples from both Euganei and Berici groups might have been saturated with quartz at temperatures higher than collection temperatures, and the supersaturation effect

would then be the result of cooling from the higher temperature. Based on this hypothesis, the predicted saturation temperatures range from 10 - 30°C higher than the temperatures at the collection point, figure 3. The Abano samples, however, are saturated with quartz at their collection temperatures.

The temperature range of the samples does not permit the variations in sample compositions to be adequately interpreted. Therefore, activity diagrams are also constructed to represent temperature variations along the reaction line defined by the systematic trends in sample compositions on the activity diagrams. These trends are represented by:

$$W = [(\log a_{Ca++}/a_{H+}^2)^2 + (\log a_{Mg++}/a_{H+}^2)^2]^{1/2},$$

figures 10 - 11.

The relationship between the stability fields for alumina silicate minerals and the solution compositions, figure 6, indicates that the Abano solutions are in equilibrium with the montmorillonite and kaolinite whereas the other samples are equilibrated with only kaolinite. A few Berici and Euganei samples suggest a temperature-concentration trend toward the montmorillonite-kaolinite phase boundaries. Temperatures that were predicted on the basis of the quartz saturation surface and $a_{H_4SiO_4}$ in the samples would place all these samples closer to the phase boundary.

Six of the eight Abano samples are saturated with respect to anhydrite, and the other two are undersaturated with respect

to anhydrite, by about 15 - 20°C, figure 12. These same two samples are also supersaturated, by about 10°C, with respect to quartz. Therefore, they also can probably be considered to be saturated with anhydrite within the error limits of the data. However, all the Berici and Euganie sample compositions have $\log(a_{SO_4^=})(a^2_{H+})$ values one to two log units less than the value necessary for anhydrite saturation at the respective temperatures and log a_{Ca++}/a^2_{H+} values. Only a few samples from each of the groups are close to or saturated with respect to calcite and dolomite, figure 11, because of the relatively low P_{CO_2} values in the majority of the samples.

Conclusions

The combined isotopic and major component data suggest the waters in the general region have been derived from both local meteoric and groundwater sources, figures 2 and 4. Systematic shifts in compositions can clearly be attributed to fluid-rock reactions along pathlines at depth and mixing of these waters in shallow and deep aquifers. Major element compositions of the waters indicate the mineralogic composition of the subsurface aquifers through which the waters flowed, and isotopic compositions indicate the sources of the water.

Sources of the waters in the region are partially defined by the $\delta^{18}O$ values. The very low $\delta^{18}O$, -11°/oo, values of the Abano and some of the Berici and Euganei-A samples require that these waters were ultimately derived from meteoric waters at $\sim$ 1.5 km elevations. These elevations are realized in the

pre-Alps northwest of the region and, therefore, is probably the source region for these waters, figure 13, large circle Ab. Local sources in either the Berici or Euganei hills for the samples with intermediate $\delta^{18}O$ values, circa -9.5 + -8°/oo and in the intervening valley for samples with the lowest $\delta^{18}O$ values -7.5°/oo are postulated, figure 13.

Several fluid pathlines are possible from the source regions to the spring or well locations. The actual pathlines are constrained by the mineral-fluid reaction paths and mineral-fluid equilibrium relationships depicted in figures 6 - 12. These relationships require certain mineral assemblages were encountered along the pathlines as the water circulated from the sourceregions to the sample site. Samples from the Abano thermal wells are saturated with respect to anhydrite and Ca - Mg montmorillonite and are supersaturated with respect to calcite and dolomite at temperatures between 50 and 90°C. This feature suggests that at some point along their circulation paths aquifers containing anhydrite, clay minerals, calcite, and dolomite were encountered, figure 13. Rocks of this composition occur at 2 km depths below the region. They are Permian evaporites which extend northward into the source regions of the meteoric water. The fact that the Abano waters are supersaturated with the carbonates probably reflects internal solution disequilibrium as a result of circulation from low P_{CO_2} environments below the surface to higher P_{CO_2} surface environments. Samples from Euganei-B and Berici springs are

saturated with respect to calcite and dolomite, but undersaturated with anhydrite. These Berici and Euganei-B waters are also relatively concentrated in SO_4, Cl, Ca, and Mg. These characteristics require flow paths through limestones and dolomites that contain pore fluids relatively concentrated in SO_4 and Cl, or that these latter components result from mixing with Abano type waters. The Mesozoic stratigraphic section beneath the region consists of a 1.5 km thick sequence of limestones and dolomites, which accounts for these characteristics, figure 13. The Berici and Euganei-B samples which tend to have lower SO_4 and Cl, but high Ca, probably flowed through the Tertiary marine limestones and volcanics that comprise the Berici and Euganei hills, figure 13. Euganei-C and local groundwaters tend to be saturated with kaolinite, montmorillonite, and quartz, but are undersaturated with respect to calcite, dolomite, and anhydrite, suggesting flow paths through the alluvium or volcanic rocks or shale beds.

The circulation paths for waters which occur in the Abano area are from sources in the pre-Alps at an elevation of $\sim$ 1.5 km, as evidenced by the ^{18}O data. This meteoric water then circulates into subsurface aquifers which contain anhydrite, halite, calcite, and dolomite. The Permian evaporites and Mesozoic carbonates near the basement contact, figure 13, are the aquifers through which these fluids flowed. The fluid pathlines through the evaporites intersect the surface, primarily in the termes, whereas those through the Mesozoic carbonate surface near

base of the Berici and Euganei hills.

The local volcanic rocks are apparently not the source of thermal energy in these waters. Because of their Tertiary age they have cooled to ambient conditions. The thermal energy appears to be derived from the normal temperature gradient. Normal gradients of 25°C/km would account for the 75°C maximum temperatures observed in the terme waters since these waters circulated from ∿ 2 km depth. The heat content of these waters could also be augmented by exothermic reactions between circulating metoeric waters and anhydrite beds. The Abano thermal system is apparently a forced convection system driven by normal hydrologic artesian loads generated by aquifer recharge ∿ 1.5 km above the Abano region.

Acknowledgements

This research was supported by funds from NSF-EAR74-03515-AO1 to Norton. We wish to acknowledge the Istituto Internazionale per la Richerche Geotermiche - Pisa for sponsoring the original study and making the data available for analyses and to express our thanks to the Istituto staff for their assistance in this study. We wish to thank Lynn McLean for editorial improvements in the manuscript and numerous rough drafts and R. Capuano, J. Knight, and R. Knapp for assistance in the study and discussion of the results.

Figure Captions

Figure 1. Topographic and sample location map for the Abano region, northern Italy.

Figure 2. Composition diagram showing relative amounts of major anions and cations in samples. Ternary plots of cations, lower left, and anions, lower right, are in terms of mEq percentages. Points from ternary plots are projected into central diamond where points represent mEq% of both anion and cation concentration, generalized from Panichi, 1976. All Abano samples plot within the very small label regions on the diagram whereas the samples from Berici and Euganei clearly have a range in bulk composition, as indicated by the points.

Figure 3. Temperature histogram for samples from the Abano region showing number of samples vs. temperature at which samples were collected, solid line, and temperature predicted by assuming quartz saturation for each sample, dotted line.

Figure 4. Oxygen isotope map of the Abano region. $\delta^{18}O$ values in $^{o}/oo$ are contoured for both artesian wells and spring samples. Sample points are also accordingly coded to bulk composition groups as defined in figure 2. $\delta^{18}O$ values for meteoric waters in the Euganei and Berici hills and for the terme wells are also indicated.

Figure 5. Oxygen isotope variations, expressed as δO^{18}, $^{o}/_{oo}$, as a function of total chloride concentration in water samples, generalized from Panichi et al., 1976. Systematic increases in δO^{18} values are noted for each of the sample groups except Euganei-C samples, which are not represented.

Figure 6. Theoretical activity diagram for the system $CaO-MgO-Al_2O_3-SiO_2-CO_2-H_2SO_4-HCl-H_2O$ in the presence of an aqueous phase at 75°C, 1 bar, and unit activity of H_2O and of the mineral phases, log $a_{H_4SiO_4}$ = -3.4 and log P_{CO_2} = -2. Compositions of samples from the Abano Terme are projected into the equilibrium diagram.

Figure 7. Theoretical activity diagram for the system $CaO-MgO-Al_2O_3-SiO_2-CO_2-H_2SO_4-HCl-H_2O$ in the presence of an aqueous phase at 25°C, 1 bar, and unit activity of H_2O and of the mineral phases, log $a_{H_4SiO_4}$ = -4.0 and log P_{CO_2} = -2. Compositions of samples from the Berici area are projected onto diagrams in two groups.

Figure 8. Theoretical activity diagram for the system $CaO-MgO-Al_2O_3-SiO_2-CO_2-H_2SO_4-HCl-H_2O$ in the presence of an aqueous phase at 25°C, 1 bar, and unit activity of H_2O and of the mineral phases, log $a_{H_4SiO_4}$ = -4.0 and log P_{CO_2} = -2.

Compositions of Euganei samples are projected onto diagrams.

Figure 9. Theoretical activity-temperature diagram for SiO_2-H_2O system relating the saturation surface to the aqueous phase. $a_{H_4SiO_4}$ for all samples show slight supersaturation with respect to quartz at low temperatures. Log $a_{H_4SiO_4}$ vs. T line is average values of $a_{H_4SiO_4}$ in samples.

Figure 10. Temperature-composition projection for the theoretical activity diagrams, figures 6 - 8, in the CaO-MgO-Al_2O_3-SiO_2-HCl-H_2SO_4-CO_2-H_2O system at log $a_{H_4SiO_4} = -10^{-2}T - 4.2$, 1 bar, and unit activity of H_2O and the mineral phases. Compositions of samples are represented in terms of region from which samples were collected.

Figure 11. Temperature-composition projection for the theoretical activity diagrams, figures 6 - 8, in the CaO-MgO-Al_2O_3-SiO_2-HCl-H_2SO_4-CO_2-H_2O system at log $a_{H_4SiO_4} = -10^{-2}T - 4.2$, 1 bar, and unit activity of H_2O and the mineral phases. Compositions of samples which are saturated or nearly saturated with respect to calcite and dolomite are represented by respective paths. The log P_{CO_2} value for each sample appears in the point for comparison with the

saturation surfaces for calcite and dolomite at log P_{CO_2} = -2 and -1. Other samples are at least 1 log unit undersaturated and are not represented on this projection.

Figure 12. Theoretical temperature-activity diagram for $CaO-H_2SO_4-HCl-H_2O$ system at 1 bar in the presence of an aqueous phase at 1 bar and unit activity of H_2O and the mineral phases. The saturation surface for anhydrite at log $(a_{SO_4^=})(a_{H+}^2)$ = -18, -17, and -16 is shown, and the composition of samples which are close to saturation with anhydrite are represented by squares with their respective log $(a_{SO_4^=})(a_{H+}^2)$ values.

Figure 13. Schematic geologic cross section of Abano region from NE to SW relating geologic units and fluid circulation paths deduced from this study. Sources of various sample groups are indicated by large circles with group names: Abano = Ab, Euganei-C = EC, and Berici low temperature samples = BC. Pathlines of fluids are depicted by lines with arrows and large squares with sample group letters as above, plus Euganei-A = EA, Euganei-B = EB, Berici high temperature = BT, and Berici low temperature samples = BL. Note subsurface mixing, particularly of Berici and Euganei-A and Euganei-B samples.

References

Garrels, R. M., MacKenzie, F. T., 1967, Origin of the chemical composition of some springs and lakes, in Equilibrium Concepts in Natural Water Systems, Advances in Chemistry Series 67: Am. Chem. Soc., p. 222-242.

Helgeson, H. C., 1969, Thermodynamics of hydrothermal systems at elevated temperatures and pressures: Am. Jour. Sci., v. 267, p. 729-804.

Helgeson, H. C., and James, W. R., 1968, Activity coefficients in concentrated electrolyte solutions at elevated temperatures (abs.): Abstracts of Papers, 155th Natl. Mtg., Am. Chem. Soc., April, 1968, San Francisco, Cal., S-130.

Knight, J., 1967, DIST-computer program for distribute solution composition: Dept. of Geosciences, University of Arizona, Tucson, Arizona.

Norton, D., 1974, Chemical mass transfer in the Rio Tanama system, west-central Puerto Rico: Geochim. et Cosmochim. Acta, v. 38, p. 267-277.

Norton, D., 1977, Sourceregions, sourcelines, and pathlines for fluids in hydrothermal systems related to cooling plutons: Econ. Geol., in press.

Paces, T., 1972, Chemical characteristics and equilibration in natural water-felsic rock-CO_2 systems: Geochim. et Cosmochim. Acta, v. 36, p. 217-240.

Panichi, C., et al., 1976, Geochimica delle acque termali euganeo-beriche, in Il sistema idrotermale euganeo-berico e la geologia dei Colli: Mem. Ist. Geol. Mineral., Universita di Padova, v. XXX, p. 113-141.

Piccoli, G., et al., 1973, Contributo alla conoscenza del sistema idrotermale euganeo-berico: Atti Acc. Naz. Lincei, Memorie Classe Sc. Fis. Mat. Nat., VIII, v. 11, p. 103-133.

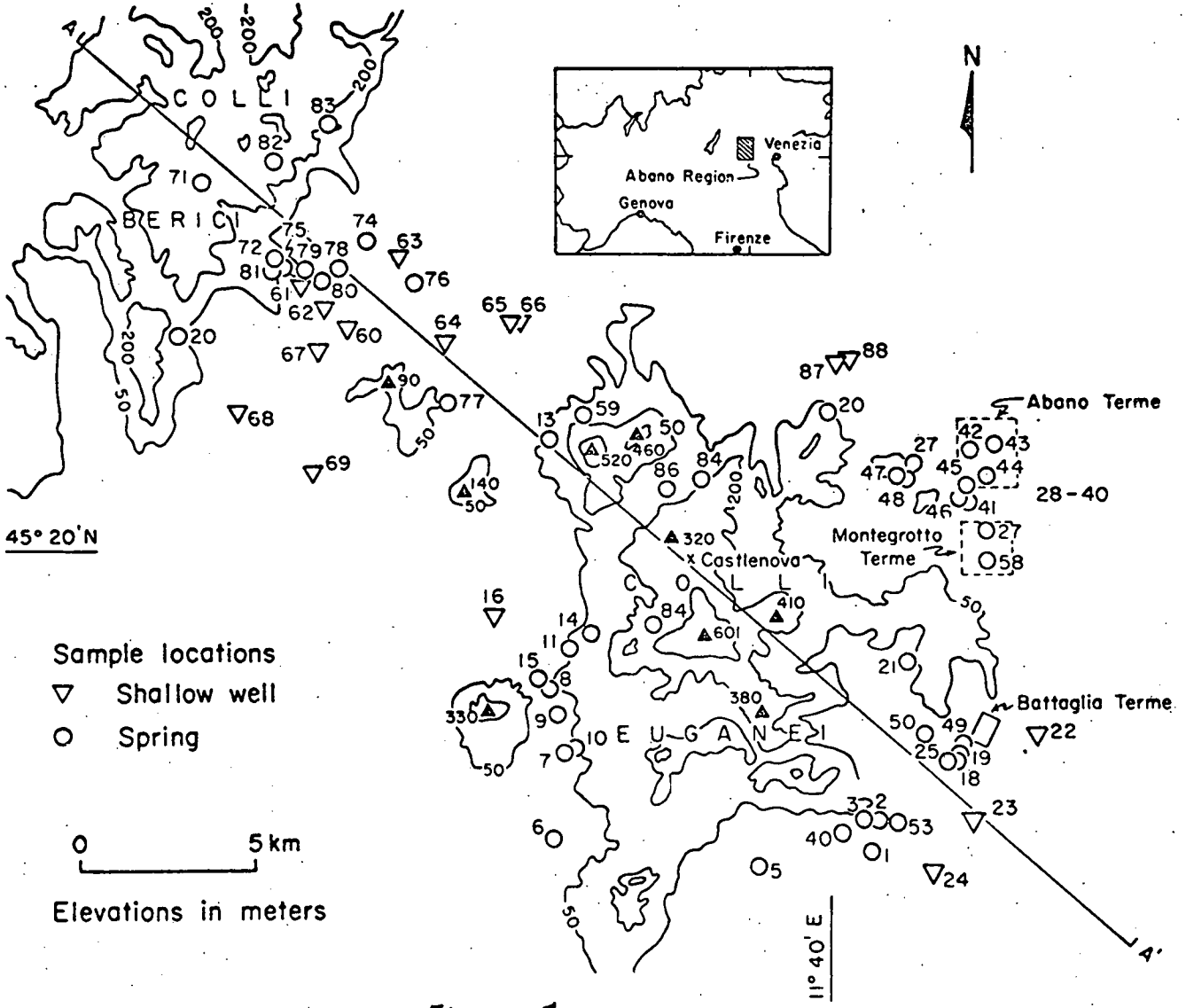
A
A'
COLLI
BERICI
EUGANEI
Venezia
Abano Region
Genova
Firenze
N
Abano Terme
Montegrotto Terme
Battaglia Terme
x Castlenova
28-40
45° 20'N
11° 40'E
Sample locations
Shallow well
Spring
0
5 km
Elevations in meters

Figure 1

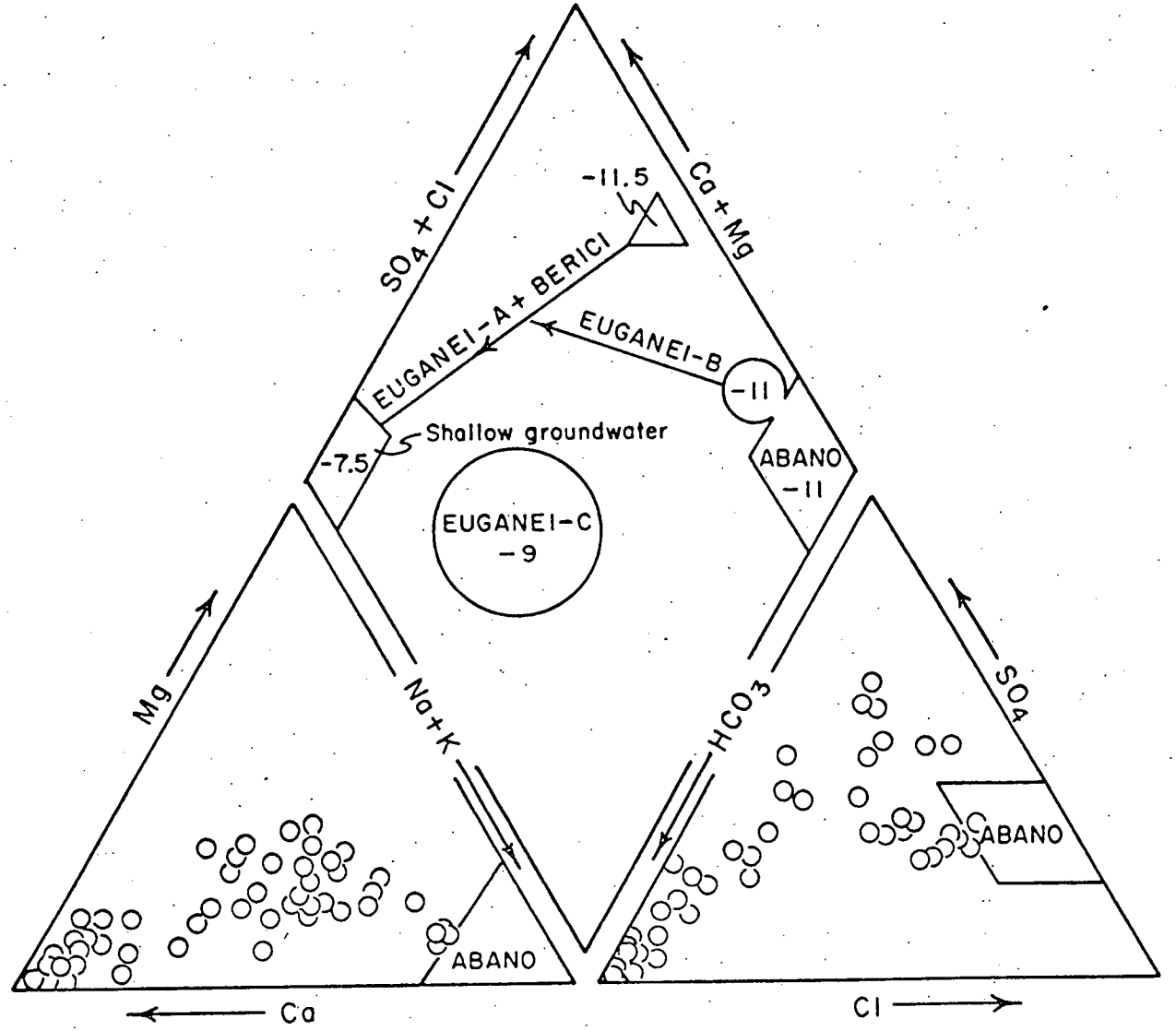
SO4 + Cl
Ca + Mg
-11.5
EUGANEI-A + BERICI
EUGANEI-B
-11
Shallow groundwater
-7.5
ABANO
-11
EUGANEI-C
-9
Mg
Na + K
HCO3
SO4
ABANO
ABANO
Ca
Cl

Figure 2

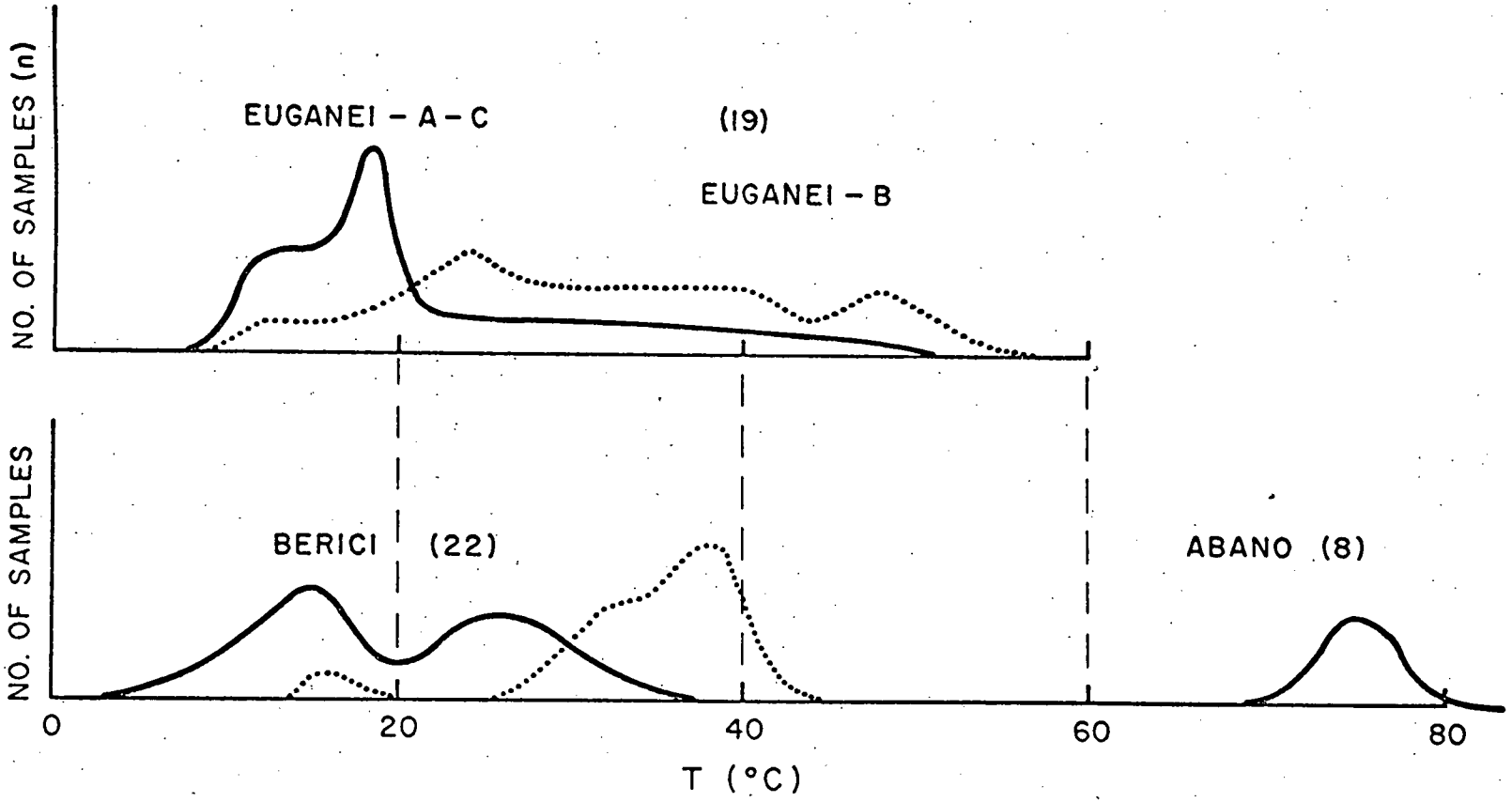
NO. OF SAMPLES (n)
EUGANEI – A – C
(19)
EUGANEI – B
NO. OF SAMPLES
BERICI
(22)
ABANO (8)
0
20
40
60
80
T (°C)

Figure 3

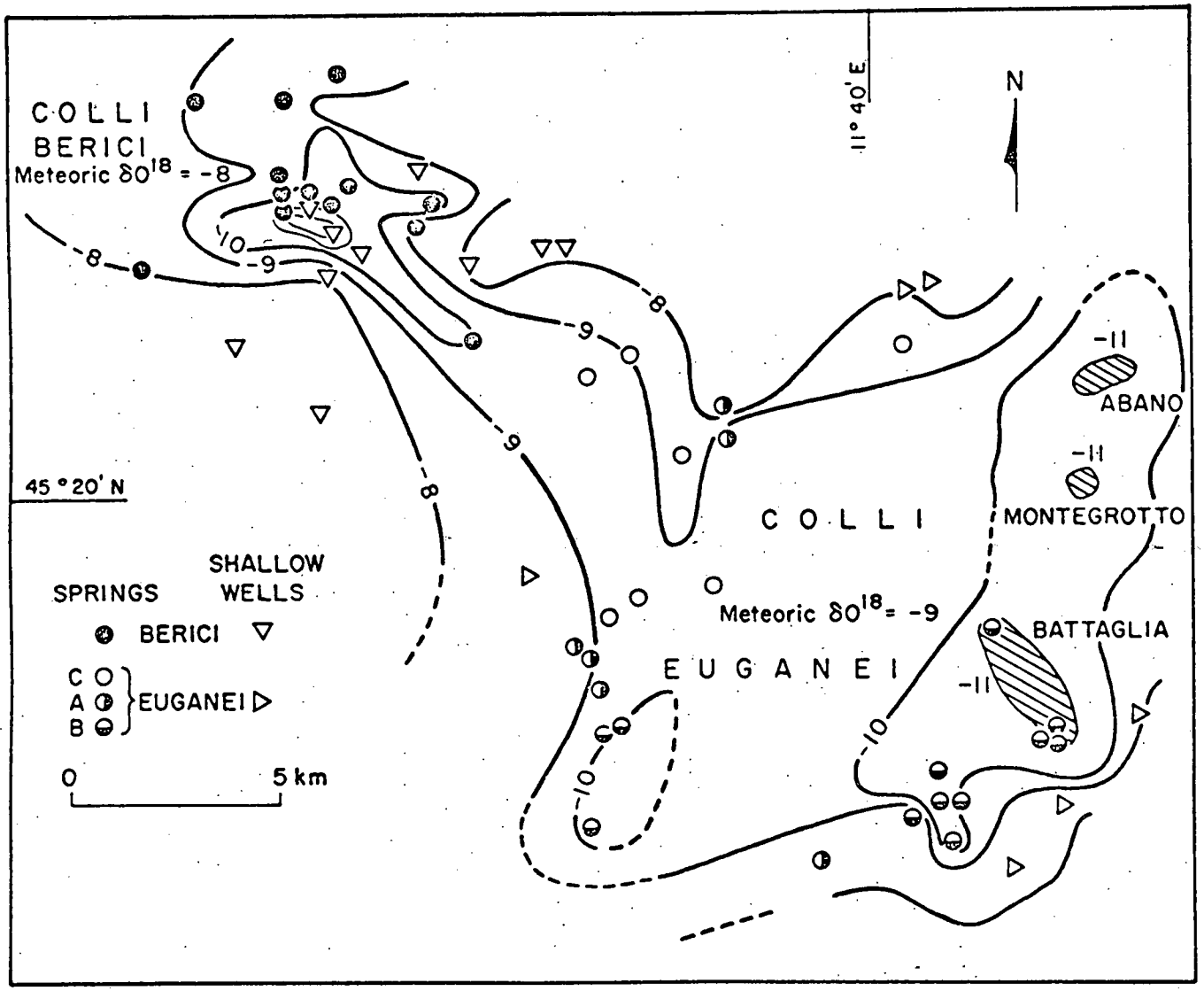
COLLI
BERICI
Meteoric δO18 = -8
11° 40' E
N
45° 20' N
-8
-9
-10
-11
ABANO
MONTEGROTTO
BATTAGLIA
COLLI
EUGANEI
Meteoric δO18 = -9
SHALLOW
WELLS
SPRINGS
BERICI
C
A
B
EUGANEI
0
5 km

Figure 4

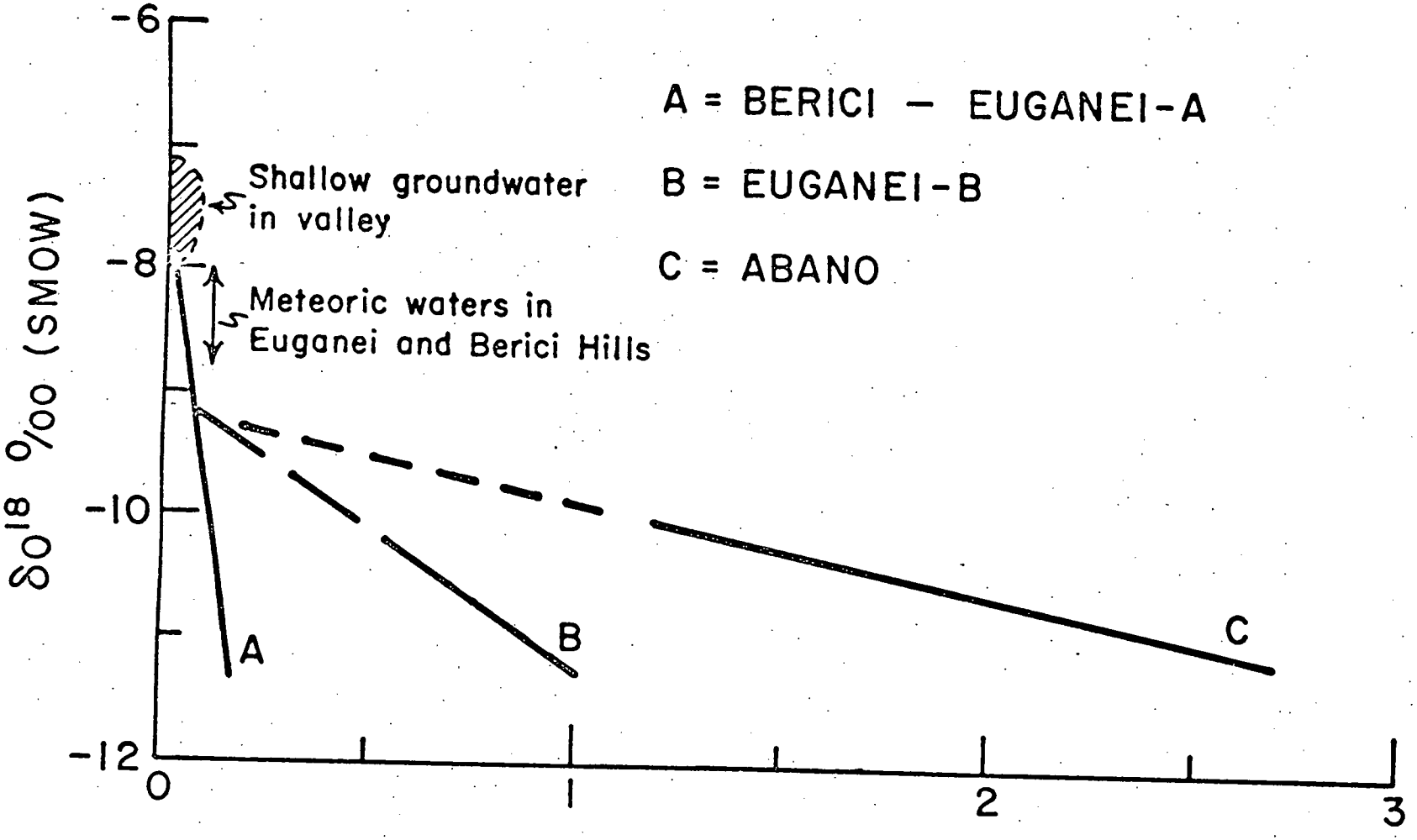
A = BERICI – EUGANEI-A
B = EUGANEI-B
C = ABANO
Shallow groundwater in valley
Meteoric waters in Euganei and Berici Hills
δO^{18} ‰ (SMOW)
-6
-8
-10
-12
A
B
C
0
1
2
3
CHLORIDE (g/l)

Figure 5

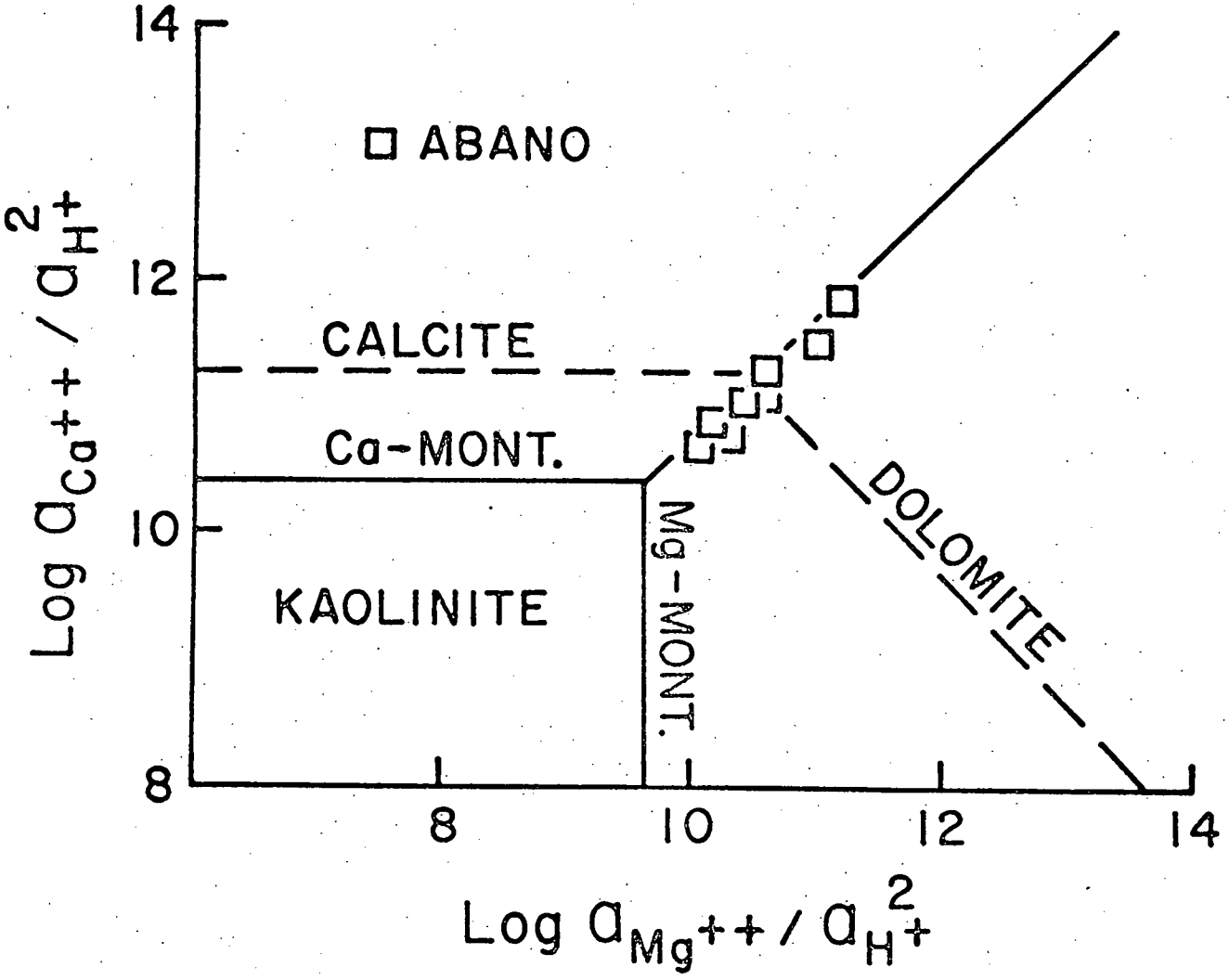
14
12
10
8
ABANO
CALCITE
Ca-MONT.
KAOLINITE
Mg-MONT.
DOLOMITE
8
10
12
14
Log $a_{Ca^{++}} / a_{H^+}^2$
Log $a_{Mg^{++}} / a_{H^+}^2$

Figure 6

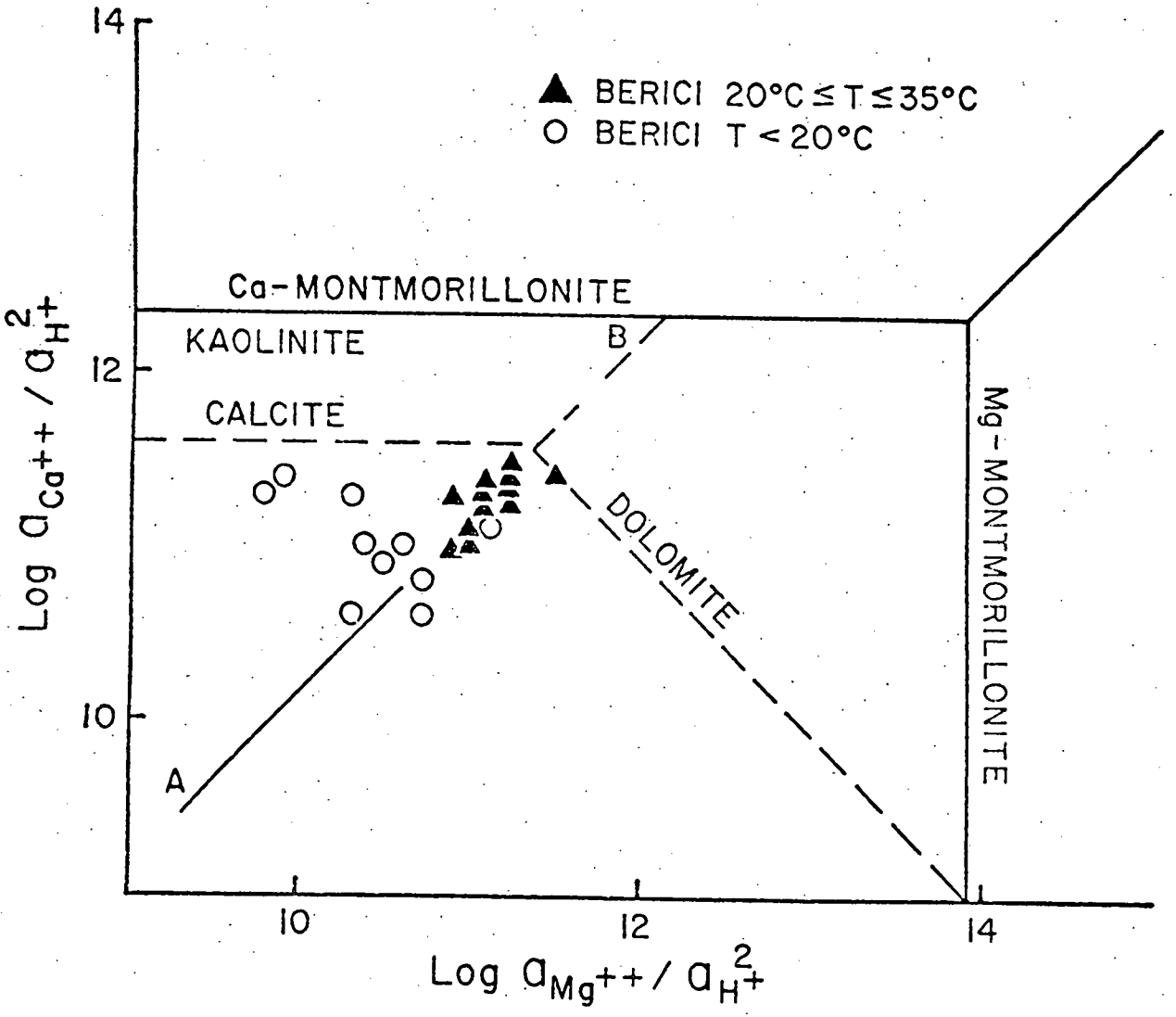
▲ BERICI 20°C ≤ T ≤ 35°C
○ BERICI T < 20°C
Ca-MONTMORILLONITE
KAOLINITE
CALCITE
B
DOLOMITE
Mg-MONTMORILLONITE
A
C
14
12
10
10
12
14
Log $a_{Ca^{++}} / a_{H^+}^2$
Log $a_{Mg^{++}} / a_{H^+}^2$

Figure 7

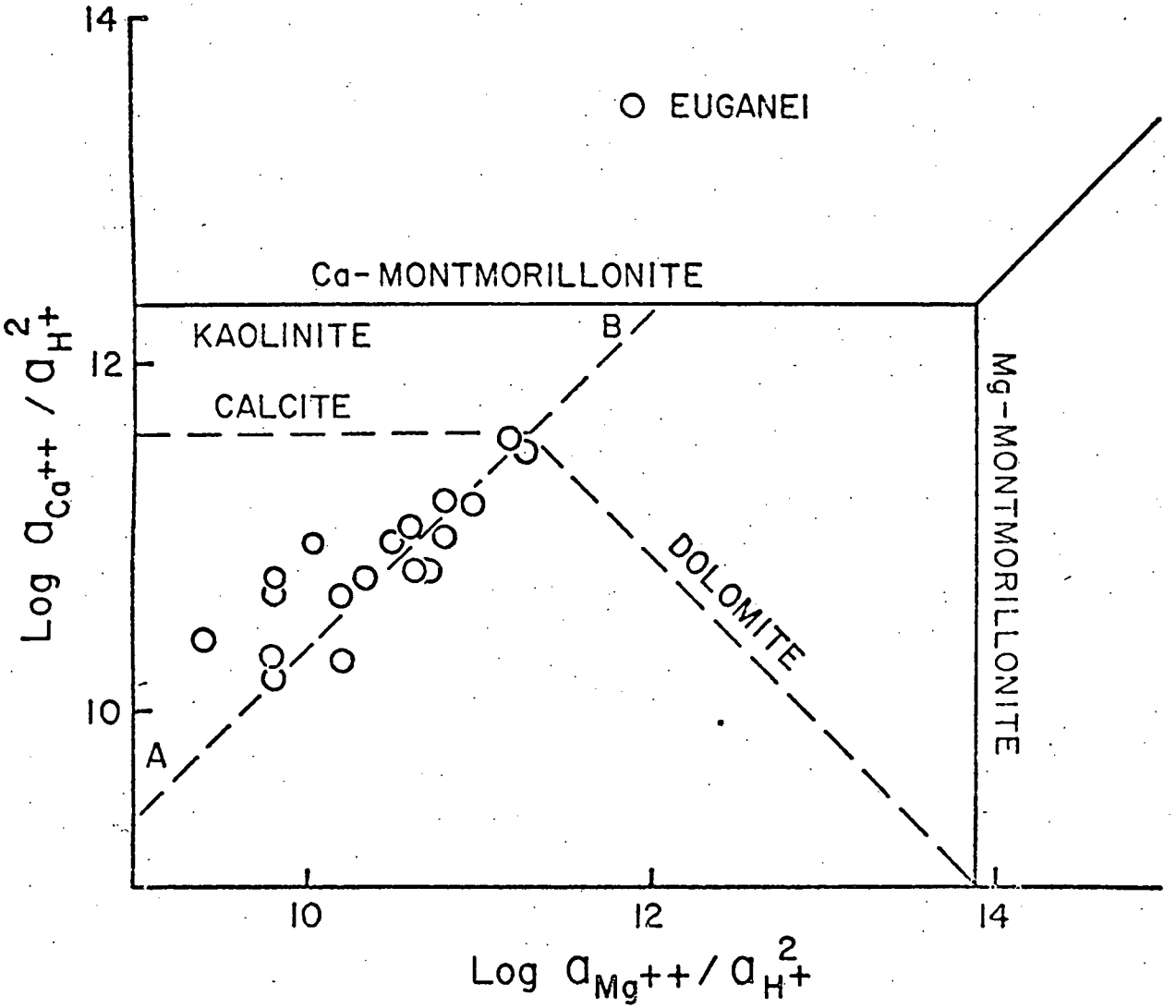
14
12
10
O EUGANEI
Ca-MONTMORILLONITE
KAOLINITE
CALCITE
B
A
DOLOMITE
Mg-MONTMORILLONITE
Log $a_{Ca^{++}} / a_{H^+}^2$
10
12
14
Log $a_{Mg^{++}} / a_{H^+}^2$

Figure 8

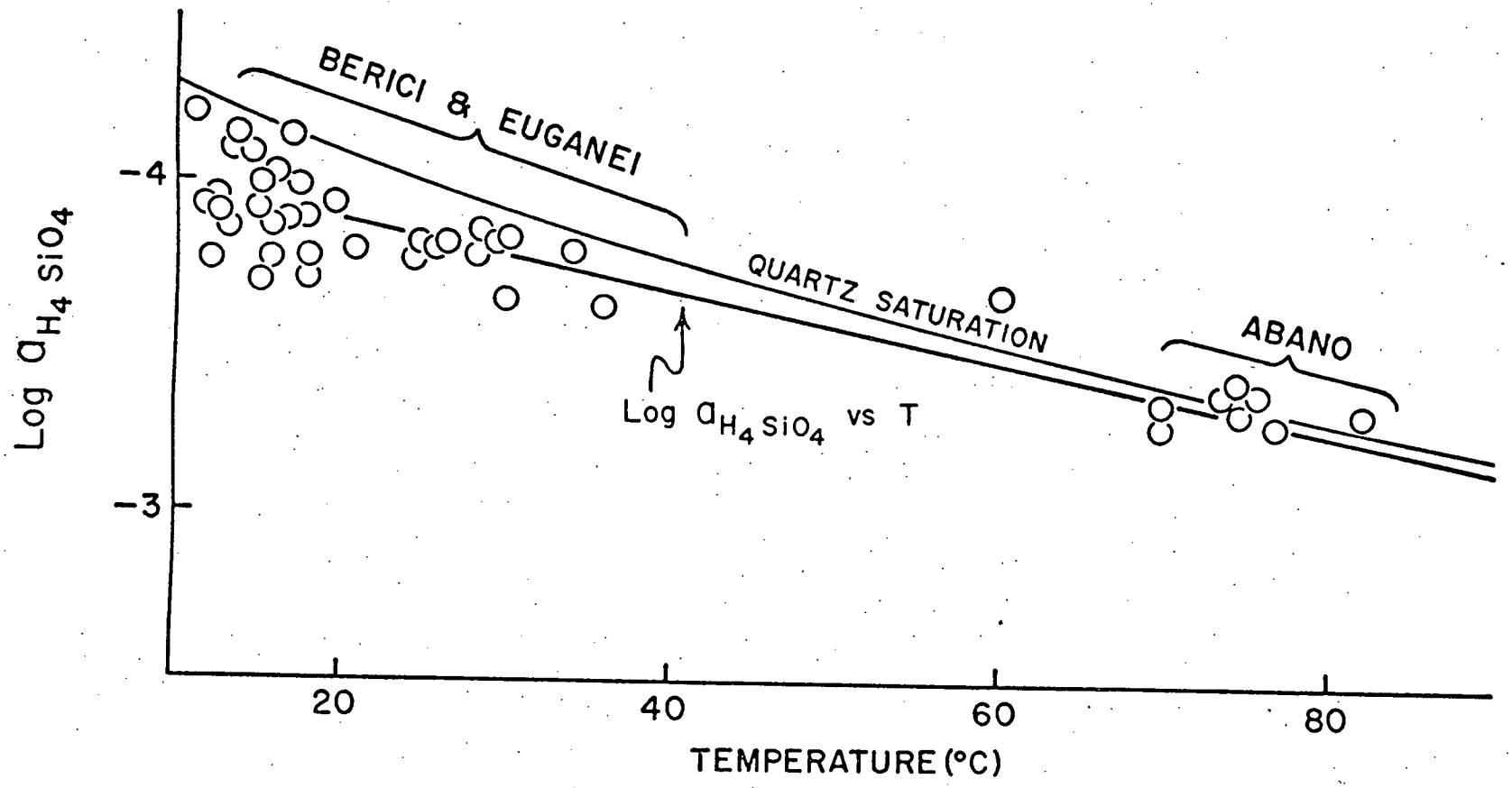
BERICI & EUGANEI
QUARTZ SATURATION
ABANO
Log $a_{H_4SiO_4}$ vs T
Log $a_{H_4SiO_4}$
-4
-3
20
40
60
80
TEMPERATURE (°C)

Figure 9

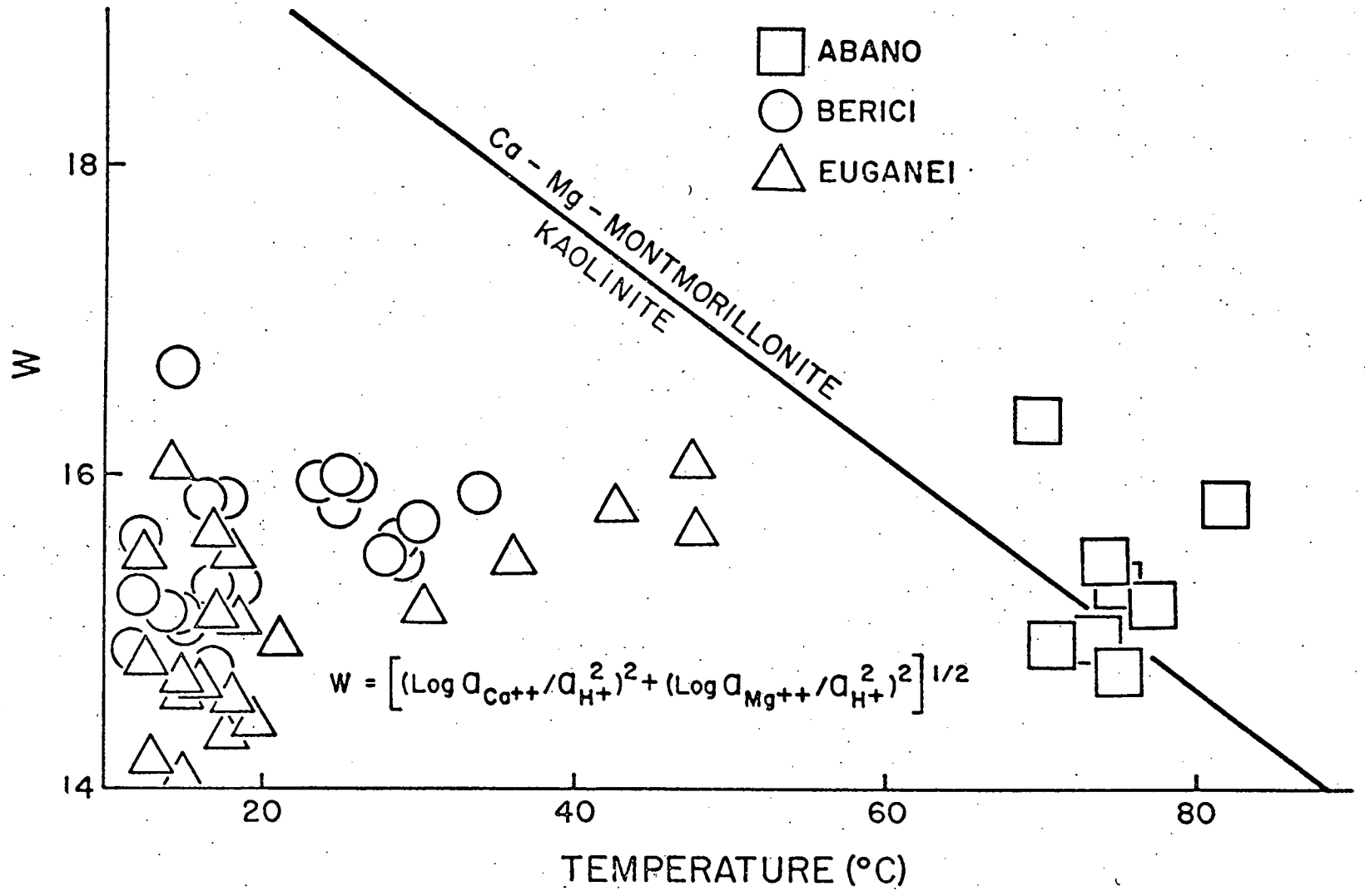
ABANO
BERICI
EUGANEI
Ca - Mg - MONTMORILLONITE
KAOLINITE
W
18
16
14
20
40
60
80
TEMPERATURE (°C)
$W = \left[(\text{Log } a_{Ca^{++}}/a^2_{H^+})^2 + (\text{Log } a_{Mg^{++}}/a^2_{H^+})^2\right]^{1/2}$

Figure 10

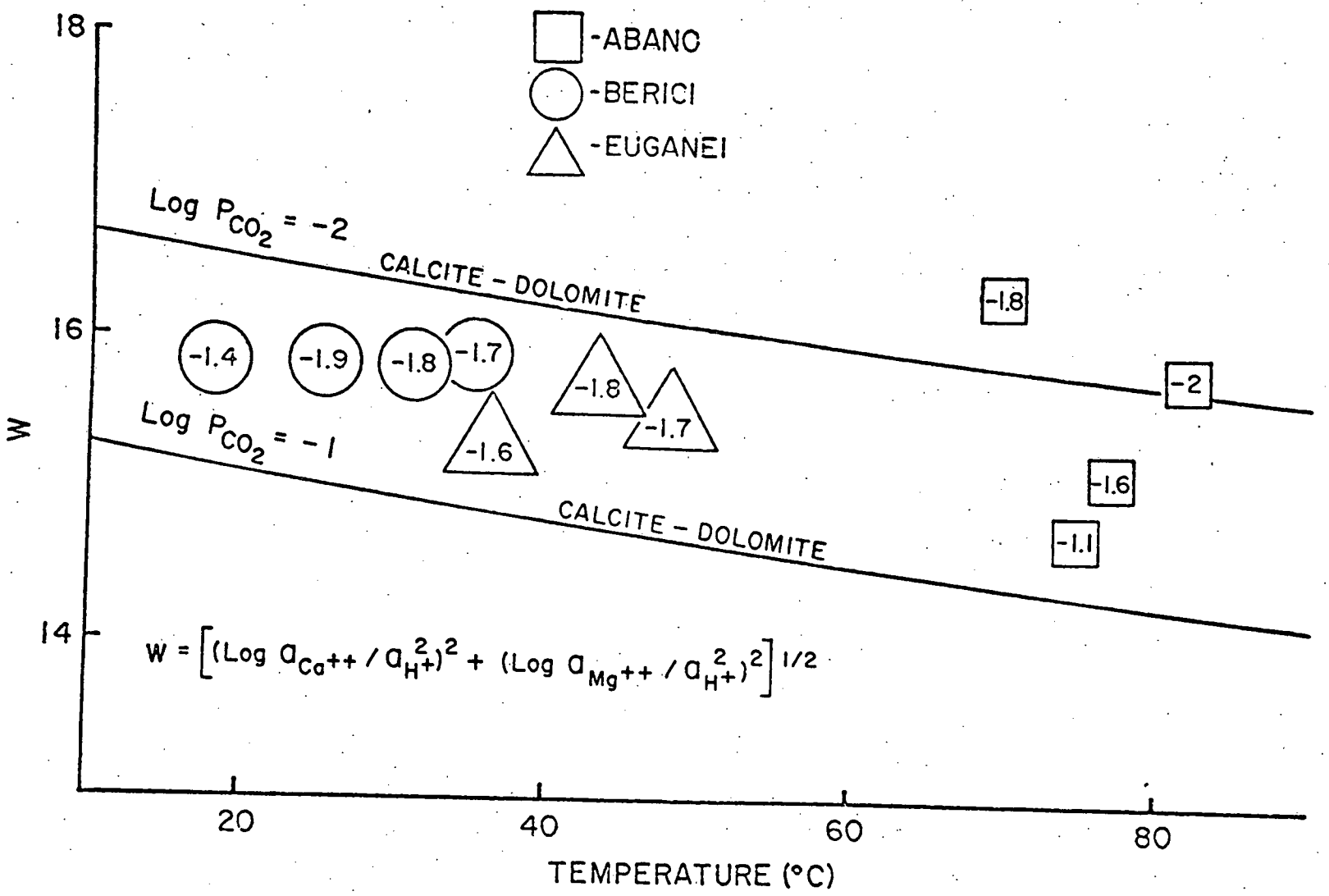
-ABANO
-BERICI
-EUGANEI
Log P_{CO_2} = -2
CALCITE - DOLOMITE
Log P_{CO_2} = -1
CALCITE - DOLOMITE
-1.4
-1.9
-1.8
-1.7
-1.6
-1.8
-1.7
-1.8
-2
-1.6
-1.1
$W = \left[(\text{Log } a_{Ca^{++}} / a_{H^+}^2)^2 + (\text{Log } a_{Mg^{++}} / a_{H^+}^2)^2\right]^{1/2}$
W
18
16
14
20
40
60
80
TEMPERATURE (°C)

Figure 11

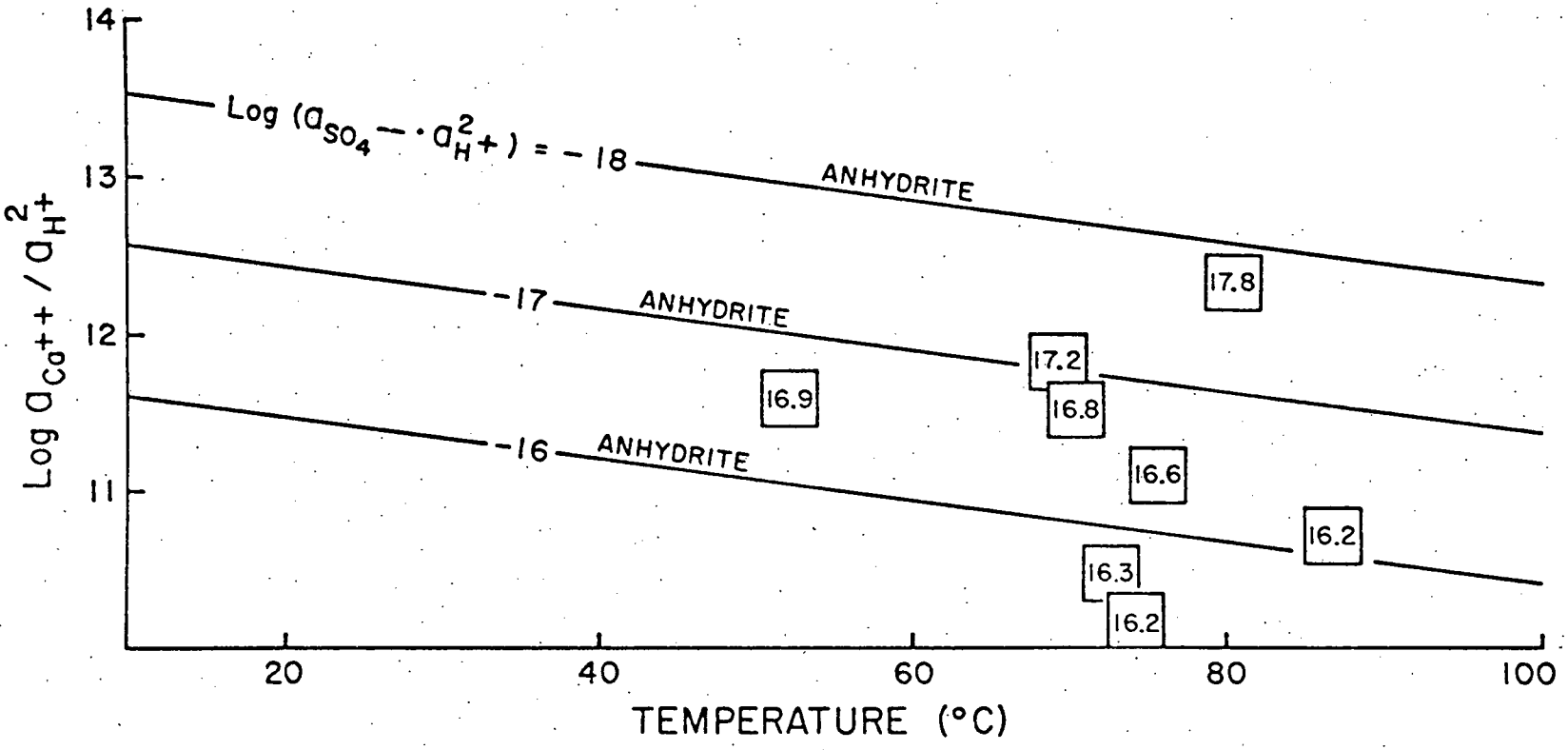
14
13
12
11
Log $a_{Ca^{++}} / a_{H^+}^2$
Log $(a_{SO_4^{--}} \cdot a_{H^+}^2) = -18$
ANHYDRITE
-17
ANHYDRITE
-16
ANHYDRITE
17.8
17.2
16.8
16.9
16.6
16.2
16.3
16.2
20
40
60
80
100
TEMPERATURE (°C)

Figure 12

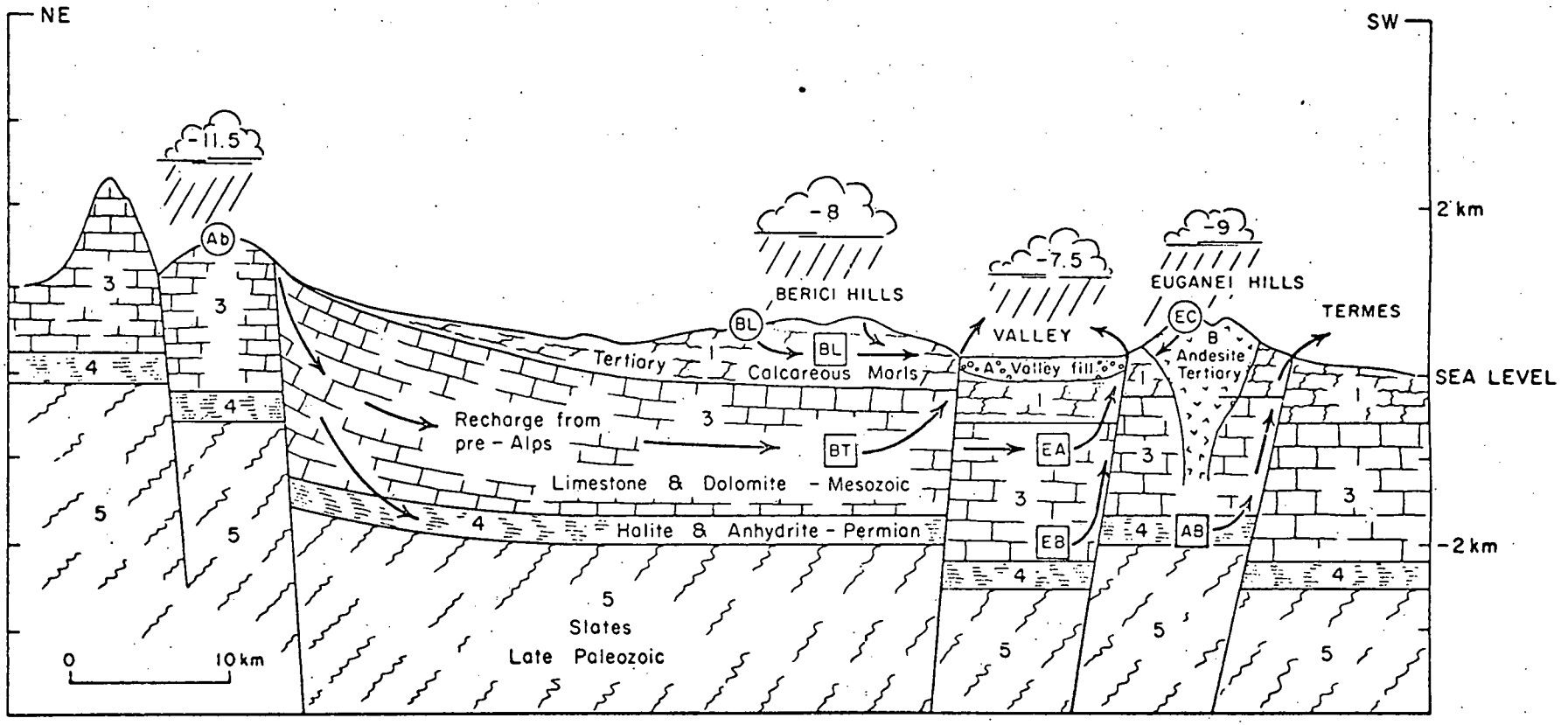
NE
SW
-11.5
-8
-7.5
-9
Ab
BERICI HILLS
VALLEY
EUGANEI HILLS
TERMES
BL
EC
EA
EB
AB
BT
Tertiary
Calcareous Marls
Recharge from
pre - Alps
Limestone & Dolomite - Mesozoic
Halite & Anhydrite - Permian
Slates
Late Paleozoic
Andesite
Tertiary
Valley fill
2 km
SEA LEVEL
-2 km
0
10 km

Figure 13

THIS PAGE
WAS INTENTIONALLY
LEFT BLANK

References

Alexander, G. B., Heston, W. M., and Iller, R. K., 1954, The solubility of amorphous silica in water: Jour. Phys. Chem., v. 58, p. 453-455.

Apps, J. A., 1970, The stability field of analcine: Ph.D. Dissertation, Harvard University, Cambridge, Massachusetts.

Archie, G. E., 1942, The electrical resistivity log as an aid in determining some reservoir characteristics: Trans. AIME, Petrol. Br., v. 146, p. 54-62.

Atwater, R., 1970, Relationship of plate tectonics to Cenozoic tectonics of western North America: Geol. Soc. America Bull., v. 81, p. 3513-3536.

Bailey, R. A., 1976, Volcanism, structure, and geochemistry of Long Valley Caldera, Mono County, Calif.: Jour. Geophys. Res., v. 81, no. 5, p. 725-744.

Baker, A. A., Calkins, F. C., Crittenden, M. D., Jr., and Bromfield, C. S., 1966, Geologic Map of the Brighton Quadrangle, Utah: U.S. Geol. Survey.

Barker, C., 1972, Aquathermal pressuring--role of temperature in development of abnormal-pressure zones: Am. Assoc. Pet. Geol. Bull., v. 56, p. 2068-2071.

Barnes, M. P., and Simos, J. G., 1968, Ore Deposits of the Park City District, With a Contribution on the Mayflower Lode, in Ore Deposits of the United States, 1933-1967, Ridge, J. R., Jr., ed., The Granton-Sales vol., no. 2, AIME, p. 1002-1126.

Bath, M., Earthquake energy and magnitude: Physics and Chemistry of the Earth, v. 7, p. 117-165, 1966.

Beane, R. E., 1972, A thermodynamic analysis of the effect of solid solution on the stability of biotite: Unpublished Ph.D. dissertation, Northwestern University, 195 p.

Beane, R., 1974, Biotite stability in porphyry copper environment: Econ. Geol., v. 69, no. 2, p. 241-256.

Bear, Jacob, 1972, Dynamics of fluids in porous media: New York, Am. Elsevier, 764 p.

Belytschko, T., and Kennedy, J. M., Finite element study of pressure wave attenuation by reactor fuel subassemblies: Jour. Pres. Vessel Tech., v. 97, p. 172-177, 1975.

Benard, M., 1901, Les tourbillons cellularies dans une nappe

liquide transportant de la chaleur par convection en regime permanent: Am. Chim. Phys., v. 23, p. 62-144.

Bianchi, L., and Snow, D. T., 1969, Permeability of Crystalline rocks interpreted from neasured orientations and apertures of fractures: The Arid Zone Research of India, Jodphur (Rajasthan), Annals of Arid Zone, v. 8, no. 2, p. 231-245.

Birch, F., Compressibility, elastic constants, in Clark, S. P., ed., Handbook of Physical Constants, Geol. Soc. America Mem. 97: New York, Geol. Soc. America, p. 97-174, 1966.

Boardman, C. R., and Skrove, J., 1966, Distribution in fracture permeability of a granitic rock mass following a contained nuclear explosion: Jour. Petrol. Tech., v. 18, p. 619-623.

Boutwell, J. M., 1912, Geology and Ore Deposits of the Park City District, Utah, With Contributions by L. H. Woolsey: U.S. Geol. Survey Prof. Paper 77, 231 p.

Bowden, C., 1975, The impact of energy development on water resources in arid lands: Arid Lands Res. Info. Paper, no. 6, 278 p.

Brace, W. F., 1971, Resistivity of saturated crustal rocks to 40 km based on laboratory measurements, in Heacock, J. B., ed., The Structure and Physical Properties of the Earth's Crust: Geophys. Mon. Ser. 14, Washington, D.C., Am. Geophys. Union, p. 243-255.

Brace, W. F., Orange, A. S., and Madden, T. R., 1965, The effect of pressure on the electrical resistivity of water saturated crystalline rocks: Jour. Geophys Res., v. 70, p. 5669-5678.

Brace, W. F., Walsh, J. B., and Frangos, W. T., 1968, Permeability of granite under high pressure: Jour. Geophys. Res., V. 73, no. 6, p. 2225-2236.

Brace, W. F., and Orange, A. S., 1968, Further studies of the effect of pressure on electrical resistivity of rocks: Jour. Geophys. Res., v. 73, p. 5407-5420.

Brock, T. D., and Mosser, J. L., 1975, Rate of sulfuric acid production in Yellowstone National Park: Geol. Soc. America Bull., v. 86, p. 194-198.

Bromfield, C. S., Baker, A. A., and Crittenden, M.D., Jr., 1970, Geologic Map of the Heber Quadrangle, Wasatch and Summit Counties, Utah: U.S. Geol. Survey.

Brown, T. H., 1970, Theoretical predictions of equilibria and mass transfer in the system CaO-MgO-Si2-H2O-CO2-NaCl-HCl: Unpublished Ph.D. dissertation, Northwestern University.

Browne, P. R. L., and Ellis, A. J., 1970, The Ohaki-Broadlands hydrothermal area, New Zealand: Mineralogy and related geochemistry: Am. Jour. Sci., v. 269, p. 97-131.

Bruges, E. A., Latto, B., and Ray, A. K., 1966, New Correlations and tables of the coefficient of viscosity of water and steam up to 1000 bar and 1000°C: Internatl. Jour. Heat and Mass Transf., v. 9, p. 465-480.

Burnham, C. W., Holloway, J. R., and Davis, N. F., 1969, Thermodynamic properties of water to 1000°C and 10,000 bars: Geol. Soc. America Spec. Paper 132, 96 p.

Burnham, C. W., and Davis, N. F., 1971, The Role of H2O in silicate melts I. P-V-T relations in the system NaAlSi3O8-H2O to 10 kilobars and 1000°C: Amer. Jour. Sci., v. 270, p. 54-79. 270, p. 54-79.

Butler, B. S., 1919, Primary (hypogene) sulfate minerals in ore deposits: Econ. Geol., v. 14, p. 581-609.

Butler, B. S., 1956, Mineralizing solutions that carry and deposit iron and sulfur: Mining Eng., p. 1012-1017.

Cadek, J., Hazdrova, M., Kacura, G., Krasny, J., and Malkovsky, M., 1969, Hydrogeology of the thermal waters at Teplice and Usti nad Labem: Sbornik Geolog. Ved, Hydrogeol., Inzenyrska Geol., Rada Hig, sv. 6, p. 1-184.

Calkins, F. C., and Butler, B. S., 1943, Geology and Ore Deposits of the Cottonwood-American Fork Area, Utah, With Contributions by V. C. Heikes: U.S. Geol. Survey Prof. Paper 201, 152 p.

Chambers, J. F., 1958, The conductance of concentrated aqueous solutions of potassium iodide at 25°C and of potassium and sodium chlorides at 50°C: Jour. Phys. Chem., v. 62, p. 1136.

Cheng, W. T., 1970, Geophysical exploration in the Tatun volcanic region, Taiwan: Geothermics Spec. Issue 2, U.N. Symp. on the Development and Utilization of Geothermal Resources, Pisa, v. 2, part 1, p. 910-917.

Christiansen, R. L., and Lipman, P. W., 1972, Cenozoic volcanism and plate-tectonic evolution of the western United States I. Late Cenozoic: Phil. Trans. R. Soc. Land., v. 217A, p. 249-284.

Clark, S. P., Jr., ed., 1966, Handbook of Physical Constants, rev. ed.: New York, Geol. Soc. America Mem. 97, 587 p.

Combs, J., Heat flow and microearthquake studies, Coso geothermal area, China Lake, California: Final rept. to Adv. Res. Proj. Agency, ARPA, order no. 2800, 65 p., 1975.

Cook, K. L., 1966, Rift system in the basin and range province,

in the World Rift System, Irvine, T. N., ed.: Paper, Geol. Survey Canada, no. 66, p. 280-289.

Cooper, John R., 1957, Metamorphism and volume losses in carbonate rocks near Johnson Camp, Cochise County, Arizona: Geol. Soc. America Bull., v. 68, p. 577-610.

Craig, J. R., and Barton, P. B., 1973, Thermochemical approximations for sulfosalts: Econ. Geol., v. 68, p. 493-506.

Criss, C. M., and Cobble, J. W., 1964a, The thermochemical properties of high temperature aqueous solutions IV. Entropies of the ions to 200° and the correspondence principle: Am. Chem. Soc. Jour., v. 86, p. 5385-5390.

Criss, C. M., and Cobble, J. W., 1964b, The thermochemical properties of high temperature aqueous solutions V. The calculation of ionic heat capacities up to 200°C: Entropies and heat capacities above 200°: Am. Chem. Soc. Jour., v. 86, p.

Crittenden, M. D., Jr., 1965, Geologic map of the Dromedary Peak Quadrangle, Utah: U.S. Geol. Survey.

Crittenden, M. D., Jr., Stockless, J. S., Kistler, R. W., and Stern, T. W., 1973, Radiometric Dating of Intrusive Rocks in the Cottonwood Area, Utah: Jour. Res., U.S. Geol. Survey, v. 1, n. 2, p. 173-178.

Damon, P. E., Shafigullah, M., and Leventhal, J. S., 1974, K/Ar chronology for the San Francisco volcanic field and rate of erosion of the Little Colorado River, in Geology of Northern Arizona, Part 1, Regional Studies: Geol. Soc. Am., p. 221-235, Rocky Mt. Sec. Mtg., Flagstaff.

Damon, P. E., and Bikerman, M., 1966, K/Ar chronology of the Tucson Mountains, Pima County, Arizona: Geol. Soc. Am. Bull., v. 77, p. 1225-1234.

Davis, S. N., 1969, Porosity and permeability of natural materials, in DeWiest, R. J. M., ed., Flow through porous media: New York, Academic Press, p. 54-90.

DeWiest, R. J. M., 1965, Geohydrology: New York, John Wiley & Sons, Inc., 366 p.

Dellechaie, Frank, 1975, A hydrochemical study of the south Santa Cruz Basin near Coolidge, Arizona (abs.): 2nd United Nations Symp. on the Development and Use of Geothermal Resources, San Francisco, California, May 20-2.

Donaldson, I. G., 1962, Temperature gradients in the upper layers of the earth's crust due to convective water flows: Jour. Geophys. Res., v. 67, no. 9, p. 28-48.

Donaldson, I. G., 1968, The flow of stream water mixtures through

permeable beds: a simple simulation of a natural undisturbed hydrothermal region: New Zealand Jour. Sci., v. 11, no. 1, p. 3-23.

Edler, J. W., 1965, Physical processes in geothermal areas: Am. Geophys. Union Mon. #8, p. 211-239.

Edler, J. W., 1967, Steady free convection in a porous medium heated from below: Jour. Fluid Mech., v. 27, p. 29-84.

Elder, J. W., 1965, Physical processes in geothermal areas, chap. 8, in Lee, W. H. K., ed.: Terrestrial Heat Flow: Am. Geophys. Union, Geophys. Mon. Ser. 8, Baltimore, 276 p. 276 p.

Ellis, A. J., and Mahon, W. A. J., 1967, National hydrothermal systems and experimental hot water/rock interactions (Part II): Geochim. et Cosmochim. Acta, v. 31, p. 519-538.

Fatt, I., 1956, The network model of porous media: AIME, Petroleum Trans., v. 207, p. 141-181.

Forgac, J., 1972, Genesis of alunite and metamorphic rocks near Dekys (Stiavnicke Porhorie Mountains): Geol. PR., v. 58, p. 189-199 (in Slovic): Chem. Abst. CA07904021557H.

Fournier, R. O., and Rowe, J. J., 1966, Estimation of underground temperature from the silica content of water from hot springs and wet-steam wells: Am. Jour. Sci., v. 264, p. 685-697.

Fournier, R. O., and Truesdell, A. H., 1973, An empirical Na-K-Ca geothermometer for natural waters: Geochim. et Cosmochim. Acta, v. 37, p. 1255-1275.

Garrels, R. M., Dreyer, Z. M., and Howland, D. L., 1949, Diffusion of ions through intergranular spaces in water saturated rocks: Geol. Soc. America Bull., v. 60, p. 1809-1828.

Gilluly, J., 1963, The tectonic evolution of the western United States: Q. Jl, Geol. Soc. Land., v. 119, p. 133-174.

Gilluly, James, 1946, The Ajo mining district: U.S. Geol. Survey Prof. Paper 209.

Gonzales, Arsenio Geronimo, 1959, Geology and genesis of the Lepanto Copper Deposit, Mankayan, Mountain Province, Philippines: Unpublished Ph.D. dissertation, Stanford University.

Goranson, R. W., 1938, Silicate-Water Systems: Phase Equilibria in the $NaAlSi_3O_8$-H_2O and $KAlSi_3O_8$-H_2O Systems at High Temperatures and Pressures: Am. Jour. Sci., 5th Series, v. 35A, p. 71-91.

Graton, L. C., and Bowditch, Samuel I., 1936, Alkaline acid solutions in hypogene zoning at Cerro de Pasco: Econ. Geol., v. 31, p. 651.

Greenberg, R. J., and Brace, W. F., 1969, Archie's Law for rocks modeled by simple networks: Jour. Geophys. Res., v. 74, p. 2099-2102.

Grindley, G. W., 1965, The geology, structure, and exploration of the Wairakei geothermal field, Taupo, New Zealand: New Zealand Geol. Survey Bull. n.s. 75, 131 p.

Gunning, H. E., and Gordon, A. R., 1942, The conductance and ionic mobilities for aqueous solutions of K and NaCl at T = 15°C - 45°C: Jour. Chem. Phys., v. 10.

Gustafson, L. B., 1963, Phase equilibria in the system Cu-Fe-As-S: Econ. Geol., v. 58, p. 667-701.

Gustafson, L. B., and Hunt, John P., 1975, The porphyry copper deposit at El Salvador, Chile: Econ. Geol., v. 70, p. 857-912

Haas, H., 1972, Equilibria in the system Al2O3-SiO2-H2O involving the stability limits of diaspore and pyrophyllite, and thermodynamic data of these minerals: Am. Mineralogist, v. 57, p. 1375-1385.

Hamilton, W., and Myers, W. B., 1966, Cenozoic tectonics of the western United States: Rev. Geophys., v. 4, p. 509-550.

Harbour, J., 1966, Stratigraphy and sedimentology of the upper Safford Basin sediments: Unpublished Ph.D. Dissertation, University of Arizona.

Heard, H. C., 1967, The influence of environment on the brittle failure of rocks, in Failure and Breakage of Rocks, Eighth Symposium on Rock Mechanics, AIME (New York), p. 82-93.

Helgeson, H. C., 1968, Evaluation of irreversible reactions in geochemical processes involving minerals and aqueous solutions - I. Thermodynamic relations: Geochim. et Cosmochim. Acta, v. 32, p. 853-877.

Helgeson, H. C., 1969, Thermodynamics of hydrothermal systems at elevated temperatures and pressures: Am. Jour. Sci., v. 267, p. 729-804.

Helgeson, H. C., 1970, A chemical and thermodynamic model of ore deposition in hydrothermal systems: Min. Soc. of Am. Spec. Paper #3, p. 155-186.

Helgeson, H. C., Brown, T. H., Nigrini, A., and Jones, T. A. 1970, Calculation of mass transfer in geochemical

processes involving aqueous solutions: Geochim et Cosmochim. Acta, v. 34, p. 569-592.

Helgeson, H. C., Garrels, R. M., and Mackenzie, F. T., 1969, Evaluation of irreversible reactions in geochemical processes involving minerals and aqueous solutions - II. Applications: Geochim. et Cosmochim. Acta, v. 33, p. 455-481.

Helgeson, H. C., and Kirkham, D. H., 1974a, Theoretical predictions of the thermodynamic behavior of aqueous electrolytes at high pressures and temperatures; I. Summary of the thermodynamic/electrostatic properties of the solvent: Am. Jour. Sci., v. 274, p. 1089-1198.

Helgeson, H. C., and Kirkham, D. H., 1974b, Theoretical predictions of the thermodynamic behavior of aqueous electrolytes at high pressures and temperatures; II. Debey-Huckel parameters for activity coefficient and relative partial molal properties of the source: Am. Jour. Sci., v. 274, p. 1199-1261.

Hemley, J. J., Hostetler, P. B., Gude, A. J., and Mountjoy, W. T., 1969, Some stability relations of alunite: Econ. Geol., v. 64, p. 599-612.

Henley, R. W., 1973, Some fluid dynamics and ore genesis: Trans/section B, Inst. Min. and Metall., v. 2, p. B1-B8.

Holst, P. H., and Aziz, K., 1972, Transient three-dimensional natural convection in confined porous media: Internatl. Jour. Heat and Mass Transf., v. 15, p. 73-90.

Horikoshi, E., 1969, Volcanic activity related to the formation of the Kuroko-type deposits in the Kosaka District, Japan: Mineralium Deposita, v. 4, p. 321-345.

Horn, M. K., and Adams, J. A. S., 1966, Computer-derived geochemical balances and elemental abundances: Geochim. et Cosmochim. Acta, v. 30, p. 279-297.

Huang, C. K., 1955, Gold-copper deposits of the Chinkaushih Mine, Taiwan, with special reference to the mineralogy: ACTA Geol. Taiwanica, no. 7, p. 1.

Hubbert, M. K., 1940, The theory of ground-water motion: Jour. Geol., v. 48, p. 785-944.

Hubbert, M. K., and Rubey, W. W., Role of fluid pressure in mechanics of overthrust faulting. I: Geol. Soc. America Bull., v. 70, p. 115-166, 1959.

Hubbert, M. K., and Willis, D. G., Mechanics of hydraulic fracturing: Petrol. Trans., AIME, v. 210, p. 153-166, 1957.

Ishihara, S., Kanehira, K., Sasaki, A., Sato, T., and Shimazaki, Y., eds., 1974, Geology of Kuroko deposits, Japan: Soc. Mining Geol. Japan, Spec. Issue 6, 435 p.

Jackson, D. B., 1966, Deep resistivity probes in the southwestern United States: Geophysics, v. 31, p. 1123-1144.

Jacobs, D. C., and Parry, W. T., 1976, A comparison of the geochemistry of biotite from some Basin and Range stocks: Econ. Geol., v. 71, no. 6, p. 1027-1035.

Jaeger, J. C., 1968, Cooling and solidification of igneous rocks, in Hess, H., ed., Basalts, v. II: New York, John Wiley & Sons, p. 504-535.

Jaques, A. L., and Webb, A. Q., 1975, Geochronology of porphyry copper intrusives from Manus Island Papua New Guinea: Geol. Survey of Papua New Guinea, rpt. 75/5.

Jarzabek, D., and Combs, J., Microearthquake survey of the Dunes KGRA, Imperial Valley, Southern California: Geol. Soc. Am., Abs. with Prog., v. 8, p. 939, 1976.

Johnson, D. M., and Combs, J., Microearthquake survey of the Kilbourne Hole KGRA, South Central New Mexico: Geol. Soc. Am., Abs. with Prog., v. 8, p. 942, 1976.

Kajiwara, Y., 1973, A simulation of the Kuorko type mineralization in Japan: Geochem. Jour., v. 6, p. 193-209.

Keenan, J. H., and Keyes, F. G., 1969, Steam Tables: New York, John Wiley & Sons, 162 p.

Keller, G. V., 1970, Induction methods in prospecting for hot water: Geothermics Spec. Issue 2, U.N. Symp. on the Development and Utilization of Geothermal Resources, Pisa, v. 2, part 1, p. 318-332.

Keller, G. V., Anderson, L. A., and Pritchard, J. I., 1966, Geological survey investigations of the electrical properties of the crust and upper mantle: Geophysics, v. 31, p. 1078-1087.

Keller, G. V., 1971, Electrical studies of the crust and upper mantle in Heacock, J. G., ed., The Structure and Physical Properties of the Earth's Crust: Am. Geophys. Union Mon. 14, p. 107-126, 1971.

Keller, G. V., and Frischknecht, F. C., 1966, Electrical methods in geophysical prospecting: Pergamon Press, Oxford.

Kelley, K. K., 1960, Contributions to the data on theoretical metallurgy. XIII. High-temperature heat content, heat capacity, and entropy data for the elements and inorganic compounds: U.S. Bur. Mines Bull. 584, 232 p.

Kelley, K. K., Shomate, C. Y., Young, F. E., Naylor, B. F., Salo, A. E., and Huffman, E. H., 1946, Thermodynamic properties of ammonium and potassium alums and related substances with reference to extraction of alumina from clay and alunite: U.S. Bur. Mines, Technical Paper 688.

Kelley, Vincent C., 1935, Paragenesis of the Colorado copper sulfides, Cananea, Mexico: Econ. Geol., v. 30, p. 663.

Kennedy, G. C., 1950, A portion of the system silica-water: Econ. Geol., v. 45, p. 629-653.

Kerr, Paul F., 1951, Alteration features at Silver Bell, Arizona: Geol. Soc. America Bull., v. 62, p. 451.

Kim, Gung Rae, I. K. Song Kim, Man Ung Pak, and Gyung Tae Shin, 1971, Metasomatic zonality of low-temperature hydrothermal secondary quartzites and argillaceous rocks with alunite: Chijil Kwa Chiri, v. 11, p. 21-25 (in Korean): Chem. Abst. CA07614074817N.

King, P. B., 1959, The evolution of North America: Princeton University Press, 189 p.

Kitahara, S., 1960, The polymerization of silicic acid obtained by the hydrothermal treatment of quartz and the solubility of amorphous silica: Rev. Phys. Chem. Japan, v. 30, p. 131-137.

Knapp, R. B., 1975, An analysis of the porosities of fractured crystalline rocks: Unpublished M.S. Thesis, University of Arizona, 160 p.

Knapp, R., and Knight, J., 1977, Decrease in effective pressure by differential thermal expansion of pore fluids: Jour. Geophys. Res., accepted for publication.

Knapp, R., and Knight, J., 1977, Permeability of rocks in hydrothermal systems: Fracture propagation by pore fluid expansion: Jour. Geophys. Res., in press.

Knight, Jerry E., 1976, A thermochemical study of alunite and copper arsenic sulfosalt deposits: Unpublished M.S. Thesis, University of Arizona.

Kofman, R. G., 1971, Interrelations between alunitization and kaolinitization in the Zaglik Deposits: Tr. Kavhar. Inst. Miner. Syr'ya No. 9 Geol. Tekhnol, p. 195-207. (in Russian): Chem. Abst. CA07806032584V.

Krieger, M. H., 1969, Ash-flow tuffs in the northern Galiuro Mountains, Arizona (abs): Geol. Soc. America Spec. Paper no. 121, p. 523.

Lachenbruch, A. H., and others, 1976, Geothermal setting and simple heat conduction models for the Long Valley

Caldera: Jour. Geophys. Res., v. 81, no. 5, p. 769-784.

Lambert, J. B., and Sato, T., 1974, The Kuroko and associated ore deposits of Japan: A review of their features and metallogenesis: Econ. Geol., v. 69, p. 1215-1236.

Landisman, M., Mueller, S., and Mitchell, B. J., Review of evidence for velocity inversions in the continental crust, in Heacock, H. G., ed., The Structure and Physical Properties of the Earth's Crust: Am. Geophys. Union Mon. 14, p. 11-34, 1971.

Lapwood, E. R., 1948, Convection of a fluid in a porous medium: Proc., Cambridge Phil. Soc. 44, p. 508-521.

Laughlin, G. F., and Behre, C. H., Jr., 1933, Classification of ore deposits, in Ore deposits of the Western States: Amer. Inst. of Mining and Metallur. Eng., New York, 797 p.

Leeman, W. P., and Rogers, J. J. W., 1970, Late Cenozoic alkali-olivine basalts of the basin-range province, USA: Contr. Mineral. and Petrol., v. 25, p. 1-24.

Lindgren, W., 1907, The relation of ore deposition to physical conditions: Econ. Geol., v. 2, p. 105-127.

Lindgren, Waldemar, 1905, The copper deposits of the Clifton-Morenci District, Arizona: U.S. Geol. Survey Prof. Paper 43.

Lister, C. R. B., 1974, On the penetration of water into hot rock: Royal Astr. Soc., Jour. Geophys., v. 39, p. 465-509.

Lodder, W., 1966, Gold-alunite deposits and zonal wall-rock alteration near Rodalaquilar, S.E. Spain: Unpublished Ph.D. Dissertation, University of Amsterdam.

Lovering, T. S., 1935, Theory of heat conduction applied to geological problems: Geol. Soc. America Bull., v. 46, p. 69-94.

Lowell, R. P., 1975, Circulation in fractures, hot springs, and convective heat transport on mid-ocean ridge crests: Royal Astr. Soc., Jour. Geophys., v. 40, p. 351-365.

Maini, Y. N. T., 1971, In situ hydraulic parameters in jointed rock--their measurement and interpretation: Unpublished Ph.D. Dissertation, University of London, 312 p.

Marine, I. W., 1966, Hydraulic correlation of fracture zones in buried crystalline rock at the Savannah River plant, near Aiken, South Carolina: U.S. Geol. Survey Prof. Paper 550-D, p. 223-227.

Marlowe, J. I., 1960, Late Cenozoic geology of the lower Safford Valley--a preliminary report: Arizona Geol. Soc. Digest, v. 3, p. 127-129.

Maske, S., and Skinner, B. J., 1971, Studies of the sulfosalts of copper. I. Phases and phase relations in the system Cu-As-S: Econ. Geol., v. 66, p. 901-918.

McKee, B. H., and Anderson, C. A., 1971, Age and chemistry of Tertiary volcanic rocks in north-central Arizona, and their relationship to the Colorado Plateaus: Geol. Soc. America Bull., v. 82, p. 2767-2782.

Mehnert, Harold H., Lipman, Peter W., and Sleven, Thomas A., 1973, Age of mineralization at Summitville, Colorado, as indicated by K-Ar dating of alunite: Econ. Geol., v. 68, p. 399.

Meidav, T., and Furgerson, R., 1972, Resistivity studies of the Imperial Valley geothermal area, California: Geothermics, v. 1, p. 47-62.

Meyer, C., Shea, E. P., Goddard, C. C., Jr., and staff, 1968, Ore deposits at Butte Montana, in Ore deposits of the United States: Amer. Inst. of Mining, Metal. and Petro. Eng., New York, p. 1373-1416.

Meyer, Charles, 1950, Hydrothermal wall rock alteration at Butte, Montana: Ph.D. Dissertation, Harvard, 329 p.

Minakami, T., Utibori, S., Yamaguchi, M., Gyoda, N., Utsunomiya, T., Hagiwara, M., and Hirai, K., The Ebino earthquake swarm and the seismic activity in the Kirisima volcanoes, in 1968-1969, Part I. Hypocentral distribution of the 1968 Ebino earthquakes inside the Kakuto Caldera: Bull. Earthquake Res. Inst., v. 47, p. 721-743, 1969.

Mitchell, B. J., and Landisman, M., 1971, Geophysical measurements in the southern great plains, in Heacock, J. G., ed.: The Structure and Physical Properties of the Earth's Crust: Am. Geophys. Union Mon. 14, p. 77-95.

Moskowitz, B., and Norton, D., 1977, A preliminary analysis of intrinsic fluid and rock resistivity in active hydrothermal systems: Jour. Geophys. Res., in review.

Moskowitz, Bruce M., 1976, Numerical analysis of electrical resistivity in hydrothermal systems: Unpublished M.S. Thesis, University of Arizona.

Muller, A. B., Battaile, J. R., Bond, L. A., Lamson, P. W., 1973, An analysis of the water quality problems of the Safford Valley, Arizona: Repts. on Natural Resource Systems, Rept. no. 15, 126 p.

Nash, T. J., 1973, Geochemical Studies in the Park City District:

I. Ore Fluids in the Mayflower Mine: Econ. Geol., v. 68, no. 1, p. 34-59.

Nield, D. A., 1968, Onset of thermohaline convection in a porous medium: Water Resources Research, v. 4, p. 553-560.

Nielson, Richard L., 1968, Hypogene texture and mineral zoning in a copper-bearing granodiorite porphyry stock, Santa Rita, New Mexico: Econ. Geol., v. 63, no. 1, p. 37-50.

Nolan, T. B., 1943, The basin and range province in Utah, Nevada, and California: U.S. Geol. Survey Prof. Paper 197-D, p. 141-196.

Norris, R. J., and Henley, R. W., Dewatering of a metamorphic pile: Geology, v. 4, p. 333-336, 1976.

Norton, D. L., and Cathles, L. M., 1975, An analysis of the physics and chemistry of pluton environments, Part II: Applications: Unpublished manuscript.

Norton, D., and Knight, J. E., 1977, Transport phenomena in hydrothermal systems: Cooling plutons: Am. Jour. Sci., v. 277, p.

Norton, D., and Knapp, R., 1977, Transport Phenomena in Hydrothermal Systems: Nature of Porosity: Am. Jour. Sci., v. 277, p.

Norton, D., 1972, Concepts relating anhydrite deposition to solution flow in hydrothermal systems: 24th IGC, sec. 10, p. 237-244, Ottawa.

Norton, D., Gerlach, T., DeCook, K. J., and Sumner, J. S., 1975, Geothermal water resources in Arizona: Feasibility study: Technical Completion Rept., Office of Water Research and Technology, Project A-054-ARIZ.

Norton, D., and Gerlach, T., 1975a, Preliminary analysis of the energy and water requirements for developing geothermal energy in Arizona, in Proceedings of a Symposium on Water Requirements for Lower Colorado River Basin Energy, ed., Foster, K: Office of Arid Lands Studies, Univ. of Arizona, in press.

Norton, D., and Gerlach, T., 1975b, Characteristics useful in exploration for thermal energy resources as suggested by field observation and computer models (abs.): 2nd United Nations Symposium on the Development and Use of Geothermal Resources, San Francisco, California, May 20-29, 1975.

Norton, Denis, 1977, Fluid circulation in the earth's crust: Am. Geophys. Union Mon. 20, in review.

Nur, A., and Simmons, G., 1970, The origin of small cracks in igneous rocks: Int. Jour. Rock Mech. Min. Sci., v. 7, p. 307-314.

Nur, A., and Simmons, G., 1969, The effect of saturation on velocity in low porosity rocks: Earth and Planet Sci. Letts., v. 17, p. 183-193.

Ohle, E. L., 1951, The influence of permeability on ore distribution in limestone and dolomite: Econ. Geol., v. 46, p. 667-706.

Ohmoto, H., and Rye, R. O., 1974, Hydrogen and oxygen isotope compositions of fluid inclusions in the Kuroko deposits, Japan: Econ. Geol., v. 69, p. 947-953.

Okamoto, G., Okura, T., and Goto, K., 1957, Properties of silica water: Geochim. et Cosmochim. Acta, v. 12, p. 123-132.

Osmond, J. C., 1960, Tectonic history of the basin and range province in Utah and Nevada: Mining Eng. v. 12, p. 251-265.

Peaceman, D. W., and Rachford, H. H., Jr., 1955, The numerical solution of parabolic and elliptic differential equations: Soc. Indust. Appl. Math. Jour., v. 3, no. 1, p. 28-41.

Percious, J. K., 1968, Geology and Geochronology of the Del Bac Hills, Pima County, Arizona, in Titley, S. R., ed., Southern Arizona Guidebook: Arizona Geol. Soc., p. 199-208.

Peterson, D. W., 1960, Geology of the Haunted Canyon quadrangle, Arizona: U.S. Geol. Survey Geol. Quad. Map, GQ-128.

Peterson, D. W., 1969, Geologic map of the Superior quadrangle, Pinal County, Arizona: U.S. Geol. Survey Geol. Quad. Map GQ-818.

Peterson, D. W., 1968, Zoned ash-flow sheet in the region around Superior, Arizona, in Titley, S. R., ed., Southern Arizona Guidebook III: Arizona Geol. Soc., p. 215-222.

Peterson, N. P., 1962, Geology and ore deposits of the Globe-Miami District, Arizona: U.S. Geol. Survey Prof. Pap., no. 342, 151 p.

Plauff, D., 1966, Magneto-telluric soundings in the southwestern United States: Geophysics, v. 31, p. 1145-1152.

Pratt, H. R., Black, A. D., Brace, W. F., and Norton, D. L., 1974, In situ joint permeability in a granite: EOS, Trans. Am. Geophys. Union, v. 55, p. 433.

Quillen, R., and Combs, J., Microearthquake survey of the Radium Springs KGRA, South Central New Mexico: Geol. Soc. America, Abs. with Prog., v. 8, p. 1055, 1976.

Quinlan, J. J., and Simos, J. G., 1968, The Mayflower Mine, in Park City District, Utah: A. J. Erickson, ed., Utah

Geol. Guidebook n. 22, p. 40-55.

Quist, A. S., and Marshall, W. L., 1968, Electrical conductances of aqueous sodium chloride solutions from 0°C to 200°C and at pressures to 4000 bars: Jour. Phys. Chem., v. 72, p. 684-703.

Ransome, F. L., 1909, The geology and ore deposits of Goldfield, Nevada: U.S. Geol. Survey Prof. Paper 66.

Ransome, F. L., 1919, The copper deposits of Ray and Miami, Arizona: U.S. Geol. Survey Prof. Paper 115.

Ratte, J. C., Landis, E. R., and Gaskill, D. L., 1969, Mineral resources of the Blue Range Primitive Area, Greenlee county, Arizona, and Catron County, New Mexico: U.S. Geol. Survey Bull. no. 1261-E, 91 p.

Rayleigh, Lord, 1916, On convection currents in a horizontal layer of fluid, when the higher temperature is on the underside: Phis. Mag. Ser. 6, v. 32, p. 529-545.

Raymahashay, B. C., 1968, A geochemical study of rock alteration by hot springs in the Paint Pot Hill area, Yellowstone National Park: Geochim. et Cosmochim. Acta, v. 32, p. 499-522.

Ribando, R. J., Torrance, K. B., and Turcotte, D. L., 1976, Numerical models for hydrothermal circulation in the oceanic crust: Jour. Geophys. Res., v. 81, p. 3007-3012.

Ribando, R. J., and Torrance, K. E., 1975, Natural convection in a porous medium: effects of confinement, variable permeability, and thermal boundary conditions: ASME preprint 75-KW/HT-73, 9 p.

Risk, G. F., MacDonald, W. J. P., and Dawson, G. B., 1970, D.C. resistivity surveys of the Broadlands geothermal region, New Zealand: Geothermics Spec. Issue 2, U.N. Symp. on the Development and Utilization of Geothermal Resources, Pisa, v. 2, part 1, p. 287-294.

Roache, Patrick J., 1972, Computational fluid dynamics: Albuquerque, N.M., Hermosa Publishers, 434 p.

Robie, R. A., and Waldbaum, D. R., 1968, Thermodynamic Properties of Minerals and Related Substances at 298.15 °K (25° C) and one Atmosphere (1013 bars) Pressure and at Higher Temperatures: U.S. Geol. Survey Bull. 1259.

Robinson, H. H., 1913, The San Francisco volcanic field, Arizona: U.S. Geol. Survey Prof. Paper 76, 213 p.

Rubin, H., 1973, Effect of nonlinear stabilizing salinity profiles on thermal convection in a porous medium layer:

Water Resources Res., v. 9, p. 211-221.

Rye, R. O., and Ohmoto, H., 1974, Sulfur and carbon isotopes and ore genesis: A review: Econ. Geol., v. 6, p. 826-842.

Sato, K., 1970, The present state of geothermal development in Japan: Geothermics Spec. Issue 2, U.N. Symp. on the Development and Utilization of Geothermal Resources, Pisa, v. 2, part 1, p. 155-184.

Schmidt, E., 1969, Properties of water and steam in Si-units: New York, Springer-Verlag, 205 p.

Schoen, R., White, D. E., Man Ung Pak, and Tae Gyung, 1971, Metasomatic zonality of low-temperature hydrothermal secondary quartzites and argillaceous rocks with alunite: Chiji Kwa Chiri, v. 11, p. 21-25. (in Korean): Chem. Abst. CA0761407481 7N.

Schwartz, George M., 1953, Geology of the San Manuel Copper Deposit, Arizona: U.S. Geol. Survey Prof. Paper 256.

Shankland, T. J., and Waff, H. S., 1974, Conductivity in fluid bearing rocks: Jour. Geophys. Res., v. 79, p. 4863-4868.

Shaw, D. R., 1965, Strike-slip control of basin-range structure indicated by historical faults in western Nevada; Geol. Soc. America Bull., v. 76, p. 1361-1378.

Snaw, H. R., and Swanson, D. A., 1970, Eruption and flow rates of flood basalts, in Gilmour, E. H., and Stradlin, G. D., eds., Proc. 2nd Columbia River Basalt Symp.: Pullman East. Wash. State College Press, p. 271-299.

Sheridan, M. F., and Fodor, R. V., 1969, Orogin of silicic ash-flow tuffs and lavas in the Goldfield Mountains, Arizona (abs.): Geol. Soc. America Spec. Paper no. 121, p. 557-558.

Sheridan, M. F., and Stuckless, J. S., 1969, Volcanics related to Black Mesa Caldera, central Arizona (abs.): Geol. Soc. America Spec. Paper no. 121, p. 60-61.

Simons, F. S., 1964, Geology of the Klondike Quadrangle, Graham and Pinal counties, Arizona: U.S. Geol. Survey Prof. Paper 461, 173 p.

Skinner, B. J., 1960, Assemblage enargite-famatinite, a possible geologic thermometer (abs.): Geol. Soc. America Bull., v. 71, p. 1975.

Skinner, B. J., 1966, Thermal expansion, in Clark, S. P., ed., Handbook of Physical Constants, Geol. Soc. America Mem. 97: New York, Geol. Soc. America, p. 75-96.

Smiley, T. L., 1958, The geology and dating of Sunset Crater,

Flagstaff, Arizona, in New Mexico Geol. Soc. Guidebook: 9th Field Conf., Black Mesa Basin, p. 186-190.

Smith, R. B., and Sbar, M. L., 1974, Contemporary tectonics and seismicity of the western United States with emphasis on the Intermountain Seismic Belt: Geol. Soc. America Bull., v. 85, p. 1205-1218.

Snow, D. T., 1965, A parallel plate model of fractured permeable media: Unpublished Ph.D. Dissertation, University of California, Berkeley, 331 p.

Snow, D. T., 1968, Rock fracture spacings, openings, and porosities: Jour. Soil Mech. and Foundations Div., ASCE, v. 94, p. 73-91.

Snow, D. T., 1970, The frequency and aperture of fractures in rocks: Jour. Rock Mech., v. 7, p. 23-40.

Ssu-hsiao, 1250, in Brower, ed., Of All Things Most Yielding: San Francisco, California, McGraw-Hill, Friends of the Earth, 128 p.

Summers, W. K., 1965, Chemical characteristics of New Mexico thermal waters: New Mexico Bureau of Mines Circ. 83, 87 p.

Takahashi, T., and Kiyonori, S., 1974, Geology and ore deposits of the Hanaoka belt, Akita Prefecture: Soc. Mining Geologists Japan, Spec. Issue 6, p. 101-113.

Takashima, I., 1972, Hydrothermal rock alteration in Takenoyu geothermal area, Kumamoto Prefecture, Japan: Chishitsu Chosajo Geppo, v. 23, p. 721-732 (in Japanese): Chem. Abst. CA07908044422Z.

Tatsumi, T., ed., 1970, Volcanism and ore genesis: Tokyo, University of Tokyo Press, 448 p.

Taylor, H. P., Jr., 1971, Oxygen isotope evidence for large-scale interaction between meteoric ground waters and Tertiary granodiorite intrusions, Western Cascade Range, Oregon: Jour. Geophys. Res., v. 76, p. 7755-7873.

Taylor, Hugh P., Jr., 1974, The application of oxygen and hydrogen isotope studies to problems of hydrothermal alteration and ore deposition: Econ. Geol., v. 69, no. 6, p. 843-883.

Tellier, A. H., 1973, Geothermal waters of Arizona: Unpublished M.S. Thesis, Arizona State University, 31 p.

Thoenin, J. R., 1941, Alunite resources of the United States: U.S. Bur. of Mines Res. Rept. 3561, 48 p.

Thompson, G. A., 1960, Problem of the Late Cenozoic structure of

the Basin Ranges: 20th Internatl. Geol. Cong., pt. 18, p. 62-68.

Tono, N., 1974, Minor elements distribution around Kuroko deposits of northern Akita, Japan: Soc. Mining Geologists Japan, Spec. Issue 6, p. 399-420.

Ulbrich, H. H., and Merino, E., 1974, Examination of standard enthalpies of formations of selected minerals in the SiO2-Al2O3-Na2O-K2O-H2O system: Am. Jour. Sci., v. 274, p. 510-542.

Van Hise, C. R., 1901, Some principles controlling the deposition of ores: Am. Inst. Min. Eng. Trans., v. 30, p. 27.

Veronis, G., 1968, Effect of stabilizing gradient of solute on thermal convective: Jour. Fluid Mech., v. 34, p. 315-336.

Villas, Netuno R., 1975, Fracture analysis, hydrodynamic properties, and mineral abundance in altered igneous rocks at the Mayflower Mine, Park City District, Utah: Unpublished Ph.D. Dissertation, University of Utah.

Villas, R. N., and Norton, D., 1977, Irreversible mass transfer between circulating hydrothermal fluids and the Mayflower stock: Econ. Geol., v. 72, in press.

Wagmen, D. D., Evans, W. H., Parker, V. B., Halow, I., Vailey, S. M., and Schumm, R. H., 1968, Selected values of chemical thermodynamic properties: Natl. Bur. Standards, Tech. Note 270-3, 264 p.

Walsh, J. B., The effects of cracks on the compressibility of rock: Jour. Geophys. Res., v. 70, p. 381-389, 1965.

White, D. E., 1974, Diverse origins of hydrothermal ore fluids: Econ. Geol., v. 69, no. 6, p. 954-973.

Willden, R., 1964, Geology of the Christmas Quadrangle, Gila and Pinal counties, Arizona: U.S. Geol. Survey Bull., no. 1161-E., 64 p.

Williams, H., 1932, History and character of volcanic domes: Univ. Calif. Pub., Dept. Geol. Sci., Bull. 21, p. 51-146.

Williams, N. C., 1952, Wall rock alteration, Mayflower Mine, Park City, Utah: Unpublished Ph.D. Dissertation, Columbia University, 58 p.

Wilson, J. C., 1967, Geology of the Alta Stock, Utah: Unpublished Ph.D. Dissertation, California Institute of Technology, 236 p.

Winograd, I. J., 1971, Hydrogeology of ash flow tuff: a preliminary statement: Water Resources Research, v. 7,

p. 994-1006.

Wooding, R. A., 1957, Steady state free thermal convection of liquid in a saturated permeable medium: Jour. Fluid Mech., v. 2, p. 273-285.

Wright, J. J., 1971, The occurrence of thermal groundwater in the Basin and Range Province of Arizona, in Hydrology and Water Resources in Arizona and the Southwest: Proc. 1971 Mtgs., Arizona Sec., Tempe, Arizona, April 22-23.

Zen, E., 1972, Gibbs free energy, enthalpy, and entropy of ten rock-forming minerals: Calculations, discrepancies, implications: Am. Miner., v. 57, p. 524-553.

Zienkiewicz, O. C., The finite element method in engineering science: McGraw-Hill, London, 521 p., 1971.

Zohdy, A. A. R., Anderson, L. A., and Muffler, L. J. P., 1973, Resistivity, self potential, and induced polarization surveys of a bapor-dominated geothermal system: Geophysics, v. 38, p. 1130-1144.

*U.S.GOVERNMENT PRINTING OFFICE: 1977- 740062/1006